EXERGY ANALYSIS AND HEAT INTEGRATION OF A PULVERIZED COAL OXY COMBUSTION POWER PLANT USING ASPEN PLUS

Prepared by

Neo Khesa

Student name

0405717G

Student number

A dissertation submitted to the faculty of Engineering and the Built Environment, University of the Witwatersrand, in fulfillment of the requirements for the degree of Master of Science in Engineering.

Supervisor: Dr. J.L Mulopo

Co-Supervisor: Dr. B.O Oboirien

21 November 2016

Declaration

I declare that this thesis is my own unaided work. It is being submitted to the degree of Master of Science to the University of the Witwatersrand, Johannesburg. It has not been submitted before any degree or examination to any other University.

.....

(Signature of candidate)

.....

(Signature of Supervisor)

.....day of.....year.....

Abstract

In this work a comprehensive exergy analysis and heat integration study was carried out on a coal based oxy-combustion power plant simulated using ASPEN plus. This is an extension on the work of Fu and Gundersen (2013). Several of the assumptions made in their work have been relaxed here. Their impact was found to be negligible with the results here matching closely with those in the original work. The thermal efficiency penalty was found to be 9.24% whilst that in the original work was 9.4%. The theoretical minimum efficiency penalty was determined to be 3% whilst that in the original work was 3.4%. Integrating the compression processes and the steam cycle was determined to have the potential to increase net thermal efficiency by 0.679%. This was close to the 0.72% potential reported in the original work for the same action.

Acknowledgements

I'd like to thank Dr Mulopo and Dr Oboirien for helping me select this topic, for having faith that I'd eventually be able to complete the work and for all the assistance (both financial and advisory) they gave me along the way. I'd also like to thank the University of the Witwatersrand school of Chemical and Metallurgical Engineering for allowing me to use their world class facilities, senior staff who I consulted from time to time, the CSIR for funding the work and my family.

Contents

List of Figures

Page

List of tables

Page

NOMENCLATURE

c	Mass fraction of carbon in coal (Dry basis)
n	Mass fraction of nitrogen in coal (Dry basis)
o	Mass fraction of oxygen in coal (Dry basis)
e_{ch}^{0}	Standard chemical exergy, MJ/mole
$e_{ch,coal}^{0}$	Chemical exergy of coal, MJ/kg
$\dot{E}^{in}$	Exergy in, MW
$\dot{E}^{out}$	Exergy out, MW
$\dot{E}_{ch}$	Chemical exergy component, MW
$\dot{E}_{mix}$	Exergy of mixing component, MW
$\dot{E}_{ph}$	Physical exergy component, MW
$\dot{E}_{tot}$	Total exergy, MW
$\dot{E}_{tot}^{feed}$	Exergy of material streams fed, MW
$\dot{E}_{tot}^{product}$	Exergy of material streams leaving, MW
$\dot{F}$	Molar flow, moles/s
h	Molar enthalpy, MJ/mole; Mass fraction of hydrogen in coal (Dry basis)
HHV	Higher heating value, MJ/kg
$\dot{I}$	Irreversibility, MW
LHV	Lower heating value, MJ/kg
$\dot{m}$	Mass flowrate, kg/s
P	Pressure, bar
Q	Heat, MW
s	Molar entropy, MJ/(mole.˚C)
T	Temperature, ˚C
T_{gas}	Temperature of compressed gas, ˚C
$\dot{W}$	Work, MW
$\dot{W}_{min}$	Minimum work, MW

Greek Letters

φ	Chemical exergy/Lower heating value

Subscripts

0	Reference state (Environmental state)
00	Dead state
i	Component index

Abbreviations

ASU	Air separation unit
CCS	Carbon capture and storage

CPU	Compression and purification unit
CW	Cooling water
DCA	Direct contact aftercooler
ESP	Electrostatic precipitator
FGD	Flue gas desulphurization
FWH	Feed water heater
GCC	Grand composite curve
HHV	Higher heating value
HP	High pressure
IP	Intermediate pressure
LP	Low pressure
MAC	Main air compressor
MHE	Main heat exchanger
NETL	National Energy Technology Laboratory
PPU	Pre-purification unit
LHV	Lower heating value
PR	Peng-Robinson
RFG	Recycled flue gas
SCR	Selective catalytic reduction
SSR	Steam seal regulator
TSA	Temperature swing adsorption

1. Introduction

There is consensus among scientists that the recent increase in average global temperatures is a result of man-made emissions of CO_2 (Houghton et al., 2001). Most of the growth in CO_2 emissions (around 47%) between the years 2000 and 2010 can be attributed to energy supply sector alone; outstripping the contribution made by industry (30%), the transport sector (11%) and the building sector (3%). If no mitigating action is taken it's predicted that emissions within the sector will as much a triple by the year 2050. Of all the fossil fuels used to generate power, coal is the most utilised and is responsible for as much as 40% of the world's electricity generation. Carbon capture and sequestration (CCS): a process whereby CO_2 emissions are captured, transported and stored in geological formations is today seen as the best means of reducing CO_2 emissions from coal fired power plants to an acceptable level in the near term (Edenhofer et al., 2014).

There are three main carbon capture and sequestration (CCS) strategies for coal power plants: Post combustion capture, pre combustion capture and oxy-combustion. Post combustion capture is where the carbon dioxide is scrubbed out of the combustion flue gases downstream using a solvent such as amine or ammonia. The reaction between the flue gas and the solvent take place in an absorber at lower temperatures before the loaded solvent reports to a stripper which regenerates the solvent by releasing the CO_2 at elevated temperatures (typically around 100-120℃). Pre combustion capture or integrated gasification combined cycle (IGCC) is where the carbon dioxide is removed upstream in a combined cycle plant that utilises gasification. The gasification product is syngas composed of H_2 and CO. The CO in the syngas product is converted to carbon dioxide via water gas shift reaction before removal using absorption. The hydrogen then reports to a combustion turbine to generate power. Oxy combustion is where a cryogenic air separation unit is retrofitted up stream. All this to produce a near pure oxygen feed for the furnace. This is done mainly to remove N_2. The resulting flue gas is primarily composed of CO_2 and H_2O which can be easily condensed out (Herold et al., 2011).

Though post-combustion capture is the more mature of the three capture strategies, oxy-combustion has proven itself to be an attractive alternative. One reason for this is that although oxy-combustion induces an energy penalty upon retrofit higher than that of pre combustion capture (Beér, 2007), it is slightly lower than that of post combustion capture (Ciferno et al.,

2008) . It's also been found to consume less water than the more mature post combustion alternative (Almås, 2012), it can be retrofitted to existing pulverized coal plants with little change to the main components (Mousavian & Mansouri, 2011) and it's also associated with reduced equipment size upon retrofit (Hu, 2011)..

The efficiency penalty or yield reduction is a measure of the reduction in efficiency a plant experiences upon retrofit with CCS. This efficiency penalty may be substantial enough for CCS (over 10% at times) that retrofit is advised only for plants with high baseline efficiency (Burnard & Bhattacharya, 2011). The efficiency penalty associated with oxy-combustion is around 10.1% (Ciferno et al., 2008). Although this is lower than the more popular post combustion alternative which is around 11.1% (Ciferno et al., 2008), it's still too high a value for wide spread retrofit of the worlds pulverized coal plants. For instance, if 40% efficiency is established as a cut off for retrofit, less than 10% of the current world coal fired power capacity would qualify (Burnard & Bhattacharya, 2011). This efficiency penalty also has a far reaching impact on the cost of electricity. It's been found that if you take into consideration the cost of construction, fuel, as well as operations and management, an oxy-combustion retrofit will result in a 48% increase in the cost of electricity produced from a pulverized coal plant (Kanniche et al., 2010). So for oxy-combustion to become a viable solution for carbon free electricity generation, a means of mitigating this efficiency penalty needs to be found.

The air separation unit (ASU) and downstream CO_2 compression and purification unit (CPU) are mostly responsible for the energy penalty associated with oxy-combustion ((IEAGHG, 2010), (Hu, 2011), (Fu and Gundersen, 2013)). Recently, Fu and Gundersen (2013) investigated the potential for reducing the efficiency penalty associated with oxy-combustion through exergy analysis and heat integration of a 570MW (net) plant simulated using ASPEN plus. They determined that the compression processes in the ASU and CPU are chiefly responsible for the energy penalty which they determined to be 9.4%. Their heat integration study determined that a reduction of 0.72% in the efficiency penalty is achievable if these compression processes are integrated with the steam cycle. In conducting their investigation, they made several simplifying assumptions. The research outlined in this paper is a revisit on their work. Specifically to find out what effect, if any, loosening several of the assumptions they made in their work will have on the results.

This paper is comprised of two sections. In the first section a comprehensive exergy analysis identical to that in Fu and Gundersen (2013) is conducted on an oxy-combustion plant with carbon capture. All major stream flows and the entire steam cycle are based on the NETL report (Ciferno et al., 2008). The ASU and the CPU are based on other common cases from literature ((Hands, 1986), (Pipitone and Bolland, 2009), (Fu and Gundersen, 2012)). The second part of the paper is a heat integration study that investigates the potential for utilizing the compression heat from compressors in the ASU and the CPU to preheat the boiler feed water in the steam cycle. Both sections are an extension of the work of Fu and Gundersen (2013). As such, comparisons are made in both sections between the results obtained here and those obtained by Fu and Gunderden (2013) to determine if relaxing several of the assumptions made by Fu and Gundersen (2013) makes any difference.

1.1. Problem statement

The efficiency penalty (yield reduction) is as much as 10% for an oxy-combustion setup despite the reduced energy demand on the CPU that comes with separation of carbon dioxide from an enriched flue gas (Ciferno et al., 2008). This large energy penalty is due to the high energy demand of the upstream air separation unit (Herold et al., 2011). Although this efficiency penalty is slightly lower than the 11.1% efficiency penalty associated with the post- combustion alternative that uses a 30wt% monoethanolmine (MEA) solution (Ciferno et al., 2008), it's still too high to make oxy-combustion a viable solution for producing a carbon free coal fired power plant. Although a 20% reduction in ASU power consumption has been achieved in recent years (Fu & Gundersen 2012), there may be still room for exploring the possibilities for process improvement through exergy analysis and heat integration. Exergy analysis is used to determine areas that contribute the most to work destructions or irreversibility's in a process. Understanding what causes irreversibility's in these processes gives an operator the ability to diagnose and find solutions to them and improve thermal efficiency. Heat integration is a technique that increases thermal efficiency by transferring heat from areas with excess heat to areas that have a deficit within a process.

Recently Fu and Gundersen (2013) performed and exergy analysis and heat integration study on a coal based oxy combustion power plant simulated using ASPEN PLUS. They determined the exergy flows and irreversibility's for the entire plant, the ASU, the CPU as well as the combustor

and steam cycle. The heat integration study determined the potential of reducing the oxy-combustion energy penalty through heat integration between the compression processes and the steam cycle. They found that the efficiency penalty upon retrofit was 9.4 percentage points (on the basis of the higher heating value), which was mainly caused by the ASU and the CPU. The theoretical minimum work for the ASU and the CPU combined was determined to only be 3.4 percentage points of the thermal input of the of the coal feed. The actual value though was found to be 9.7 percentage points. Their heat integration study determined that a reduction of 0.72% in the efficiency penalty is achievable. To perform the exergy analysis through ASPEN PLUS they made the following assumptions:

- The exergy of the ash is assumed to be zero
- The exergy of the limestone slurry is calculated as the exergy of its two main constituents: water (70 wt%) and calcium carbonate $(CaCO_3)$. The exergy of gypsum is calculated in similar way; as the sum of the exergy of water (10 wt%) and solid gypsum $(CaSO_4.2H_2O)$. The chemical exergy of $(CaCO_3)$ and $(CaSO_4.2H_2O)$ is obtained from (Szargut, Morris and Steward 1988).
- The reaction heat of the FGD unit is ignored. The chemical exergy of the waste water in the FGD unit is also ignored.
- Ignoring the physical exergy of the solids (coal, limestone, gypsum).
- Assuming the ambient air is composed only of N_2, O_2, Ar, CO_2 and H_2O. This ignores other noble gases and inorganic substances present in ambient air.
- The exergy of impurities (H_2O and CO_2) in the ASU are ignored.

1.1.1. Research questions:

i. What is the efficiency penalty when the assumptions made by Fu and Gundersen (2013) are included in the simulation?

ii. What effect will relaxing these assumptions have on the exergy analysis results?

iii. What effect will relaxing these assumptions have on the heat integration results?

iv. What more can be done to overcome this penalty?

1.2. Research objectives

The objective of this thesis is to revisit the work of Fu and Gundersen (2013) and include some of the assumptions which were ignored previously. This is because these assumptions have the potential to affect the efficiency penalty and the irreversibility's determined through exergy analysis, especially around the flue gas desulphurization unit and the heat integration results. In order to determine this, the following research objectives were met.

1. Simulate a pulverised coal air fired power plant without CCS using ASPEN PLUS V8.4.
2. Simulate a pulverised coal oxy-combustion power plant with CCS again using ASPEN PLUS V8.4.
3. Relax the following assumptions made by Fu and Gundersen (2013) in both simulations:
   - The exergy of the ash is not assumed to be zero
   - The exergy of the limestone slurry is not calculated only as the exergy of its two main constituents: water and calcium carbonate but will include all the other constituents within the limestone slurry
   - The reaction heat of the FGD unit is not ignored.
   - The chemical exergy of the waste water in the FGD unit is also not ignored.
   - Physical exergy of the solids are taken into account (coal, limestone, gypsum).
   - The exergy of impurities in the ASU are taken into account
4. Determine how the efficiency penalty compares to that reported by Fu and Gundersen (2013).
5. Conduct an exergy analysis on the oxy-combustion plant, and then determine how the exergy analysis results compare to that of Fu and Gundersen (2013).
6. Conduct a heat integration study on the oxy-combustion plant where the compression processes in the ASU and CPU are integrated with the steam cycle. Compare these heat integration results with those reported by Fu and Gundersen (2013).

2. Literature review

2.1. Anthropogenic climate change

There is strong evidence that the recent increase in global mean temperatures is consequence of recent human industrial activity and its associated greenhouse gas emissions. When the earth receives incoming solar radiation from the sun, a fraction of it is re-emitted from the surface as outgoing solar radiation at longer (infrared) wavelengths. Greenhouse gasses are able to absorb a fraction of the outgoing solar radiation and re-emit it at higher altitudes and lower temperatures. This phenomenon is called positive radiative forcing and tends to warm the lower atmosphere and surface (Houghton et al., 2001). Typical greenhouse gasses include species such as, CO_2, CH_4, SO_2 and even water vapour just to name a few. Greenhouse gas concentrations in the upper atmosphere have risen exponentially since the beginning of the industrial revolution. Evidence of this has been found from the inspection of atmospheric air bubbles in ice cores drilled from ice sheets in cold regions such as Antarctica and Greenland. These ice sheets are several hundred thousand years old, providing a comprehensive record of atmospheric conditions over these time scales. Strong correlations have been drawn between the concentration of greenhouse gasses trapped in these ice core air bubbles and global atmospheric temperatures. The records show an exponential increase in greenhouse gas concentrations and global atmospheric temperatures from around the time of the industrial revolution to the present day (Petit et al., 1999). This recent exponential increase in greenhouse gas emissions has also been affirmed in investigations made by the Intergovernmental Panel on climate change (IPCC). According to the (IPCC), half the cumulative anthropogenic CO_2 emissions between 1750 and 2010 have occurred in the last 40years. Results showed that greenhouse gas emissions between the years 2000 and 2010 grew at 1.0gigatonne carbon dioxide equivalent (GtCO_2eq) or 2.2%, whist those between the years 1970 and 2000 grew by only 0.4 (GtCO_2eq) or 1.3% (Edenhofer et al., 2014).

2.1.1. Future projections

The Intergovernmental Panel on climate change (IPCC) has conducted comprehensive studies forecasting the degree to which average global temperatures will change for several mitigation scenarios. The mitigation scenarios are models that forecast changes in global temperatures with differing assumptions on the degree to which governments take action and collaboratively combat climate change. The mitigation scenarios are called Representative Concentration

Pathways (RCPs). There are four predominant Representative Concentration Pathways: (RCP8.5), (RCP6.0), (RCP4.5) and (RCP2.6). RCP8.5 is a worst case scenario in which governments take little action to combat climate change. In this scenario its projected that greenhouse gas concentrations in the upper atmosphere exceed 450 parts per million (ppm) CO_2eq by 2030, and go on to reach up to 1300 ppm CO_2eq by 2100. This will result in an increase in global mean surface temperatures of between 3.7℃ and 4.8℃ compared to pre-industrial levels. RCP2.6 is a best case scenario in which governments make a concerted effort to combat climate change. It's characterized by greenhouse gas concentrations in the upper atmosphere of around 450 ppm CO_2eq by the year 2100. In this scenario mean surface temperatures grow to less than 2℃ relative to pre-industrial levels. RCP6.0 and RCP4.5 are scenarios that lie between these two extremes (Edenhofer et al., 2014). Figure 1 is a graph depicting the projected upper atmosphere greenhouse gas concentrations and total radiative forcing associated with each scenario from 2010 to 2090.

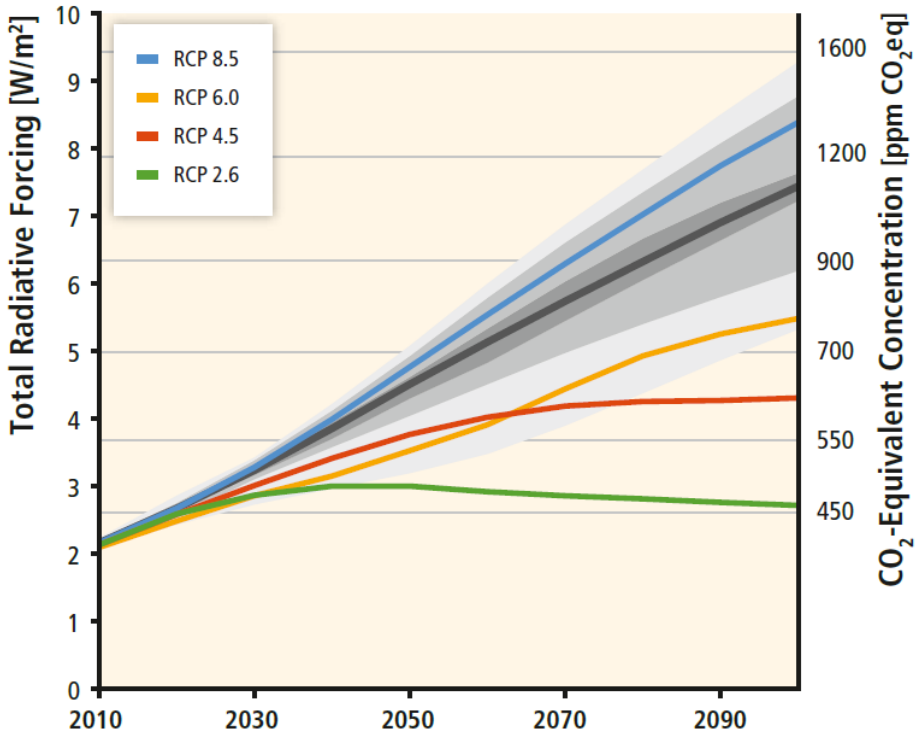

Figure 1: Projections of greenhouse gas concentrations and total radiative forcing for representative concentration pathways between the years 2010 and 2090. The solid lines represent medians, whilst the shading represents the degree of uncertainty or possible deviation. The Figure was lifted from (Edenhofer et al., 2014).

If nothing is done to mitigate the projected high concentration in greenhouse gasses by 2100 (RCP 8.5), simulations on global climate predict: extreme variations in precipitation, increased drought and flooding, enhanced El Nino, continued glacial retreat and sea level rise (Houghton et al., 2001). Average evaporation levels and precipitation are expected to increase globally. However, the precipitation won't be evenly dispersed, with excesses and shortfalls to usual patterns predicted from region to region. Furthermore, strong correlations have been drawn between seasonal variations and mean precipitation. For example, it's projected that while precipitation will increase in both summer and winter in high latitude regions, a decrease in winter rainfall is predicted for Australia, Central America and South Africa. Simulations also predict reductions in summer precipitation in mid continental areas. El Nino events, which are associated with an eastward migration in precipitation around the equatorial pacific are likely be enhanced in the event of extreme climate change. These extremes will increase the occurrences of flooding and droughts all over the world. Models also predict an overall continued retreat in glaciers and ice caps, but much like global precipitation regional discrepancies to the overall trend are predicted. For example while snow cover and sea ice are projected to decrease in the Northern Hemisphere, the Antarctic is projected to gain mass. This overall glacial and ice cap melting will result in notable sea level rise. Models predict this rise in sea level will be anywhere between 0.11m and 0.77m by 2100 (see Figure 2) (Houghtonet al., 2001).

These extreme weather patterns will change the prevailing conditions that man has become accustomed to for cultivation; threating sustainable development. These changes also affect natural systems and the earth's biosphere. Rising sea levels will threaten many coastal regions and low lying islands.

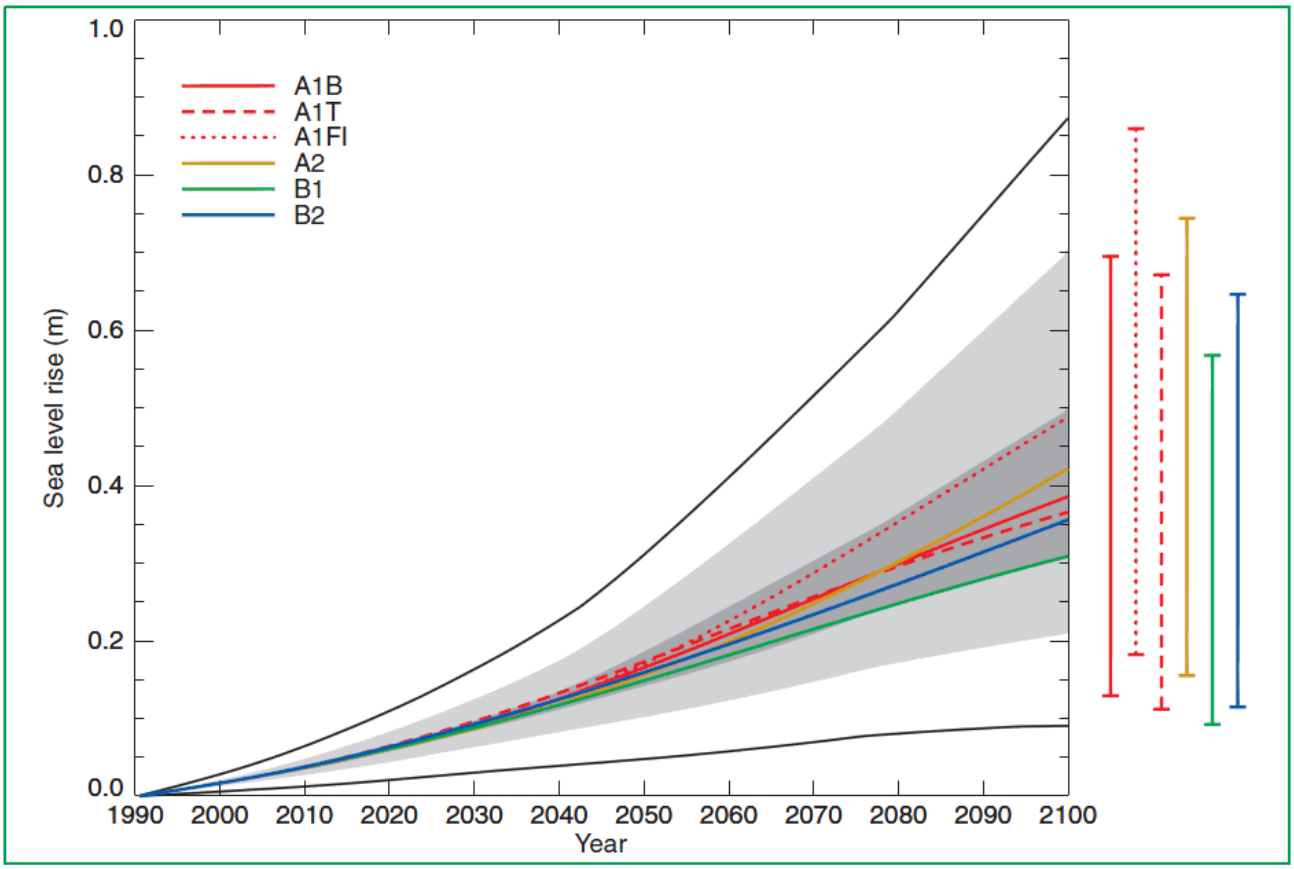

Figure 2: Figure depicting average sea level rise between the years 1900 and 2100 for 6 simulated emission scenarios. Scenario A1F1 assumes a fossil fuel intensive technology emphasis and has the highest predicted atmospheric CO_2 concentrations by 2100. Scenarios A1T and B1 broadly describe a world of reduced fossil fuel usage with greater reliance on clean resources. These two scenarios have the lowest predicted atmospheric CO_2 concentrations by 2100. This graph was lifted from (Houghton et al., 2001).

2.1.2. Contribution of energy sector

The energy sector was found to be the largest contributor (25%) to total direct anthropogenic greenhouse gas emissions in 2010. This is larger than the direct contributions made by agriculture, forestry and other land use (AFOLU) (24%), the building sector (6.4%), the transport sector (14%) and industry (21%) (see Figure 3). The energy sectors contribution to the increase in greenhouse gas emissions has also been larger than the contribution made by other sectors in recent years. For example the energy sectors contribution to the increase in annual greenhouse gas emissions between the years 2000 and 2010 is around 47%. This was greater than the contributions made by industry (30%), the transport sector (11%) and the buildings sector (3%) (Edenhofer et al., 2014). One of the reasons for its large contribution could be that it's the primary energy source for all other sectors. This would explain why the indirect contributions made by other sectors to its direct percentage contribution shown in Figure 3 are so large. Another reason for this is that fossil fuel combustion is the primary means the energy supply sector produces power today (Beér, 2007). This method of producing power can be very carbon intensive; meaning the ratio of CO_2 emitted per unit of primary energy for it can be very high. Fuels with higher carbon content release a greater amount of CO_2 per unit power output. Two major fossil fuel combustion products are CO_2 and H_2O.

From the year 1850 to around the year 1975, there has been a gradual progression toward fuels with ever decreasing carbon content. From fuels such as biomass and coal with very high carbon content, to natural gas which has a very low carbon content and on to renewables which have near zero carbon content. This trend can be seen in Figure 5. From the Figure it's clear there has been a rapid decline in the use of non-commercial biomass from 1850 to the year 2000. Coal rose in usage till the year 1910 before declining steadily. This was accompanied by the steady rise of less carbon intensive alternatives such as Nuclear power. However coal has experienced a slight resurgence around the 1980's (Edenhofer et al., 2014).

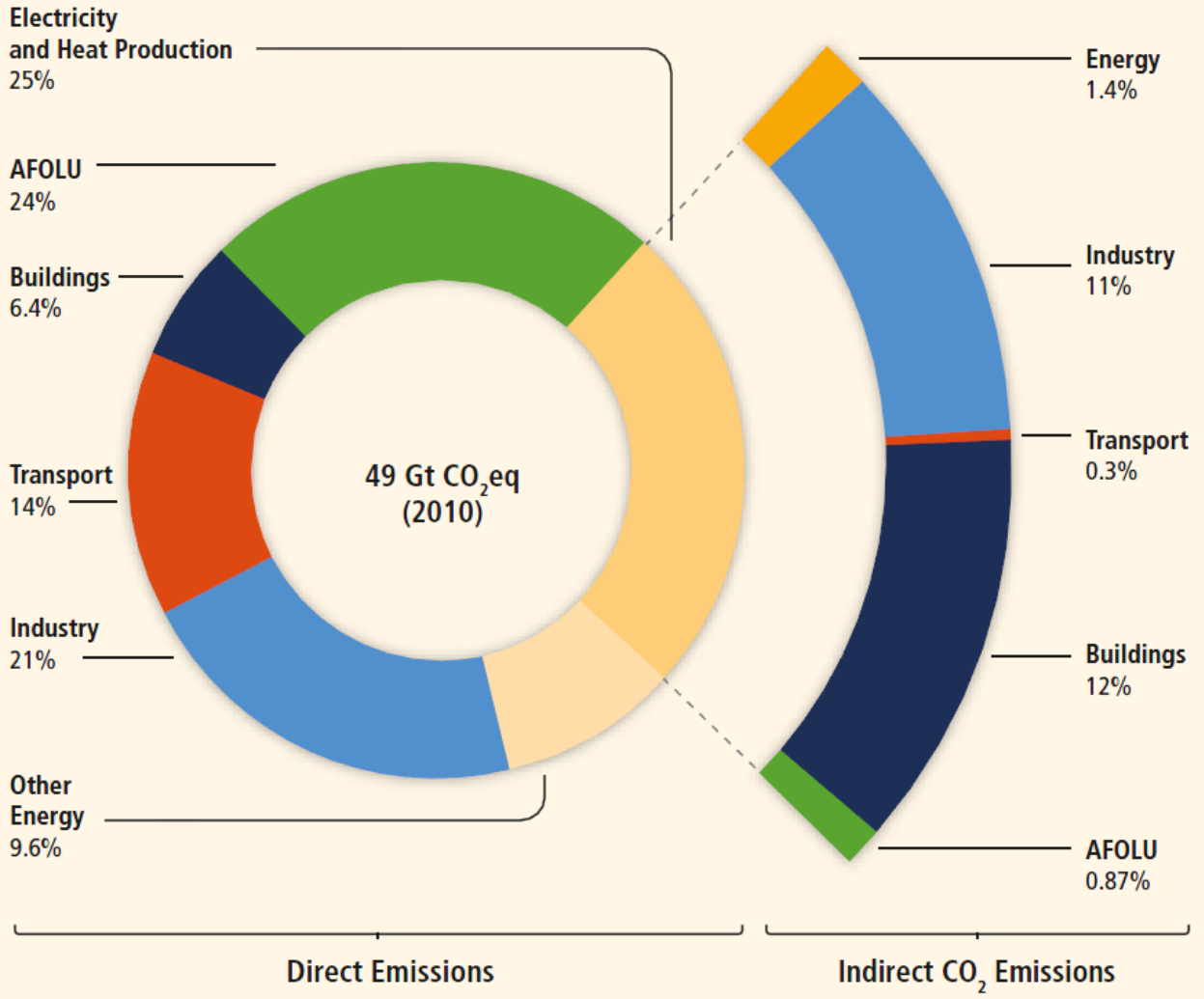

Figure 3: Direct and indirect percentage contribution to total anthropogenic greenhouse gas emissions in (Gt$\boldsymbol{CO_2}$eq/yr) made by different economic sectors in 2010. Sectors include: Agriculture, forestry and other land use (AFOLU), electricity and heat production, buildings sector, transport sector, industry sector and other energy. 'Other energy' refers to emission sources from the energy sector other than heat and electricity production. The figure was lifted form (Edenhofer et al., 2014).

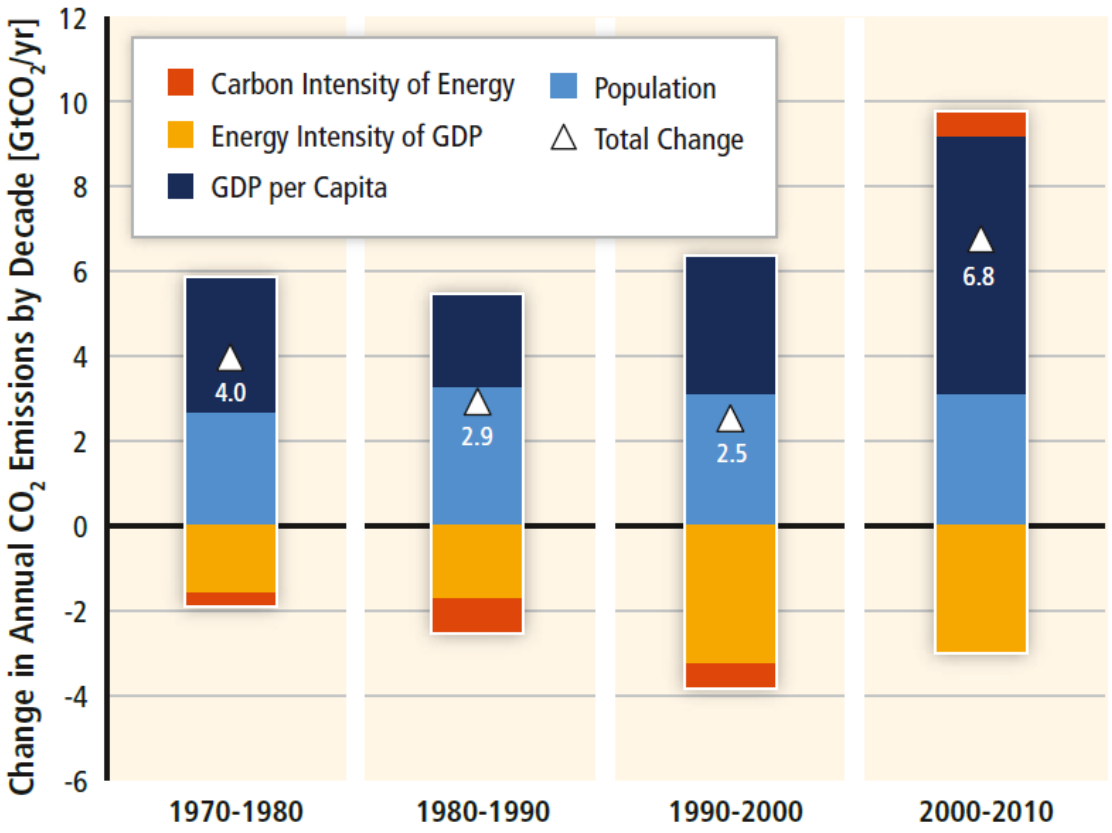

Figure 4: Contributions made over four decades to the change in annual greenhouse gas emissions made by: Population growth, GDP per capita, energy intensity and carbon intensity of the energy supply. Total emission changes are indicated by the white triangle. The graph was lifted from (Edenhofer et al., 2014).

This trend of gradual decarbonization has not been enough though to mitigate the exponential increase in greenhouse gas emissions in the upper atmosphere. There are several reasons for this. One of them is population growth, which globally went from around 3 billion in the middle of the 20th century to around 7 billion at the turn of the millennium. Its impact has been roughly linear though, with studies estimating that its contribution between the years 2000 and 2010 was roughly identical to those it made in the previous three decades. Another is economic growth. Its contribution has been much more pronounced with the current rapid economic growth in developing regions such Asia, South America and the African continent. These two factors have also outpaced improvements in energy utilization or energy intensity (Edenhofer et al., 2014). Energy intensity is the degree to which economic growth is dependent on energy output (see Figure 4).

Recent increase in carbon intensity of the energy supply has also played a role, this is because fossil fuel combustion of fuels with high carbon content is popular among developing nations as means of producing electricity for their ever growing populations. This is because these nations are under severe pressure to lift large fractions of their population out of poverty and fossil fuels (especially coal) represent the cheapest means of powering their economies. One of the reasons for this is that fossil fuel combustion is a mature and reliable means of producing power today. Another reason is that fossil fuel reserves are also very abundant in most regions. For example, it's estimated that oil reserves are up to 20,000EJ; about 120 times larger than current global production. Natural gas reserves are up to 120,000EJ; 1300 times larger than current production. While coal reserves are as high as 400,000EJ; 3500 time larger than production. At current rates of extraction these cheaper fossil fuel alternatives will only be depleted many decades from now.

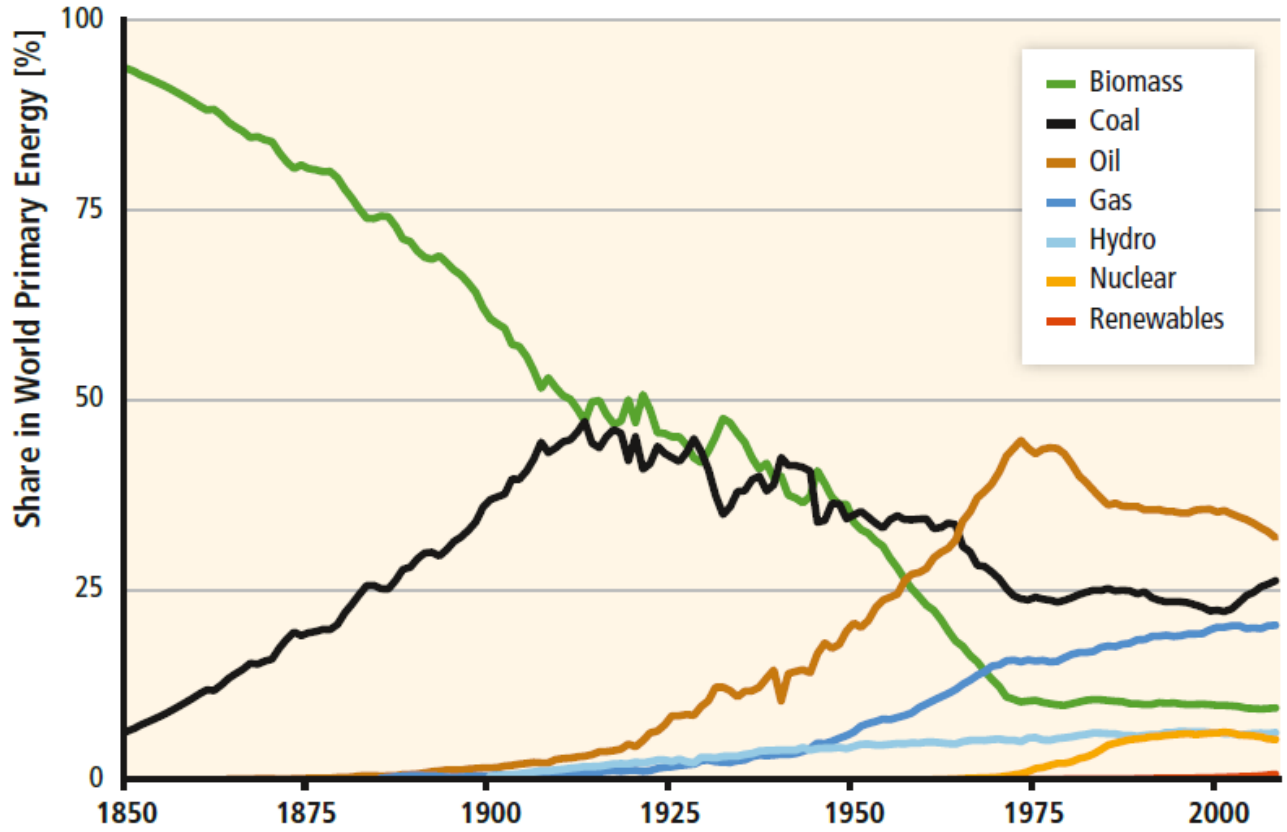

Figure 5: Share in in global primary energy supply between the years 1850 and 2000 for Biomass, Coal, Oil, Gas, Hydro, Nuclear and Renewables. Graph lifted off (Edenhofer et al., 2014)

2.1.3. Mitigation options and significance of CO_2

As mentioned in the previous section the majority of the growth in greenhouse gasses in the upper atmosphere from the years 2000 to the present day can be attributed to the energy sector. Of all the greenhouse gasses emitted in the energy sector CO_2 is the most prevalent. This is a long standing trend that has been observed since 1970 in which CO_2 emissions from fossil fuel combustion and industrial processes amount to 78% of all greenhouse gas emission growth from then until 2010 (see Figure 6 below). For reasons stated in the previous section this trend is set to continue, in fact in baseline scenarios were no mitigating action is taken (i.e. RCP8.5), CO_2 emissions from the energy supply sector are projected to double or even triple by the year 2050 compared to the levels they were in 2010, which were around 14.4(GtCO_2/year) (Edenhofer et al., 2014). It should come as no surprise then that in most optimistic mitigation scenarios (such as RCP2.6) decarbonization of the energy sector is considered pivotal in keeping greenhouse gas concentrations at acceptable levels in the upper atmosphere by 2100. Decarbonization is the name given to the observed decline in carbon intensity (CO_2 emissions) of the primary energy sector over time. Optimistic scenarios predict a required 90% reduction below 2010 levels in CO_2 emissions in the energy supply sector between the years 2040 and 2070 (Edenhofer et al., 2014). They also predict that the share of low carbon energy sources (such as renewable energy, nuclear and CCS) will need to increase from 30% to more than 80% by 2050. With a complete phase out of fossil fuel power generation without CCS required by 2100 (Edenhofer et al., 2014). Decarbonization is also projected to occur more rapidly in the energy sector; outpacing industry, buildings and the transport sectors. An explanation for these findings could be the energy sectors already mentioned large direct contribution to global emissions and its role as the primary energy source for all other sectors.

There are three main options available today for decarbonization of the world's energy sector. These options include: renewable energy sources, nuclear energy and carbon capture and sequestration (CCS) retrofit of fossil fuel power plants.

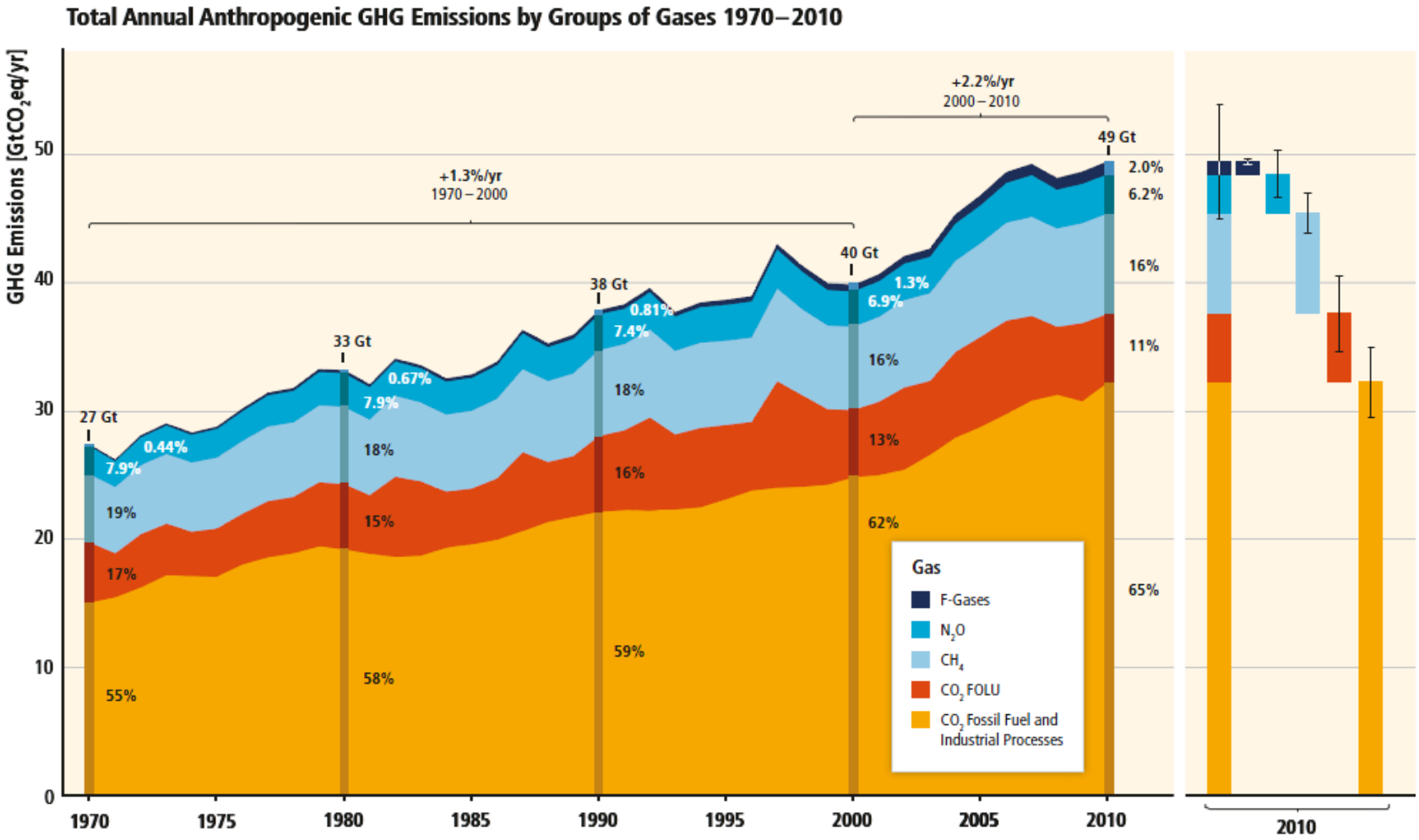

Figure 6: Growth in total anthropogenic greenhouse gas emissions (Gt$\boldsymbol{CO_2}$eq/yr) between the years 1970-2010. $\boldsymbol{CO_2}$ emissions from fossil fuel combustion and industrial processes are depicted in orange, $\boldsymbol{CO_2}$ emissions from forestry and other land use are depicted in red, $\boldsymbol{CH_4}$ emissions are depicted in light blue, $\boldsymbol{N_2O}$ emissions are depicted in sky blue and fluorinated gasses are depicted in dark blue. The Figure was lifted from (Edenhofer et al., 2014)

Renewable energy consists of all non-emitting sources that represent an idealized means of achieving the long term emissions targets set in optimistic climate models. What makes them ideal is that many of them are associated with zero emissions and are acquired from non-depleting sources. For instance, bioenergy produces liquid fuels from constantly renewable biomass. Hydroelectric power generates electricity from renewable water sources. Wind turbines produce electricity from renewable prevailing winds. Photo voltaic cells generate electricity by converting renewable solar radiation to electricity. Some of the advantages associated with renewable energy include: improved energy security, drastically reduced emissions, sustainable economic growth and improved access to electricity in remote regions where traditional grid extensions would be too costly (IEA (International energy agency), 2013). Renewable energy sources have improved substantially in performance, availability and cost over the years. Over half of new electricity generation added globally in 2012 was sourced from renewable energy technologies (Edenhofer et al., 2014). This growth though is reliant on massive subsidies doled out by governments concerned about long term energy security, human health and climate change. It's estimated that over $101 billion was paid in subsidies to renewables in 2012, an increase of 11% to those paid in 2011. Projections predict an increase to over $220 billion in subsidies by the year 2035 (IEA (International energy agency), 2013). Their current reliance on massive subsidies means their growth for the moment is occurring predominantly in more developed regions of the world. This makes them inaccessible to developing regions where currently the majority of global emissions growth is occurring and is projected to continue.

Nuclear energy is a mature technology that's already supplying cheap energy to many parts of the world. It could drastically reduce global greenhouse emissions if it were widely implemented. This is because it produces no CO_2 emissions. In the European Union for example it's estimated to have displaced around 300million tonnes of CO_2 that would have been emitted from fossil fuel power plants with similar output (European Comission, 2005). Its contribution though to global power generation has been on a steady decline since 1993 (Edenhofer et al., 2014). This can be attributed to a variety concerns centered on: waste disposal, safety, security and poor public opinion. Safety concerns stem from the many nuclear Power plant accidents over the years (such as the Chernobyl disaster (26 April 1986), and the Fukishima disaster (11 March 2011)). These accidents have the potential to render regions in which they occur uninhabitable for thousands of years. Nuclear proliferation is another safety concern that could threaten global

security. There are also major waste disposal concerns over the entire nuclear fuel chain, from mining to decommissioning and fuel storage (European Comission, 2005). Ongoing research into new fuel cycles, reactors, waste disposal and safety may make this technology a more attractive option in the future (Edenhofer et al., 2014).

Carbon capture and sequestration (CCS) involves capture of carbon dioxide from fossil fuel power plants, compression of the pure carbon dioxide stream followed by storage in geological formations. The methods employed to capture the CO_2 include downstream chemical absorption of the CO_2 from flue gasses using solvents, physical absorption of the CO_2 fraction of a gasification product that's undergone shift reaction and finally combustion of fossil fuel in a near pure oxygen atmosphere to produce a near pure CO_2 flue gas ready for compression and storage. A major advantage associated with these processes is the relative maturity of their subsystems, for example chemical absorption has been used as a means to capture CO_2 emissions from ammonia plants since the 1980's. High temperature fuel combustion in near pure oxygen atmospheres has been used by the glass and steel industries for some decades now (Herold et al., 2011). Another major advantage is that it extends the lifespan of fossil fuel power plants within the mitigation portfolio, providing a relatively affordable climate mitigation option for the developing world that serves as an energy bridged that can smooth the transition to renewable forms of non-emitting energy sources (European Comission, 2005). A challenge associated with these processes though is that they have yet to be fully implemented on a commercial scale. So many operational issues that can only be identified and solved through experience are unknown. Rules and regulations on CO_2 storage and monitoring in geological formations need to be established. There are also questions on the operational safety and long term integrity of CO_2 storage. The biggest challenge though is finding means of mitigating their associated efficiency penalties relative to their unabated counterparts. Solutions to these challenges are not that far off though. Large scale pilot plants are likely to be built in places such as the United States in the not too distant future. A lot of ongoing research is currently under way that attempts to find means of ensuring the integrity of CO_2 wells. Much research is under way on means of reducing CCS efficiency penalties through well-established methods such as heat integration, exergy analysis and mathematical optimization. Supercritical plants that will have efficiencies high enough to offset the efficiency penalties associated with CCS are already at the demonstration phase. Therefore CCS is likely to become competitive far sooner than renewables. This is also

supported by various climate mitigation models (Edenhofer et al., 2014). This makes CCS the best near term climate mitigation option for the global energy sector.

2.1.4. Significance of coal and CCS

Of the fossil fuels that have contributed to the slowing in the decarbonization of the global energy sector, coal is the most abundant. It accounts for over 55% of the world's total fossil fuel reserves. Coal reserves that are economically and technically exploitable at today's prices were determined to be around 1 040 billion tonnes at the end of 2011. These exploitable reserves grew by nearly 35 billion tonnes in 2011, with notable additions coming from countries such as: Australia, Indonesia and most importantly South Africa. Globally, coal reserves and resources are well distributed. Coals low cost and accessibility has resulted in it becoming the fossil fuel of choice in developing regions. This would explain why globally its use has increased substantially, satisfying nearly half of the increase in global energy demand over the decade ending in 2012. This growth in coal use in the developing world is predicted to continue into the near future although at a slightly slower rate than in decades passed. Despite the fact that coal use is decreasing in the developed world (driven by the desire to decarbonize through renewables) it's not enough to offset this continuing growth in the developing world. This explains why projections have indicated that coals contribution to global electricity generation by 2035 will be 33%. This would maintain its position as the leading fuel source for the energy sector (see Figure 7) (IEA (International energy agency), 2013).

Coal use has major drawbacks though. Its high carbon content (highest among all fossil fuels) means it releases a large amount of CO_2 per unit energy released. As a result coal fired power plants are largely to blame for the rising anthropogenic CO_2 emissions that have been recorded over the years.

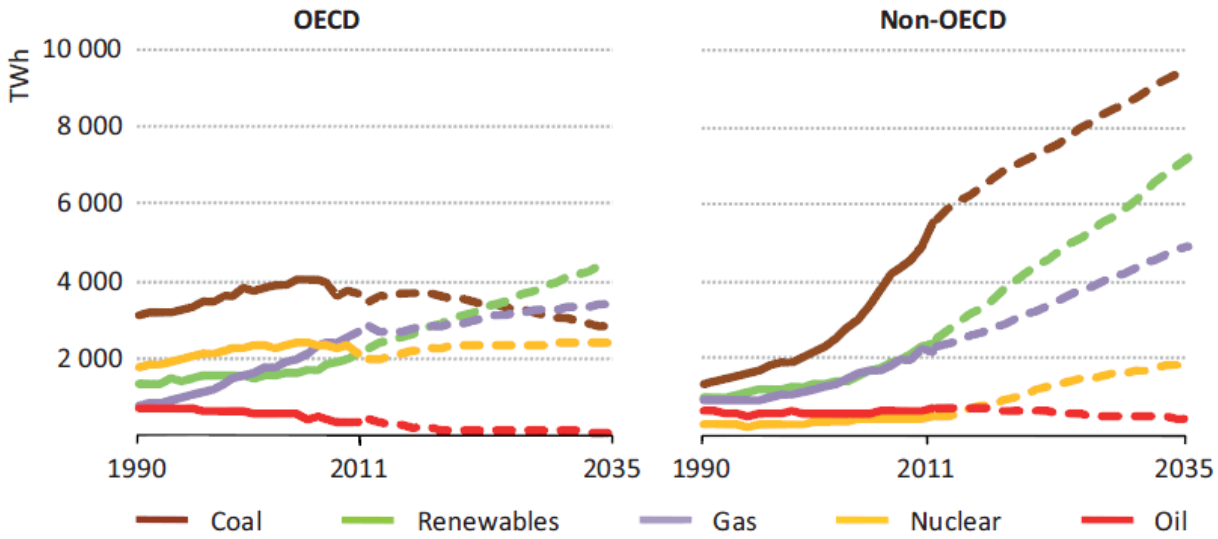

Figure 7: Projected electricity generation by Coal, Renewables, Gas, Nuclear and oil from 1990 to 2035. OECD stands for Organization for Economic Cooperation and Development, and includes mostly developed nations from America, Asia and Europe. This graph was lifted off (IEA (International energy agency), 2013).

Since CCS can be retrofitted to both new and existing plants, it can be implemented without the need to replace all of the preexisting coal fired power capacity. This, along with its relative maturity makes CCS an invaluable low cost option in a world that still requires cheap coal fired energy. In fact it's been determined that CCS could potentially reduce the overall cost of decarbonizing the energy sector by around $1 trillion between the years 2012 and 2035 (IEA (International energy agency), 2013). The optimistic mitigation scenarios (those that reach atmospheric greenhouse gas concentrations of around 430ppm-480ppm CO_2eq) ran by the IPCC predict that the cost of mitigation could increase by close to 300% in the absence of CCS (see Figure 8 left panel).The low cost of CCS also makes it a mitigation option that developing countries can implement fairly quickly. So it can also significantly reduce the costs associated with delayed mitigation. These additional costs are incurred because of things like lack of availability and reduced mitigation time frame. These could be significant as Figure 8 (right panel) shows: here, simulation results show that mitigation costs could increase by just over 100% if no action is taken by 2030.

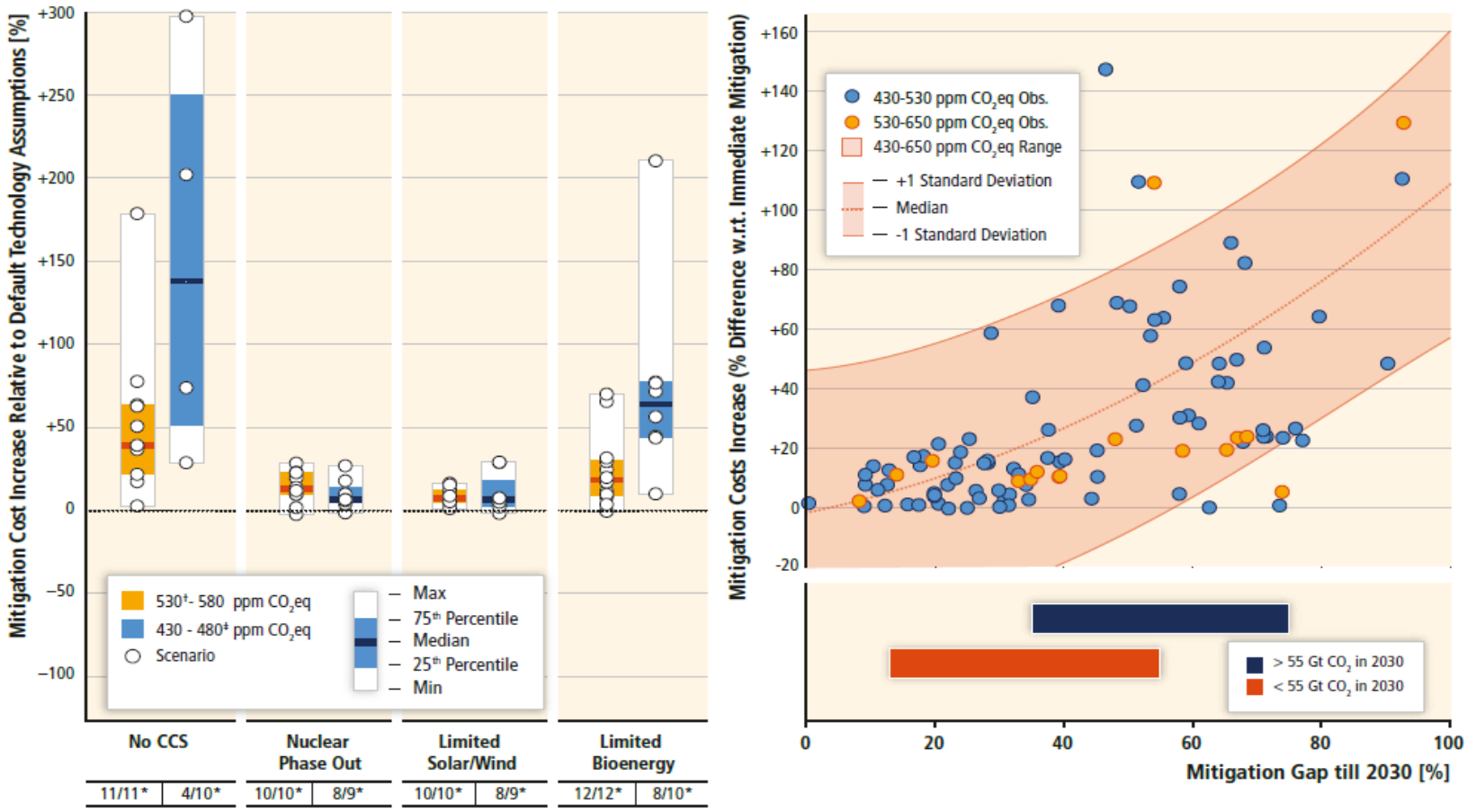

Figure 8: The left panel shows the predicted increase in net present value of mitigation costs between 2015 and 2100 (discounted at 5% per year) for four different scenarios: A scenario with no CCS, a scenario with no Nuclear energy, a scenario with no Solar or Wind energy and a scenario with limited Bioenergy. The right panel charts long term mitigation cost increases against mitigation gap. The mitigation gap defined as the difference in cumulative $\boldsymbol{CO_2}$ emission reductions between scenarios where mitigation happens immediately and those where its delayed till 2030. These graphs were lifted from (Edenhofer et al., 2014).

2.2. Coal fired power generation

In this section, well review some of the means by which one can generate power from coal. We'll be focusing on advanced cycle; next generation power plants which have efficiencies high enough for carbon capture retrofit. Doing this will give an overview of the industry, and the technology available.

2.2.1. Rankin cycle plants

2.2.1.1. Rankine cycle description

Figure 9 is a simplified diagram of a pulverised coal plant. In a conventional pulverised coal power plant, crushed or pulverised coal is combusted in a boiler which then transmits this heat to a working fluid (Which is water in this case) through a conducting surface. Once the water has turned to steam, it reports to a turbine (stream 1) which turns a generator and produces electricity. The steam exiting the turbine (stream 2) is then condensed before being pumped back to the boiler (stream 4) completing the cycle. These pulverised coal plants have been the predominant means through which power has been generated from coal since the 1920's (Beér, 2007).

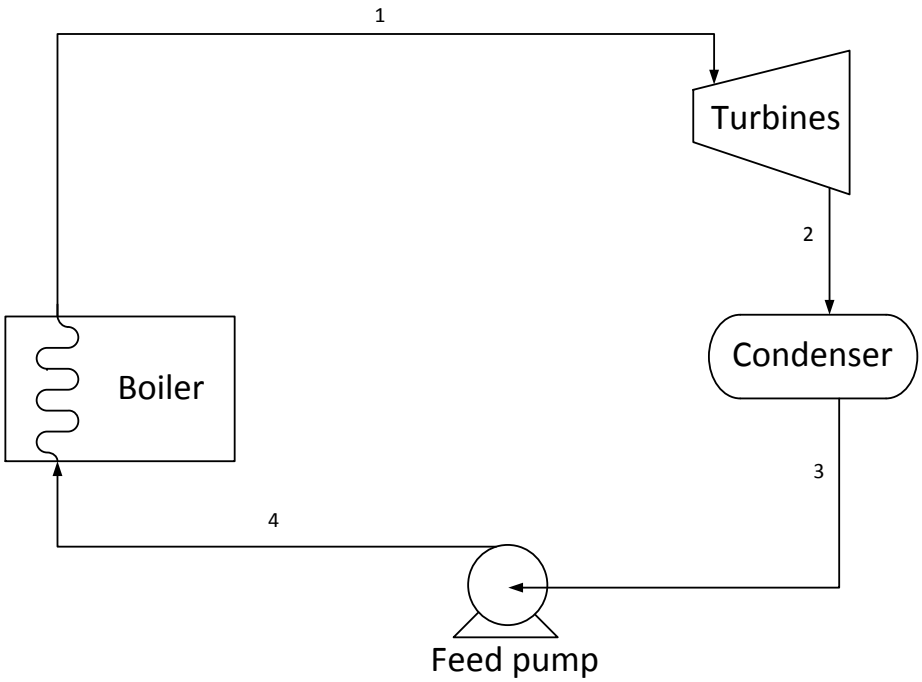

Figure 9: Simplified diagram of a pulverised coal power plant.

2.2.1.2. Rankine cycle efficiency

Figure 10 illustrates the means with which a supercritical pulverised coal plant can have its efficiency improved systematically, with the horizontal axis representing the action taken whilst the vertical axis represents the efficiency improvement this action will have. These actions can increase the efficiency of pulverised coal supercritical power plants by slightly over 45% (Beér, 2007).

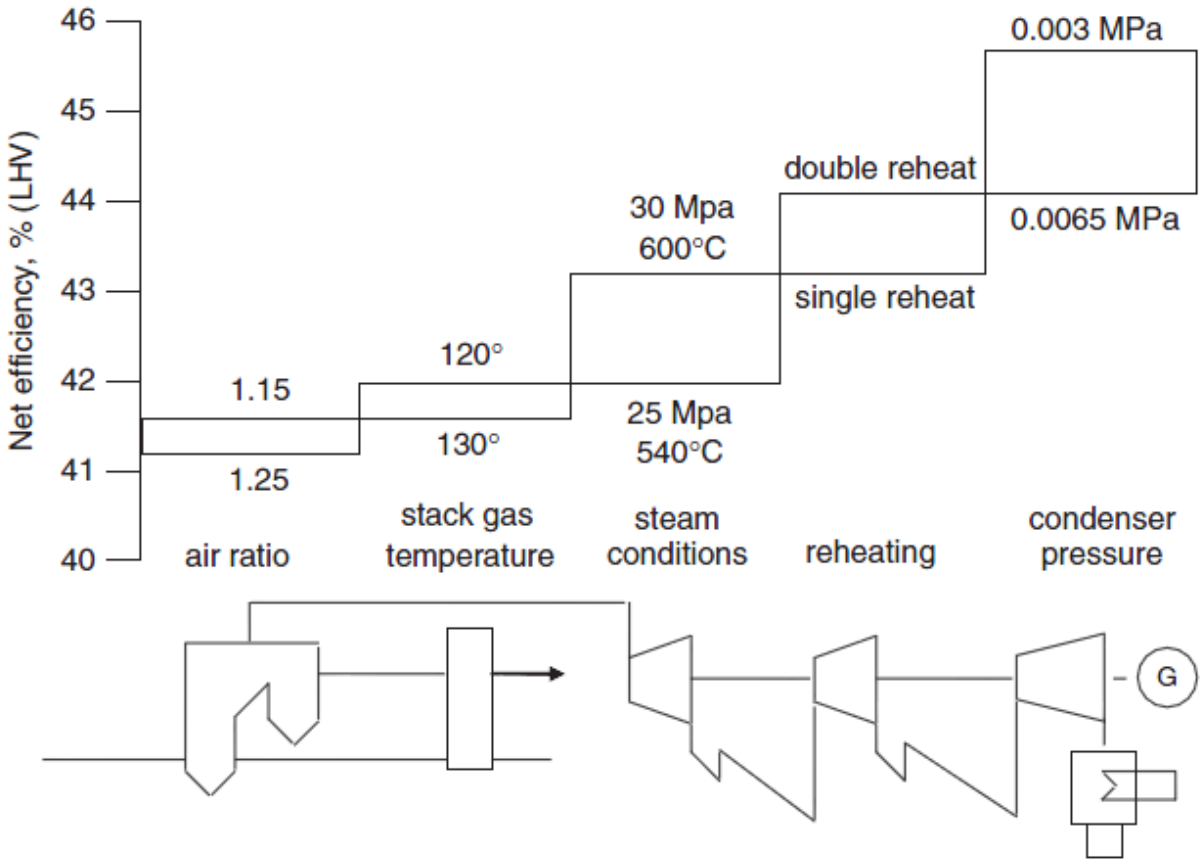

Figure 10: This figure, taken from (Beér, 2007), charts the improvements certain actions will have on the overall plant efficiency.

The air ratio by definition is the ratio between the mass of air stoichiometrically required for combustion and the mass of air actually fed. Inefficient combustion is the reason the air is fed in excess. While feeding in excess air dose increase the likelihood of complete combustion, it increases the flowrate of hot flue gasses leaving the stack. This of course increases heat losses through the stack. A number of actions can be taken to improve combustion efficiency without

increasing the air feed such as using finer coal or improving the burner design ((Beér, 2007); (Coal Industry Advisory Board, 2010)). Improved heat transfer between the working fluid and the flue gasses should bring closer their approach temperatures when they leave the vessel (much like in a heat exchanger). This might explain why lower stack gas temperatures are associated with improved efficiency. Increasing the number of times the steam goes through reheating raises the temperature of the heat addition and its exergy content (see section on exergy).

It's convenient to chart the progress of the working fluid in a Rankine power plant on temperature entropy diagrams such as Figure 11. In Figure 11 the left half of the blue line represents saturated vapour and the right half represents saturated liquid. The apex of the curve is the critical point, and in the area bound beneath the curve water is in equilibrium with vapour. To the left of the diagram the working fluid exists as liquid water and to the right its steam (Coal Industry Advisory Board, 2010). Figure 12 shows the path traced by the working fluid in a Rankine cycle on a temperature entropy diagram. The orange line represents the path taken by an ideal cycle and the green line represents the path taken by a real cycle (Zhu, 2015). Line segment (1-2) represents the path taken by the fluid as its pumps into the boiler. As the fluid is heated in the boiler it changes phase from liquid water at point 2 to steam at point 3. It then expands through the turbine from point 3 to point 4 before being condensed back to liquid water from point 4 back to point 1 (Hough, 2009). These diagrams give an indication of how far the process strays from ideality. As will be mentioned in the section on exergy a process is perfectly efficient or reversible when it goes through series of equilibrium processes between its initial and final sate. This is why in the ideal cycle line segment (4-1) (which represents condensation) and line segment (2-3) (which represents heat addition) are flat. When at equilibrium fluids will change phase at constant temperature when the pressure is held constant. So these segments are isobaric unlike those traced by the green line. Line segments (1-2) and (3-4) represent isentropic compression and expansion in the ideal cycle. Without the generation of entropy these segments are reversible and perpendicular unlike those on the actual cycle.

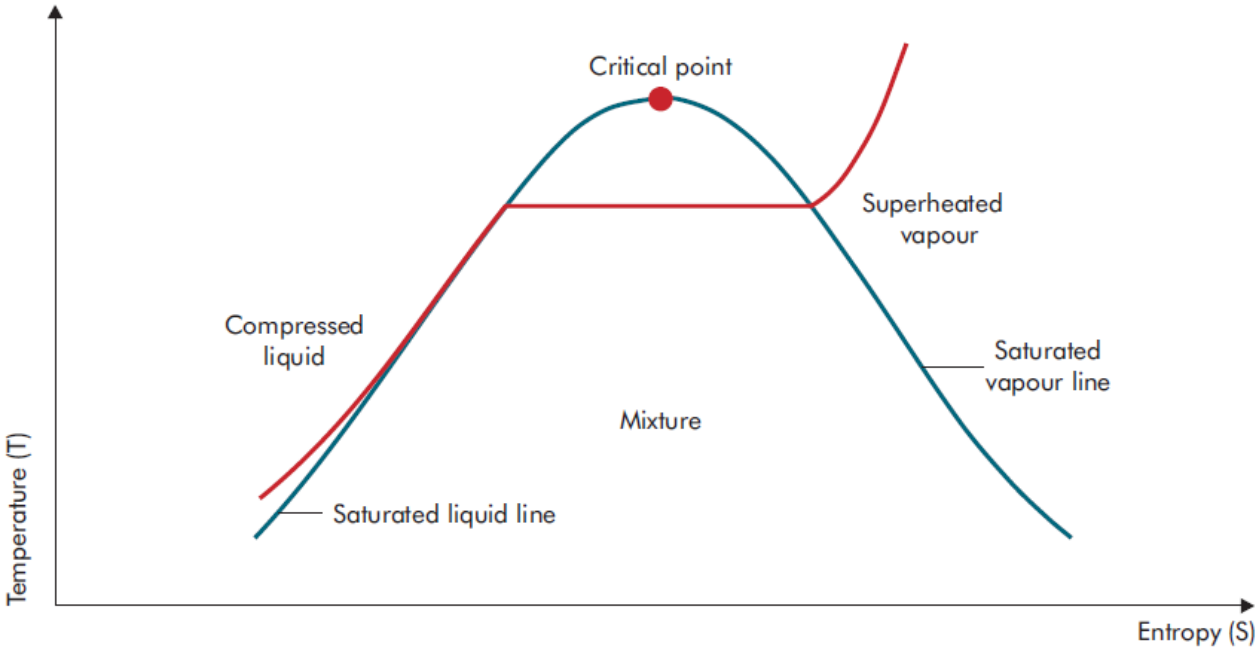

Figure 11: Temperature entropy diagram for steam and water. The graph was lifted from (Coal Industry Advisory Board, 2010).

Pulverised coal plants can also have their efficiencies improved by changing the condition of the working fluid from sub, to super or ultra-supercritical steam. This increases the operating parameters of the steam (temperature and pressure), increasing the energy content of the steam reporting to the turbine. Typical subcritical operating conditions are 163bar/538℃, those of supercritical plants are 245bar/565℃ whilst those of ultra-supercritical plants are 300bar/600℃ (Beér, 2007). The effect of this can be seen in Figure 12 by the rise in temperature of the working fluid from the horizontal line representing constant temperature heat addition to point 3. As the operating parameters of the steam increase to superheated conditions point 3 is shifted upward. Superheating the steam also ensures the working fluid remains dry as it expands through the turbine. This extends turbine life by reducing the associated damage caused by water impingement on the turbine blades (Hough, 2009). Advancements in materials of construction are what have enabled pulverised coal plants to operate at these advanced steam conditions that would otherwise damage units such as the boiler and turbine blades. For example current super alloys and coatings permit turbine inlet temperatures of up to 1290°F, and fourth generation super alloys with Ruthenium mono-crystal structures could potentially increase inlet temperatures to 2010°F in the future (Hough, 2009).

Another parameter that has a major impact on efficiency is the condenser pressure. As the condenser pressure drops point 4 in Figure 12 shifts downward. This improves efficiency by increasing the pressure drop between point 3 and 4, increasing the capacity for the steam to expand through the turbine (Hough, 2009).

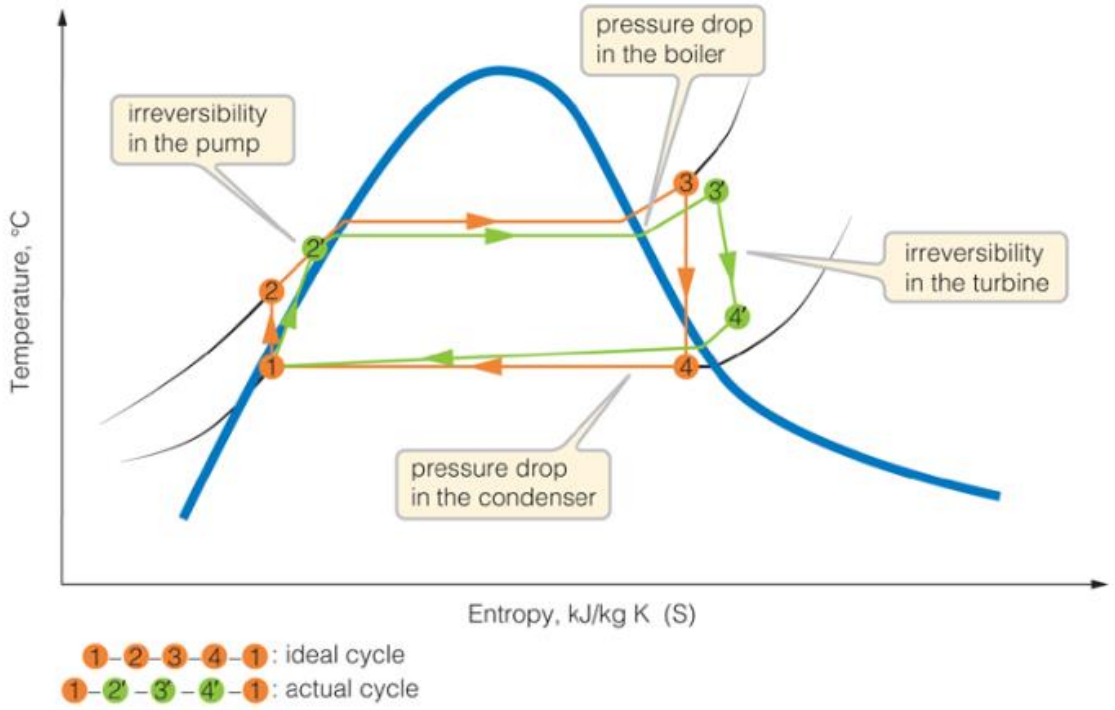

Figure 12: Temperature entropy diagram for an ideal and an actual Rankine cycle. This graph was lifted from (Zhu, 2015).

2.2.2. Circulating fluidised bed

2.2.2.1. Fluidised bed description

In this setup the coal is burned in a fluidised bed, which is a process unit that gives a bed of manufactured or crushed solid particles fluid like characteristics. The particle bed lies on a perforated floor near the base of the unit. The unit is open at either end, with a channel near the bottom to permit the injection of an oxidant (either air or oxygen) at high enough flow-rates to lift and scatter the particles up the length of the unit (In other words enough for the entire mixture to become turbid). This is what gives the bed of particles fluid like characteristics (Zhu, 2013).

2.2.2.2. Fluidised bed advantages

Removal of NOx and SOx is much simpler and cheaper with this unit. The bed has lower supercritical (SC) combustion temperatures (563℃ - 582℃) than those you'd typically find in a SC Pulverised coal facility which inhibits the formation of NOx. This is most likely due to the fact that the unit operates at temperatures lower than is required to overcome the activation energy penalty for the oxidation of nitrogen. This lower temperature also contributes to furnace flexibility, as it inhibits ash fouling along with corrosion of the heat transfer surfaces associated with certain fuels which are difficult to deal with. Removal of 90% to 95% of the SOx emissions can be achieved simply with the addition of limestone (Zhu, 2013).

Despite a lower combustion temperature these furnaces have comparable combustion efficiencies to those of Pulverised coal boilers. This can be attributed to the turbidity within the unit which improves heat transfer by reducing the temperature profiles which reduce the work potential of the heat evolved (see section on exergy). Reductions in temperature profiles will also improve heat transfer by maintain temperature driving forces between the flue gas and the working fluid throughout the length of the furnace. The increased reaction surface area (result of crushing coal to finer particles) and turbidity also insure more of the fuel is burned which makes further use of the chemical energy contained within the fuel (Zhu, 2013).

The improved combustion efficiency also makes the boiler more flexible and able to deal with a wider variety of fuels. From those with low calorific content i.e.(Waste coals and biomass) to those with higher calorific content such as Anthracite (Zhu, 2013).

2.2.2.3. Fluidised bed disadvantages

One of the major problems with these units is scale, most of the units are small (≥300MWe) compared to pulverised coal units (>1000MWe) (Zhu, 2013) so when scaling up one has to consider the added cost associated with acquiring parts made rare or unique because their unusually large or bespoke. They also operate at predominantly subcritical conditions because of the lower combustion temperatures, this makes adaptation to super-critical and especially ultra-supercritical operation difficult (Burnard & Bhattacharya, 2011).

2.2.3. Air heater, gas turbine combined cycles (AH-GTCC)

2.2.3.1. AH-GTCC description

In this setup, air is first heated by passing it through an active circulating fluidised bed. The furnace uses heat from coal combustion to heat and pressurise the air before feeding it to a gas turbine which produces power for a toping Brayton cycle. The gas turbine generates power before the outgoing hot air is fed into the furnace to act as oxidant for the combustion of the fuel coal which provides combustion heat for a Rankine cycle (Beér, 2007).

2.2.3.2. Advantages and disadvantages of (AH-GTCC)

Having a fluidised bed, the cycle will inherit all advantages associated with this process unit: Ability to deal with a wide variety of fuel qualities, simple and cost effective removal of SOx and NOx, effective furnace heat transfer along with efficient combustion (Zhu, 2013). The gas turbine operates on the Brayton cycle, whilst the steam turbine operates on the Ranking cycle. Combining the two allows for inclusion of gas turbine power production which is much more efficient than using a steam turbine alone resulting in less of the fuels exergy content being destroyed (see section on exergy). The initial conditions are also improved i.e.(Gas turbine inlet pressure and temperature), as a result the two cycles effectively enhance each other resulting in a combined efficiency of around 40.4% (LHV) (Beér, 2007), which is much higher than either cycle could achieve alone (Kumar Mohanty et al., 2014). Being air fed, the turbine feed need not go through gas cleaning more common with other gas turbine setups (Beér, 2007). This setup could provide means of improving the efficiency of a conventional coal fired power plant and make it more CCS ready. The cycle inherits all the disadvantages associated with fluidised beds mentioned above: which are lower combustion temperatures that inhibit supercritical and ultra-supercritical operation along with their smaller scale. The addition of a fluidised bed and a gas turbine will also increase cost and complexity.

2.2.4. Internal gasification, combined cycle (IGCC)

2.2.4.1. IGCC description

In this setup coal is first gasified in a pressurised fluidise bed gasifier producing syngas and char (in the case of incomplete gasification). The syngas produces power by reporting to a combustion turbine whilst the char is sent to a pressurised fluidised bed combustor (PFBC)

which generates power by transmitting the resultant heat to a steam cycle. To increase efficiency and reduce wastage even further the high pressure, oxygen laced flu gas product fraction from the fluidised bed boiler (After going through gas cleaning for removal of particulates and alkali at 870℃) also reports to the combustion turbine along with the syngas. See Figure 13 below for a basic schematic of the process (Beér, 2007).

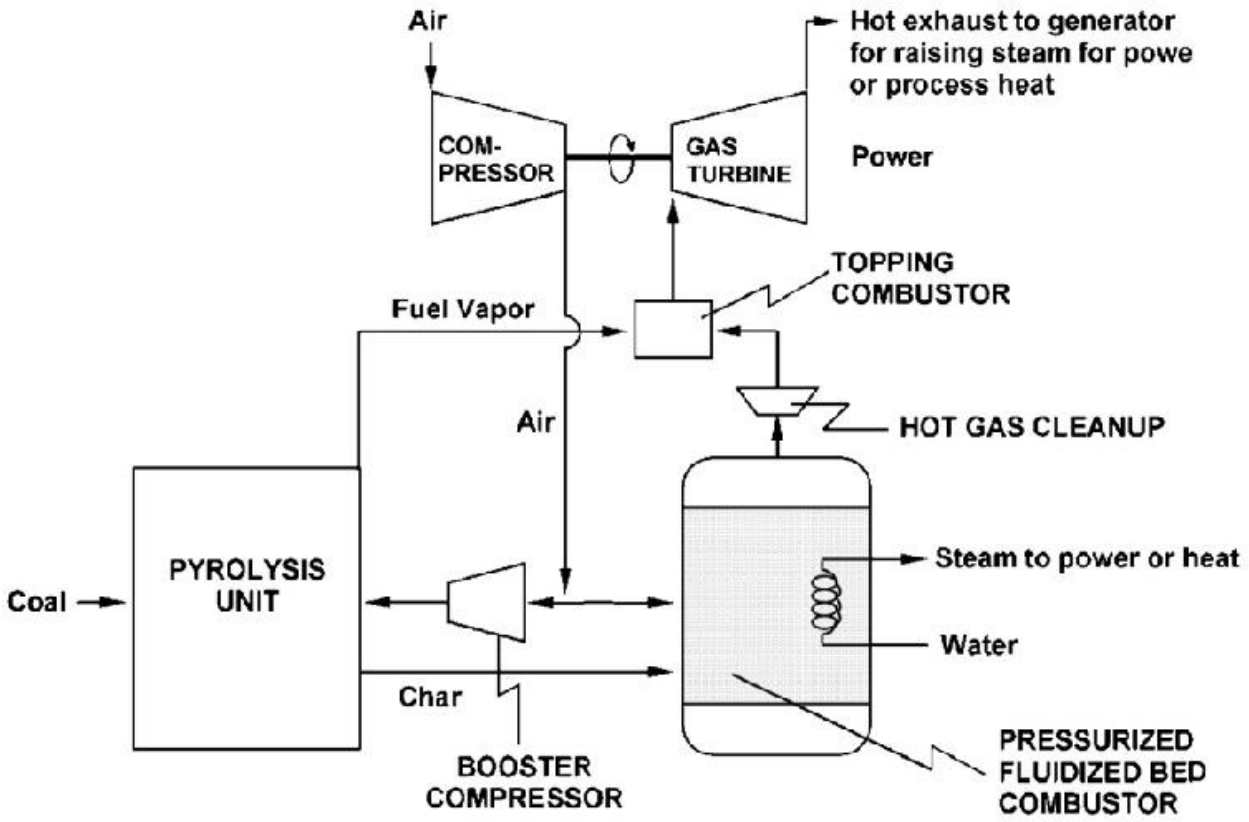

Figure 13: This Figure, lifted from (Beér, 2007), is a simplified diagram of an IGCC plant.

2.2.4.2. IGCC Advantages

Coal gasification followed by gas turbine combustion is currently the optimal manner in which to generate power from coal, overcoming many of the limitations associated with the Rankin cycle. It represents the best means of reducing global greenhouse gas emissions to 20% of those emitted in 1990 for newly built coal fired plants (Hanak et al., 2014), with some stating the

technology can potentially reach 60% efficiency and beyond. Currently the net efficiency of existing IGCC plants is around 42% (Beér, 2007). The subsections to follow explain characteristics that make this possible.

2.2.4.2.1. IGCC Furnace superiority

Having a circulating fluidised bed furnace results in the setup inheriting all the benefits associated with this combustion unit within the Rankine or steam cycle: ability to handle fuels of varying quality, convenient and inexpensive treatment of SOx and NOx, efficient Char combustion and efficient furnace heat transfer (Beér, 2007).

2.2.4.2.2. IGCC combustion turbine superiority

In IGCC it pays to have syngas with a large chemical energy to sensible heat ratio. This insures that the energy contained in the syngas stream is better conserved on route to the combustion turbine, with less of the available energy/heat radiating to the environment or reporting to the steam cycle which is a lot less efficient because of the difficulty that comes with transmitting heat (see section on exergy). This is because combustion turbines are essentially grounded jet engines that inject the gaseous fuel down the length of the turbine Producing heat, and a pressure differential down the length upon ignition. Unlike boiler steam turbine configurations the heat from combustion is transmitted to the working fluid (which in this case is a mixture of syngas and air) directly, overcoming the transmission restriction associated with boilers when they heat the working fluid (which in that case is water) through a conducing surface (transmission which we know is restricted by the temperature disparity between the hot reservoir and the ambient environment (Kotas,1985)). The nature of the working fluid also contributes: being a gas, there is no need to overcome the sensible heat barrier and destroy work before reaching saturation and producing the vapour that ultimately turns the rotor. So a greater fraction of the heat evolved increases the working fluid temperature and pressure; improving efficiency and increasing thrust. The fluid can also be compressed using power from the cycle with little chance of condensation, this is advantageous as electricity can be converted to work with very little irreversibility (Kotas,1985).

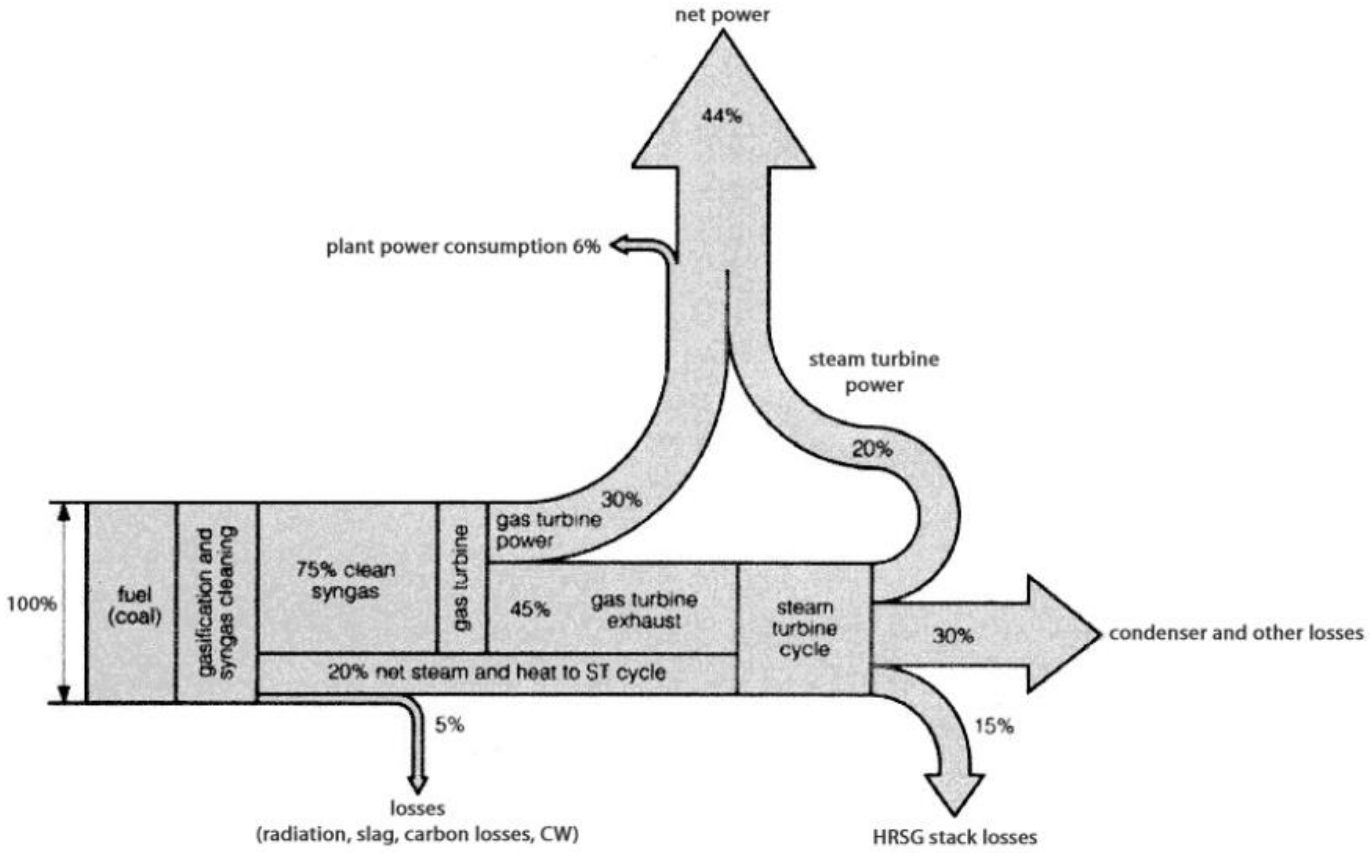

Figure 14: This Figure is an idealised energy flow diagram for IGCC. The Figure was lifted from (Beér, 2007).

The idealised energy flow diagram above (Figure 14) is pictorial confirmation of the superior efficiency associated with combustion turbine power generation. Looking at the diagram, 75% of the total fuel energy input which is labelled 75% clean syngas reports to the combustion turbine as syngas, and only 60% of that; 45% of the total fuel input which is labelled 45% gas turbine exhaust is wasted by the turbine. Whereas of the total fuel energy reporting to the steam cycle; represented by the sum of the streams labelled 20% net steam and heat to ST cycle and 45% gas turbine exhaust, 69.23% is wasted by the steam cycle. These losses being represented on the diagram by the sum of the outgoing streams labelled condenser and other heat losses and HRSG stack losses which are 30% and 15% of the total fuel energy input respectively (Beér, 2007).

2.2.4.2.3. IGCC and CCS

Once carbon capture and sequestration becomes obligatory, IGCC will become very attractive option for newly built plants because of the ease with which carbon dioxide can be captured from the setup. This is because carbon dioxide is expelled from the system at high pressures, making capture and compression a lot less energy intensive (Beér, 2007).

2.2.4.2.4. IGCC Disadvantages

Historically IGCC suffered from high capital costs brought on by lack of availability that naturally colligates with all pioneering technology. The lack of reference plants also meant operating risks, maintenance costs and any other unforeseen issues that could only be resolved through experience were unknown (Beér, 2007). In response to this, various supplier groupings (Very likely incentivised by governments) came together and produced generic IGCC plant designs on a turnkey basis with guarantees on cost, construction time, availability and efficiency. But despite all this, and the expansive research that has gone into characterizing, developing and optimizing it, the negative perception still persists, with the technology very likely spurned as a result of voluntary and involuntary organizational inertia (Burnard & Bhattacharya, 2011).

2.3. Carbon capture and sequestration (CCS)

2.3.1. Pre-combustion capture

As mentioned earlier, pre-combustion capture is a CCS strategy where carbon dioxide is removed upstream. It is only suitable for integrated gasification combined cycle (IGCC) setups. How it works is that the coal feed undergoes gasification in the presence of steam and oxygen to produce synthesis gas (a mixture of carbon monoxide and hydrogen) and char (in the case of incomplete gasification) (Beér, 2007). The carbon monoxide undergoes water gas shift reaction to convert it to carbon dioxide before it's separated out from the fuel hydrogen physically through pressure swing absorption. The hydrogen is then used to produce electricity by reporting to a combustion turbine (Herold et al., 2011). The char (in the case of incomplete gasification) is sent to a pressurised fluidised bed combustor (PFBC) which generates power by transmitting the combustion heat to a steam cycle (Beér, 2007).

The syngas product from a gasification processes is produced at relatively high pressures. It also has a relatively high CO_2 concentration (as compared to post combustion capture for example where the flue gas contains large amounts of NOx) (Folger, 2010). This makes separation of the CO_2 using physical adsorbents possible which is less expensive and less energy intensive. Other advantages associated with this strategy are: i) better plant load flexibility as carbon capture happens upstream (decoupled from the electricity production) (Herold et al., 2011), ii) it can be implemented in IGCC setups, which as mentioned before are the most efficient means today of producing power from coal (Beér, 2007). A disadvantage however of this setup is its associated complexity and high capital cost (Herold et al., 2011). Implementing it on a conventional pulverised coal plant would require replacement and purchase of major plant units. As a result, it's not a viable CCS retrofit for pre-existing plants.

2.3.2. Post combustion capture

Post combustion capture involves removal of carbon dioxide downstream from the combustion process. The carbon dioxide is captured through chemical reaction using an organic solvent. The most common solvent used is monoethanolamine (MEA), an amine compound. How the process works is that the flue gas first reports to an absorber, where it is scrubbed with the amine solution. The rich solvent then reports to a regenerator. The regenerator uses heat (supplied by steam from the steam cycle) to release the CO_2 and regenerate the solvent. The regenerator heats

the solvent to around 100-120℃ (Herold et al., 2011). The solvent is then cooled to around 40-60℃ before being recycled back to the absorber (Herold et al., 2011), and the CO_2 stream is separated out and compressed for storage (Folger, 2010). The regeneration of solvent in the stripper following the absorber using steam from the steam cycle is the most energy intensive step within the capture process.

Some of the advantages associated with post combustion include: that it's the most widely used and mature strategy of the three and that it can be readily retrofitted to existing setups without the need for modification of existing major plant units (Herold et al., 2011). A disadvantage of the processes is the high thermal efficiency penalty associated with it. This could be attributed to the fact that the technology was initially developed to clean very pure carbon dioxide streams (ammonia industry, fertilizer industry, separation of CO2 from natural gas). Another disadvantage is that the solvent degrades over time from the accumulation of pollutants that the regenerator fails to remove (Kanniche et al., 2010). Other disadvantages include use of toxic chemicals and reduced power plant flexibility to load changes (Herold et al., 2011). The process is also associated with a higher percentage increase in cost of electricity (65%) upon retrofit than oxy-combustion (48%). These Figures take into consideration the cost of construction, fuel, as well as operations and management at an assumed 11% discount rate (Kanniche et al., 2010).

2.3.3. Oxy-combustion capture

Oxy combustion is a process whereby a boiler is fed a stream of pure oxygen instead of air. The oxygen stream is derived from a cryogenic air separation unit upstream. As mentioned this results in a near pure carbon dioxide stream at the tail end containing a small amount of water vapour which can easily be condensed out. The cryogenic air separation processes is the most energy demanding unit within the retrofit, consuming up to 15% of the plants electricity production (Herold et al., 2011). The oxygen is fed to the furnace along with a stream of recycled flue gas (which is composed mostly of CO_2). This is done to control the flame temperature and improve heat transfer within the furnace (Mousavian & Mansouri, 2011). A significant disadvantage is its lack of maturity and availability, with very few pilot plants having being built to demonstrate its feasibility on a large scale (Herold et al., 2011). Despite this, oxy combustion has proven itself to be a viable alternative to the more popular post combustion strategy because of its smaller thermal efficiency penalty upon retrofit. The primary reason for this is that it

increases the partial pressure of CO_2 in the flue gasses to a great degree (Kanniche et al., 2010). It can also be retrofitted to existing coal fired power plants with little modification to the main power plant units (Mousavian & Mansouri, 2011). This makes oxy-combustion a good candidate for a viable CCS retrofit to existing coal fired power plants if a means of significantly reducing its thermal efficiency penalty can be found. Another advantage it has over the more popular chemical based post combustion alternative is that it avoids the problem of waste disposal and emission of toxic compounds. Also, when optimized the oxy-combustion boiler flue gas volume is considerably lower than that of an air fired case. This can reduce the size and cost of required boiler equipment (Lockwood, 2014).

2.4. Brief history of Oxy-combustion

Oxy combustion was first developed in the 1980's as a means of producing pure CO_2 streams for enhanced oil recovery. It's only in the 1990's that it gained interest as a possible CCS alternative to post combustion capture after early pilot scale studies (Chen et al., 2012). The first full scale oxy-combustion pilot plant was Vattenfall's 30MW facility built in Germany. Pilot plants which followed include the 30MW oxy-fuel circulating fluidized bed plant in Spain, and a 100MW plant retrofitted for ox-combustion in Australia, which also happens to be the first to generate electricity for the grid. Many other plants have been proposed and even had feed studies completed but very few have been built. This is down to lack of lack of political will and financial support. The only large scale plants still running toady are the 168 MW FutureGen 2.0 plant in the USA, the 426 MW White Rose project in the UK and the retrofitted 200MW plant in Shenmu, China (Lockwood, 2014).

2.5. Oxy-combustion characteristics

2.5.1. Air separation unit

Of all the air separation technologies available today cryogenic distillation is the most cost effective option for producing large amounts of relatively high purity oxygen. It's also a very mature technology, with several large gas companies such as Air Liquide, Linde and Air Products offering their own commercial scale versions of it (Soundararajan, 2015). This is the reason it's the technique of choice for oxy-combustion power plants. Cryogenic distillation separates out the main components of air (N_2, O_2, Ar) by taking advantage of their different volatilities. In order to do this the air needs to be compressed and cooled close to its saturation point (4-6 bar and below 170℃). It's likely that this is done to reduce reboiler duty. As mentioned before, the cryogenic air separation unit is very energy intensive, consuming around 15% of the of a plants electricity production. The specific energy consumption value is around 0.24(kWh/kgO_2) (Chen et al., 2012). This value can increase significantly for oxygen mole fractions higher than 97%. It's for this reason that an oxygen mole fraction of around 95% was determined to be optimal (Soundararajan, 2015). The air compressor is chiefly responsible for this large energy consumption. A possible means of mitigating this is through process integration: Specifically, to use the compression heat to pre heat boiler feed water. This reduces the amount of steam extraction for boiler feed water preheating in the steam cycle and increases the plants gross power output (Fu and Gundersen, 2013).

2.5.1.1. Compression cleaning and cooling

The moment the air is fed into the unit it's compressed to around 4-6bar in a multistage compressor with water intercooling (Lockwood, 2014). This is done to approximate isothermal compression which minimizes compression work (Kotas,1985). This is vital as this unit is mostly responsible for the high specific power consumption of the ASU. The compressed air is then cooled to around 12℃ in a direct contact tower using chilled water which is cooled by the cryogenic Nitrogen product form the distillation unit. This cooling is essential as it brings the air closer to saturation and makes it easier to separate out less volatile impurities in the adsorption step that follows. CO_2 and water are the less volatile impurities separated out using Temperature swing adsorption (TSA) in the next step. TSA processes separates out the CO_2 and water in two columns packed with molecular sieves that adsorb the impurities at low temperatures and release

them when heated. The use of two columns enables continuous operation by having one column adsorb the impurities at lower temperature whilst the second column regenerates its saturated sieves by releasing the adsorbed impurities upon heating. Once one column is saturated the air flow is then switched to the next column whose sieves at that point would have been regenerated. The heating is done by the Nitrogen product from the distillation unit which is heated by low pressure steam form the steam cycle. Prior to being fed to the distillation unit the air is further cooled to around 172℃ in in the main heat exchanger against the cryogenic Oxygen and Nitrogen products from the distillation unit (Lockwood, 2014).

2.5.1.2. Distillation

The distillation unit in this work is comprised of a high pressure rectification column and a low pressure stripping column with heat integration between the condenser and the reboiler. Between them is a heat exchanger that that cools the bottom product from the high pressure column against the cool nitrogen distillate from the low pressure column (see Figure 15 below) (Fu and Gundersen, 2012). After being cooled to near due point in the main heat exchanger the compressed air reports to the bottom of the low pressure column. The most likely reason for it being at only near due point is to eliminate the need for a reboiler. This column then separates the air feed into a near pure Nitrogen distillate and crude bottoms oxygen product with composition: O_2-39.3%, Ar-1.5%, N_2-59.2% (stream A2-1 in Figure 15) (Fu and Gundersen, 2012b). An early challenge in cryogenic distillation was to find a means of condensing the cryogenic vapour distillate to provide sufficient reflux. This was accomplished by recovering the high quality cold energy in the liquid oxygen product (Lockwood, 2014). In the distillation unit used in this study this is achieved through heat integration between the low pressure rectification column and high pressure stripper. The nitrogen distillate is then used a reflux in both columns. The nitrogen is only partially condensed though, and the remaining vapour fraction reports to a gas turbine which recovers power and aids in reducing the energy penalty associated with air separation. The temperature difference between the condenser and reboiler is maintained at 1.5K and can be adjusted by changing the operating pressure of the high pressure column. The saturation temperature of the Nitrogen distillate at the top of the high pressure column is dependent on the outlet pressure from the main air compressor. This outlet pressure is adjusted so that the liquid nitrogen distillate from the top of the high pressure column can be condensed by the boiling oxygen at the bottom of the low pressure column (Fu and Gundersen, 2012b). One

likely reason for this is to ensure none of the stages dry up in the low pressure column. Another would be to ensure the bottom stage within the unit reaches equilibrium. Before the nitrogen distillate from the high pressure column is fed to the low pressure column it reports to the central heat exchanger along with the crude oxygen product from the high pressure column. Here their both cooled against the nitrogen distillate from the low pressure column. The reason for this is to avoid vaporization after their depressurized in valves on their way into the high pressure column (Lockwood, 2014).

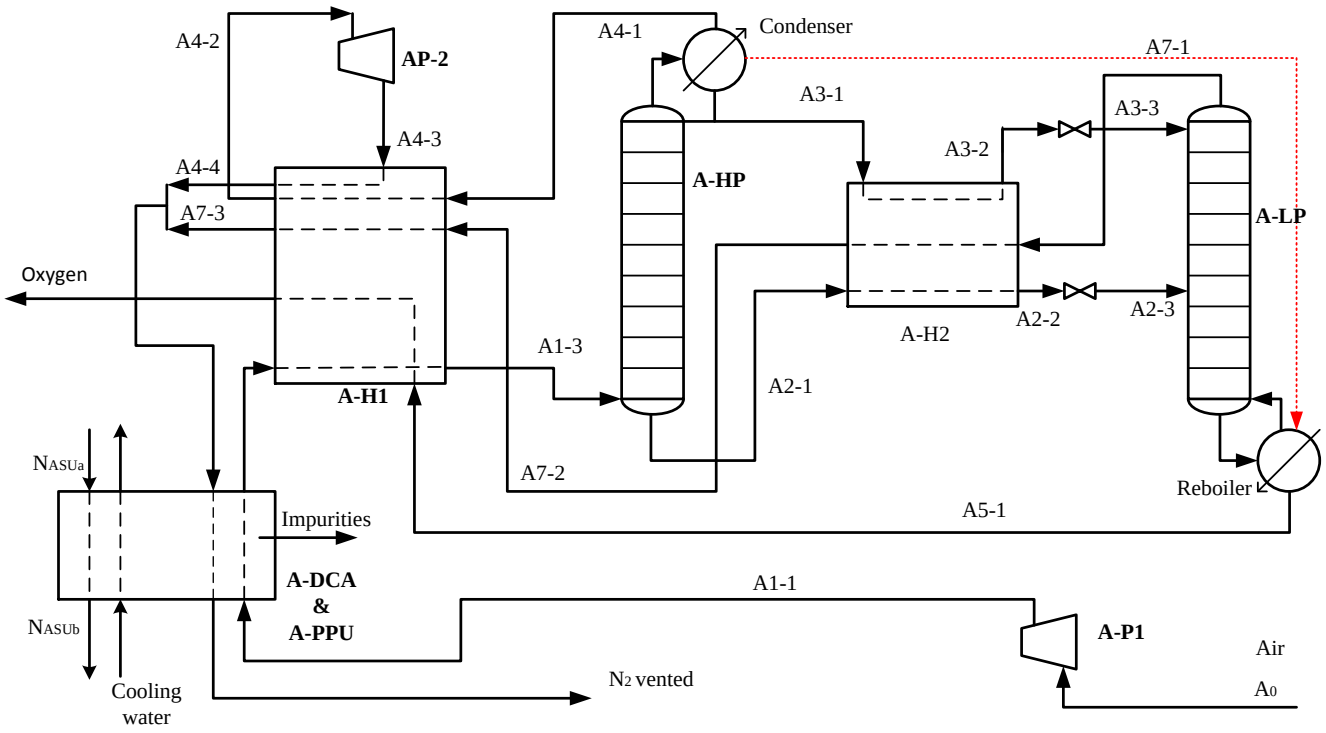

Figure 15: Diagram of the double column distillation processes used in this work. The diagram was adapted from a similar diagram in Fu and Gundersen (2013).

2.5.2. CO_2 compression and purification unit

The carbon dioxide compression and purification unit consists of a dewatering step, compression and cryogenic separation. The unit can be retrofitted without the need to remove selective catalytic reduction step (SCR), the electrostatic precipitator (ESP) or the flue gas desulfurization unit (Chen et al., 2012). The need for NOx removal is limited. The nitrogen free oxygen feed means the only nitrogen sources are the fuel nitrogen, and nitrogen associated with air ingress. Another reasons for this is that there is an associated reduction of around twenty five percent in

oxidation of fuel nitrogen (Buhre et al., 2005). This can be attributed to low NOx burners and staged combustion. There is also a rapid reduction of nitrogen due to the re-burning effect, which is a process were recycled NOx is converted to HCN and NH_3in the flame. Particulates are removed using an electrostatic precipitator before the recycle. This is done to avoid them building up in the recycle loop (Soundararajan, 2015). There's a dehydration step before compression, which serves to purify the flue gas, remove condensable gasses and lower the compression work by reducing the flue gas volume. The reduction in compression work can be significant as the flue gas after desulphurization contains around 15% water by volume (Fu and Gundersen, 2013). Sulphur dioxide is removed via wet flue gas desulfurization (FGD). The FGD unit is fed pure oxygen from the air separation unit to minimize flue gas contamination. It's important to have flue gas desulphurization before cryogenic separation of inert gasses. This is because sulphur dioxide has properties very similar to that of CO_2, which would make the final separation step very energy intensive (Toftegaard et al., 2010). The final cryogenic separation step can either be a flash or a distillation process. Flashing is less energy intensive whilst distillation can produce very pure product (Soundararajan, 2015). The final CO_2 product must be delivered to meet pipeline and reservoir specifications. It also needs to be at a high enough pressure to overcome frictional and static pressure drops and avoid flashing the gas along the way. The carbon dioxide is delivered at pressure between 80-200bar and temperatures between 0-50℃. It's preferred though to deliver it at between 100-110bar and temperatures above the critical value (31.1℃) (Toftegaard et al., 2010).

2.5.3. Boiler Island

An important consideration in oxy-combustion retrofits is ensuring that combustion and heat transfer characteristics in the oxy-combustion boiler match those of a conventional air fed boiler. This is because feeding pure oxygen with a recycled flue gas composed primarily of CO_2 changes the boiler gas combustion characteristics. The two altered combustion gas properties that have greatest impact on combustion and heat transfer are the gas radiative properties, and the gas heat capacity (Toftegaard et al., 2010). Another process characteristic that can impact on the boiler island is the flue gas recycle location.

2.5.3.1. Flue gas recycle location

In oxy-combustion plants the flue gas recycle is necessary as it feeds in CO_2 as diluent to the boiler. This CO_2 helps regulate the flame temperature and spreads the combustion heat up the length of the boiler (Mousavian & Mansouri, 2011). The CO_2 is fed into the boiler by the secondary recycle which can be done before or after wet flue gas desulphurization (see Figure 16 below). Recycling the flue gas after the wet flue gas desulphurization step avoids the buildup of SOx in the boiler which are associated with low and high temperature corrosion within the unit. It is thermally prudent though to recycle the flue gas before the wet flue gas desulfurization step as this unit robs the flue gas of valuable heat it could carry into the boiler (Lockwood, 2014). To compensate the flue gas has to be heated against boiler feed water from the steam cycle which represents an efficiency penalty (Fu and Gundersen, 2013). The decision on whether the secondary recycle is taken from before or after the wet flue gas desulphurization step will depend largely on the sulphur content of the feed coal. Most pilot plants choose to sacrifice efficiency and recycle after flu gas desulphurization. Having secondary recycle streams both before and after flue gas desulphurization is an option that attempts to lower the efficiency penalty whilst removing a sufficient amount of SOx. The Sulphur content of the feed coal would then determine the contribution made by either recycle stream. An alternative for coals with very low Sulphur content is to use a form of semi-dry FGD or even dry sorbent injection which induces much lower efficiency penalties whilst achieving sufficient SOx removal (Lockwood, 2014). There is also what is known as the primary recycle that assists with coal transportation and drying. It's normally taken off after the flue gas condenser in what is known as dry flue gas recycle as opposed to of wet flue gas recycle. The reason for this is that the water contained in the flue gas prior to flue gas condensation hinders coal drying and can cause coal agglomeration problems. It dose however need to be reheated to around 250℃ - 300℃ for effective coal drying (Mancuso et al.et al., 2013).

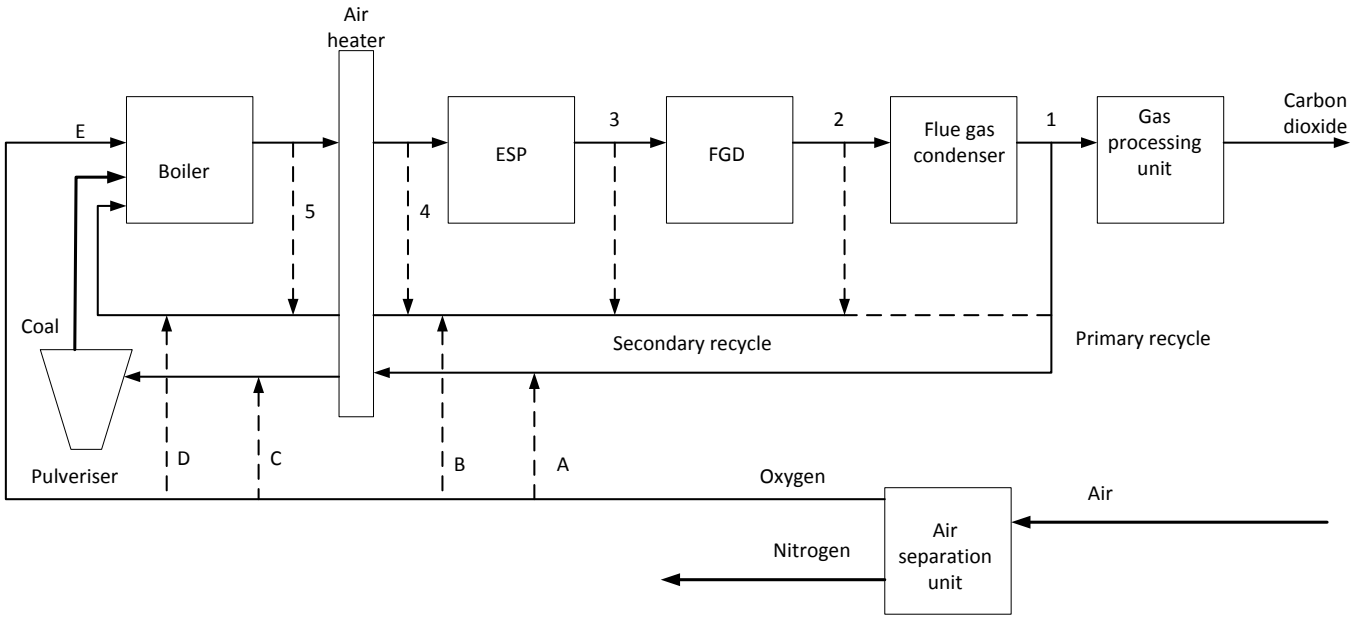

Figure 16: Diagram showing possible primary and secondary recycle locations in oxy-combustion power plant. Diagram was lifted from (Lockwood, 2014).

2.5.3.2. Flame stabilization

Studies have shown that oxy-combustion results in poor flame stability and that the flame exists in narrower air fuel ratios and oxygen dilutions (Chen et al., 2012). It's also been found that the laminar flame speed is lowered which delays coal ignition, reduces temperatures and increases the likelihood of the flame detaching from the burner and being extinguished((Molina and Shaddix, 2007); (Suda et al., 2007)). Studies have shown that flame propagation in coal dust clouds is a factor of as much as six slower when CO_2 is used as diluent as opposed to Nitrogen. This can be mostly attributed to Carbon dioxides high specific heat which lowers reaction temperatures and reaction rates. Simulations of the processes using theoretical models that use methane gas to approximate coal volatilities show that flames speeds up to 10 times higher are achieved when nitrogen is used a diluent as opposed to carbon dioxide (see Figure 17 below) (Lockwood, 2014).

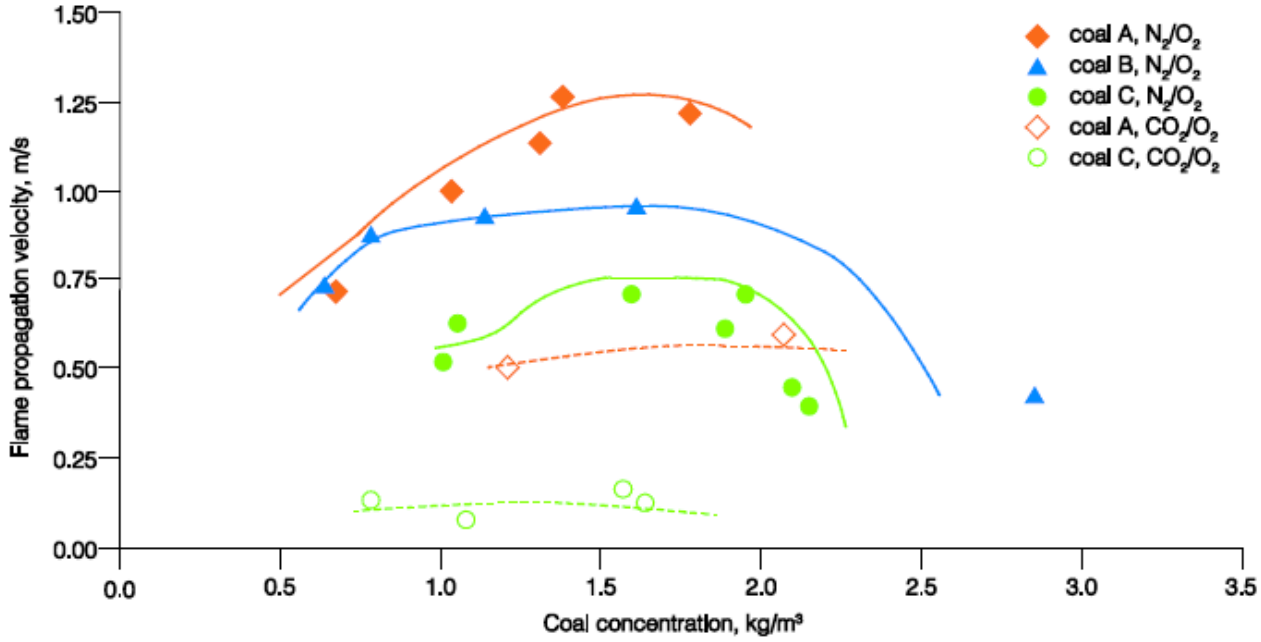

Figure 17: Graph depicting change in flame propagation speed in air and oxy fired burners with varying concentrations of diluent ($\boldsymbol{CO_2}$ and $\boldsymbol{N_2}$) for different coal types. The graph was lifted from (Lockwood,2014).

A characteristic that plays a smaller role in reducing flame speeds is the reactivity of CO_2 with radicals such as O, H and CH. A possible explanation for this is that the reactions are endothermic, and effectively rob the furnace of heat. A study on methane combustion under oxy-fuel conditions which used a chemically inert CO_2 species as reference found that the chemical effect induces a roughly two fold reduction in flame speed. This was much less than the influence of physical properties (such as specific heat) which they found to induce a tenfold reduction in flame speed (Lockwood, 2014).

2.5.3.3. Heat transfer

Upon retrofit, the flue gas recycle ratio needs to be optimized. This is because the nitrogen that predominates in the feed air in a conventional air fired pulverised coal combustion setup serves as diluent; distributing the combustion heat throughout the furnace. So air fired pulverised coal boilers were initially designed to make use of this phenomenon to maximise the amount of heat transmitted to the working fluid within the limits of material constraints associated with whatever the boiler was fashioned. So in order to make the most of existing infrastructure it is

prudent then to find a cost effective alternative to nitrogen for newly retrofitted plants. Carbon dioxide was determined to be a cheap (as it is a free combustion product) and suitable replacement, whose concentration can easily be altered through recycle ratio optimization once fed back. The optimization is done in an effort to produce heat transfer characteristics similar to an air fired case within existing boilers. This optimal boiler flue gas flow will be different to the initial flow in an air fired case because of the altered boiler gas combustion characteristics mentioned before (Mousavian & Mansouri, 2011).

There are two predominant heat transfer regions recognized in pulverized coal boilers: there's the radiant boiler section (which is near the flame) and the convective boiler section (which is further up). Each section, characterized by the predominant type of heat transfer mechanism it receives combustion heat (Mousavian & Mansouri, 2011).The volume of flue gas flowing through the boiler is inversely proportional to the heat transfer within the radiant section and directly proportional to the heat transfer within the convective section. As the volume of flue gas through the boiler reduces, it exposes the radiant section to the furnace flame; increasing temperatures within the region. It also has a detrimental impact on the membrane walls of the steam generator. The maximum heat transfer these membrane walls can manage without degrading is a metallurgical constraint imposed on the boiler by design (Mousavian & Mansouri, 2011). So the retrofitted boiler must have radiant section heat transfer characteristics no greater than that of a conventional air fired case to ensure the membrane wall isn't damaged. The convective boiler section has been so named because its likelihood of receiving heat is proportional to the flow of gas through the unit. Increasing progressively with the decrease in heat transfer to the radiant section with increased flue gas flow (Boiler passed flow) (see Figure18).

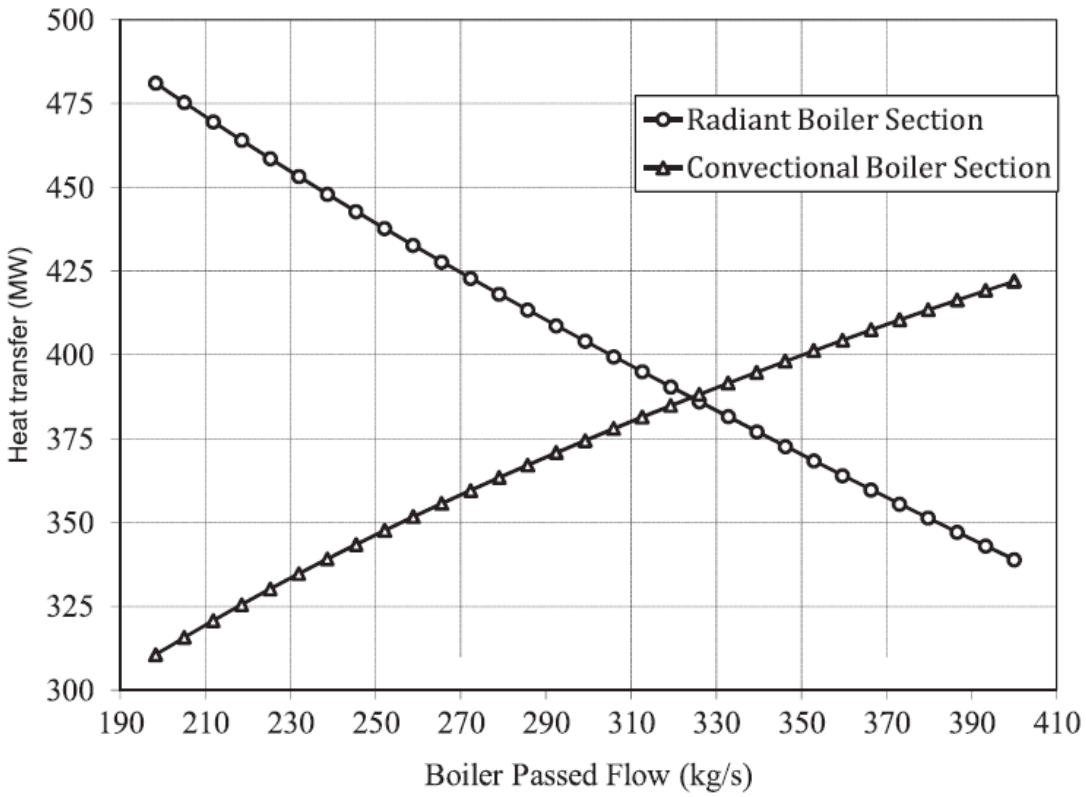

Figure 18: Heat transfer in radiative and convective section of oxy-combustion boiler against boiler flue gas flowrate (boiler passed flow). This graph was lifted from (Mousavian and Mansouri, 2011).

It's been found that an optimum flue gas flow rate exists that is a compromise on the heat transfer in the radiant and convective sections. At this optimum the heat transfer to the working fluid is maximized along with the power generated. This can be seen in Figure 19 which charts the change in overall thermal power generation against boiler flue gas flow rate (boiler passed flow) in an oxy-combustion power plant. The curve roughly takes the shape of a parabola with negative gradient and has a maximum or peak at a flowrate of around 273(kg/sec) (Mousavian and Mansouri, 2011).

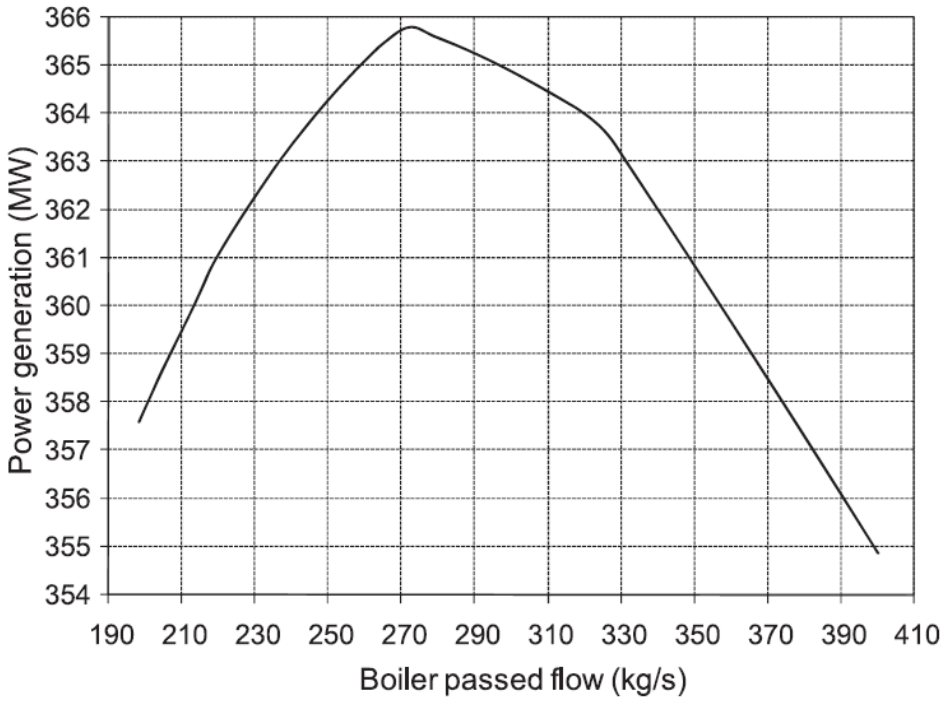

Figure 19: This graph, taken off (Mousavian & Mansouri, 2011), shows the change in thermal plant power generation with boiler flue gas flow rate (boiler passed flow) in an oxy-combustion plant.

2.6. Pressurized oxy-combustion

Pressurized oxy-combustion has recently been suggested as a viable means of increasing oxy-combustion thermal efficiencies. In this setup flue gas water is condensed out from combustion flue gasses in a flue gas condenser. The heat released is used to preheat boiler feed water. This is made possible because increasing the flue gas pressure increases the saturation temperature of the water it contains, which makes heat integration with the higher temperature feed water heaters feasible. As a result, less steam is extracted for feed water preheating from the steam cycle turbines which increases gross power output. Another benefit of this strategy is that it reduces both boiler air ingress and flue gas volume. Although this strategy increases the compression work in the air separation unit, this is counterbalanced by the reduced compression work requirements in the downstream compression and purification unit. Studies have shown this strategy to reduce the associated oxy-combustion thermal efficiency penalty by around 3%. Among the challenges associated with this strategy is altered boiler flue gas heat transfer characteristics under higher pressures and safety concerns related to CO_2 poisoning (Chen et al., 2012).

2.7. Exergy analysis

Exergy by definition is the maximum amount of work one can draw from a stream of matter or quantity of heat as it moves toward equilibrium with the environment. This makes exergy analysis a powerful tool for determining the thermodynamic efficiency of a process as it accounts for losses in work as processes moves towards this equilibrium state. This is because the concept of exergy takes into account the second law of thermodynamics. This is unlike an energy analysis which takes into account only the first law of thermodynamics which states that energy is conserved, making it unable to account for work losses (Kotas,1985).

2.7.1. Significance of the second law

The second law states that the entropy of an isolated system (the system and surrounding) is forever increasing. An amount of work is lost as this happens that cannot be harnessed using any means derived from the technology in our present day. Accounting for the second law allows one not only to more accurately determine what plant layouts are most efficient; it's also a tool with which sections in the plant and their accompanying process units can be accurately ranked according to work losses or irreversibility's. Ranking plant sections according to irreversibility's helps determine which areas are most wasteful and have the greatest potential for improvement. The work output that isn't destroyed as a result of entropy production is called the material or heat streams exergy/useful work content (Kotas,1985).

2.7.2. Carnot efficiency, equilibrium and reversibility

There exists an upper limit to the amount of work (which in this case is called usable work or exergy) an amount of heat accepted or rejected by thermal reservoir can do called the Carnot efficiency. This limit is dependent on the temperature disparity between the thermal reservoir that rejects (T_H) or accepts the heat and that of the ambient environment (T_a). Equation 2.7.2a is a means of determining Carnot efficiency for a reservoir rejecting heat, and Equation 2.7.2b is a means of using the Carnot efficiency to determine the amount of usable work that can be harnessed from an amount of heat (Q) rejected by the reservoir (Kotas,1985).

$$\eta_{carnot} = \frac{T_H - T_a}{T_H} \qquad 2.7.2a$$

$$W_{usable} = Q\left[\frac{T_H - T_a}{T_H}\right] \quad 2.7.2b$$

Carnot efficiency was developed through the conception of an idealized power cycle that transmits heat from a hot reservoir to a working fluid through a conducting surface i.e.(an ideal Rankine cycle). As the fluid goes round the cycle it goes through a series of processes that are infinitesimally close to equilibrium. This makes the idealized process perfectly efficient and its work output an idealized maximum for the quantity of heat rejected by the hot reservoir (Wallace& Linning,1970). It can also by extension be used to determine the amount of usable work attainable from a quantity of heat (Q) transmitted through a conducting surface (Kotas,1985).

Reversibility can be thought of as the ability of a process to be run in reverse, where the work output from the process is used to return the process and surroundings to their original state. This in theory is impossible as there will always be work losses. A practical way of imagining this is through the acknowledgment that a fluid equilibrates (reaches homogeneity) through fluid movements (eddies and currents etc.) that flow down property gradients (i.e. temperature gradients, concentration gradients etc…). As theses pockets of fluid move they do work (which causes cooling) that can never be retrieved. These property gradients are associated with non-equilibrium processes that have the tendency of pulling work flows away from the desired path between the processes initial and final state. So the closer the processes are to equilibrium (or the more homogenous they are) along the desired path, the more efficient or reversible the process between the initial and final states along the desired path is. Formally, these un-retrievable work flows are caused by: solid fluid friction (viscous dissipation), mechanical or electrical hysteresis, ohmic resistance (Kotas,1985).

The fraction of work that isn't usable and is destroyed as a result of an increase in entropy of the isolated system (which is combination of the system and the surroundings) can be determined using Equation 2.7.2c below (which is the product of the entropy production of the isolated system (ΔS_{isol}), and the prevailing ambient temperature, T_0) (Kotas,1985).

$$W_R = (T_0)\Delta S_{isol} \quad 2.7.2c$$

2.7.3. Exergy of material flows

In summary the total exergy content of a material stream can be described as the amount of work obtainable when the stream of matter goes from its initial state to the dead state. The dead state is characterized by thermal, mechanical and chemical equilibrium with the environment. The total exergy content ($\dot{E}_{tot}$) of a stream of matter can be divided into four components (see Equation 2.7.3): the kinetic exergy ($\dot{E}_K$), the potential exergy ($\dot{E}_P$), the physical exergy ($\dot{E}_{ph}$) and the chemical exergy ($\dot{E}_0$). The kinetic and potential exergy are associated with high grade exergy and will be ignored in this thesis (Kotas,1985).

$$\dot{E}_{tot} = \dot{E}_K + \dot{E}_P + \dot{E}_{ph} + \dot{E}_0 \qquad 2.7.3$$

2.7.3.1. Physical exergy

By definition the physical exergy of a material stream is the maximum amount of work one can harness from it when the said stream is brought from its initial state (T, P) to the environmental state by physical processes involving only thermal interaction with the environment. The environmental state is characterized by thermal equilibrium (where the stream is at the ambient environmental temperature; T_0) and isolated stream (the stream by definition cannot exchange matter with the environment) mechanical equilibrium (where the total stream pressure is one atmosphere; P_0) with the environment (Kotas,1985). This can be imagined as the total amount of usable work retrievable from thermomechanical disequilibrium. It's exhausted once a stream ceases to flow and is at the prevailing ambient temperature downstream. Equation 2.7.3.1 is the expression used to determine the physical exergy of a stream.

$$\varepsilon_{ph} = (h_i - h_0) - T_0(s_i - s_0) \qquad 2.7.3.1$$

Here:

- ε_{ph} = physical exergy of a stream
- h_i = initial enthalpy of the stream
- h_0 = environmental state enthalpy of the stream
- T_0 = ambient temperature
- s_i = initial stream entropy
- s_0 = environmental state stream entropy

2.7.3.2. Chemical exergy

The chemical exergy of a stream of matter is defined as the maximum amount of work one can harness from the said stream when each of its components are brought form the environmental state to the dead state. The dead state is characterized by thermal equilibrium (where the stream is at the ambient environmental temperature; T_0) and chemical equilibrium (here each component exists in its environmental chemical state and partial pressure; P_{00}) with the environment. Equation 2.7.3.2a below is an expression for determining the chemical exergy content of a material stream (Kotas,1985). γ_i is the activity coefficient for component i (For ideal solutions this term falls away).

$$\tilde{\varepsilon}_{0M} = \sum_i x_i \tilde{\varepsilon}_{0i} + \tilde{R}T_0 \sum_i x_i \ln \gamma_i x_i \qquad 2.7.3.2a$$

The term to the right of Equation 2.7.3.2a represents the amount of work that needs to be expended to get each gas mixture component to the environmental state that forms the basis for the determination of chemical exergy. This exergy expended is always negative since we were trying to determine the exergy content of the combined mixture at the environmental state (Each component has to then be compressed from its initial state (which is only a fraction of the total environmental state pressure of the mixture), this can be considered the exergy of mixing and represents the amount of work destroyed upon mixing with the environment (Kotas,1985). The term to the left represents the change in exergy of a pure component as it moves from the environmental state to the dead state (see Equation 2.7.3.2b). Values of standard chemical exergy for many reference species can be found in literature.

$$\tilde{\varepsilon}_0 = \tilde{R}T_0 \ln \frac{P_0}{P_{00}} \qquad 2.7.3.2b$$

2.7.4. Exergy and flowsheeting simulators

A more convenient means of determining the exergy content of material streams in flowsheet simulators such as ASPEN plus was developed by Hinderink, et al.,(1996). Unlike the method mentioned above, this method separates the material stream into its pure unmixed components at the initial stream conditions (T, P) before determination of the physical and chemical exergy. This separates the exergy of mixing term from the chemical exergy and greatly simplifies the calculation of total stream exergy for flowsheet simulators. So when using this method the total

exergy content of a material stream is divided into three distinct components: the exergy of mixing ($\dot{E}_{mix}$), the physical exergy ($\dot{E}_{ph}$) and the chemical exergy ($\dot{E}_{ch}$) (Hinderink et al., 1996).

$$\dot{E}_{tot} = \dot{E}_{ch} + \dot{E}_{ph} + \dot{E}_{mix} \qquad 2.7.4$$

2.7.4.1. Exergy of mixing

First the stream at its initial conditions (T, P) is separated out into its pure unmixed components (all of them at conditions (T, P)) using the exergy of mixing. Much like the exergy of mixing in Equation 1.3.2a it too is always negative (see Equation 2.7.4.1) (Hinderink et al., 1996).

$$\dot{E}_{mix} = \left[\dot{F}h - \sum_i^n\left(\dot{F}_i h_i\right)\right] - T_0\left[\dot{F}s - \sum_i^n\left(\dot{F}_i s_i\right)\right] \qquad 2.7.4.1$$

Here, $\dot{F}$ is the total stream molar flow, $\dot{F}_i$ is the component molar flow, h is the total stream enthalpy, h_i is the component molar enthalpy, s is the total stream molar entropy and s_i is the component molar entropy.

2.7.4.2. Physical exergy

Then the physical exergy of the pure unmixed components is determined as they each move from processes conditions (T, P) to the environmental state (T_0, P_0) (Hinderink et al., 1996).

$$\dot{E}_{ph} = \left[\sum_i^n\left(\dot{F}_i h_i\right) - \sum_i^n\left(\dot{F}_{0,i} h_{0,i}\right)\right] - T_0\left[\sum_i^n\left(\dot{F}_i s_i\right) - \sum_i^n\left(\dot{F}_{0,i} s_{0,i}\right)\right] \qquad 2.7.4.2$$

Here, $h_{0,i}$ and $s_{0,i}$ are the component enthalpy and entropy at reference conditions (T_0, P_0) respectively.

2.7.4.3. Chemical exergy

Then the change in chemical exergy is determined as each of the pure unmixed components go from the environmental state (T_0, P_0) to the dead state (T_0, P_{00}). Here, $e^0_{ch,i}$ is the standard chemical exergy which can be determined using Equation 2.7.4.3 above or it can be lifted from literature (Hinderink et al., 1996).

$$\dot{E}_{ch} = \sum_i^n\left(\dot{F}_i e^0_{ch,i}\right) \qquad 2.7.4.3$$

2.7.4.4. Benefits of methodology

With this method you don't need to find the activity coefficients (γ_i) for each component in a stream, neither do you need to assume the stream is an ideal solution. ASPEN is able to return

the pure component properties of each constituent in a mixture along with the properties of the mixture as whole. This allows one to determine the exergy of mixing accurately through simple subtraction. When dealing with multi-phase streams each phase is dealt with separately before their exergy contents are summed together to give the total stream exergy. Separation of streams with a liquid and gas phase can be accomplished by simply flashing the stream at the processes conditions (T, P) (Hinderink et al., 1996). In this thesis streams not at the environmental state (T_0, P_0) containing liquid-solid phases were dealt with by having their liquid phase's separated out using a hydrocyclone. An imaginary stream with identical composition to a completely dry stream of the solid phase at initial conditions (T, P) is then simulated to, and used to approximate the exergy of the solid phase. This was done because the solid product from a hydrocyclone always contains a small amount of water, and ASPEN plus dose not return the pure component thermodynamic properties of solids in a multi-phase stream. The exergy of the two streams are then summed together to get the total stream exergy much like with gas-liquid streams. This method of dealing with phases separately is an ideal means of determining material stream exergies with flowsheet simulators since it's easy to implement and a lot more accurate than determining the exergy of a multi-phase streams directly.

Another benefit of using this method is that by dealing with pure processes components its more accurate since thermodynamic properties such as entropy and enthalpy change of pure components can more accurately be determined than those of a mixture from state to state (Hinderink et al., 1996).

3. Process description

The pulverized coal plants simulated in this work are based on the work of Fu and Gundersen (2013). All major stream flows in the coal to power processes are based on the NETL report (Ciferno et al., 2008). The ASU and the CPU are based on other common cases from literature ((Hands, 1986), (Pipitone and Bolland, 2009), (Fu and Gundersen, 2012)). The oxy-combustion and air fired power plant steam cycles are based on the work of Almas (2012).

3.1. Oxy-combustion process description

Figure 20 is a simplified diagram of the oxy-combustion plant investigated in this work. Stream data for all material streams can be found in the appendix.

3.1.1. Steam cycle

The supercritical oxy-combustion steam cycle is represented by system boundaries: CU2, CU3 and CU4. A more detailed flowsheet of the steam cycle is given in Figure 26 and stream data for its material streams in the appendix. System boundary CU2 encircles the high pressure turbine section. CU3 represents the stream flows (incoming and outgoing), the turbines and their work output in the low and intermediate pressure sections of the steam cycle. CU4 represents s the electricity generator which converts 98.5% of the total turbine work output to electricity (Szatkowski, 2009).

3.1.2. Air separation unit

A double column air separation unit is retrofitted upstream to produce the required 95mol% oxygen feed. The ambient air feed (A0) is first compressed to 5.6 bar by a 3 stage compressor (A-P1) with inter-stage cooling. The compressed air is then reported to a direct contact after cooler (A-DCA) before being sent to temperature swing adsorption pre-purification unit (A-PPU). Here H_2O, CO_2 and various other impurities are removed. Low pressure steam from the steam cycle (N_{ASUa}) provides heat for regenerating the sieves. The dried compressed air then reports to the main heat exchanger (A-H1) were it is cooled to near dew point. The cooled air is then separated into three streams: one with a 95mol% composition of O_2 (A-51) and two with a 97mol% composition of N_2 (A7-2 and A4-1). The condenser in the high pressure column (A-HP) is integrated with the reboiler in the low pressure stripping column (A-LP). The temperature difference of the condenser/reboiler is maintained at 1.5℃. The N_2 stream (A4-1) from the top of

the high pressure column reports to the tail gas turbine (A-P2) to recover power, before being mixed with the N_2 stream (A7-3) from the top of the low pressure column. The mixed nitrogen stream then provides additional cooling in the pre purification unit (A-PPU) before being vented to the atmosphere. The oxygen product (A5-2) with molar composition (O_2-95.63%; N_2-1.29%; Ar-3.07%) is split into two: the minor part of it (C2-2) is sent to the serve as oxidant for the flue gas desulphurization unit and the major part of it (C2-1) serves as oxidant for the boiler.

3.1.3. Boiler and flue gas desulphurization

A pulverized coal feed (C0) with characteristics given in Table 1 serves as fuel. To ensure complete combustion, the oxygen fed to the boiler is set to produce a boiler flue gas with an oxygen mole fraction of around 2% (Ciferno et al., 2008). The oxidant is provided by stream (C4-1) and a small amount infiltration air. The combustion takes place at 1.01bar and the combustion heat is converted to power by the steam cycle. The particulate matter in the flue gas stream (C1-1) is removed in an electrostatic precipitator (ESP) with close to 100% efficiency. The flue gas then reports to a wet flue gas desulphurization system (FGD) where around 98% of the SO_2 is removed. To reduce the combustor flame temperature, around 72% of the flue gas leaving the FGD (C1-3) is recycled back to the boiler. The remainder (R1-1) reports to the compression and purification unit. The relatively cool recycle stream (C3-1), is then heated by around 9℃ to prevent entrained water droplets from passing through the air fans (C-P3). The recycle stream (C3-3) is mixed with the major part of the oxygen product from the ASU (C2-1) before being fed to the boiler.

3.1.4. Compression and purification unit

The flue gas entering the compression and purification unit (R1-1) is first cooled to around 35℃ in a direct contact aftercooler (R-DCA) with condensate knockout. The gasses are then compressed to 32bar by a three stage compressor (R-P1) with water intercooling. The gas is then dewatered in a molecular sieve twin bed drier (R-S1) to avoid ice formation in the sub ambient heat exchangers. Steam from the steam cycle (N_{CPUa}) provides the heat required to regenerate the molecular sieves. The flue gas is then cooled to -25℃ in the sub ambient heat exchanger (R-H1) before being flashed into a vapor and liquid stream by flash drum (R-S2). The CO_2 rich liquid stream (R2-1) is then expanded in a Joule-Thompson valve before being heated against the incoming flue gas in heat exchanger (R-H1).

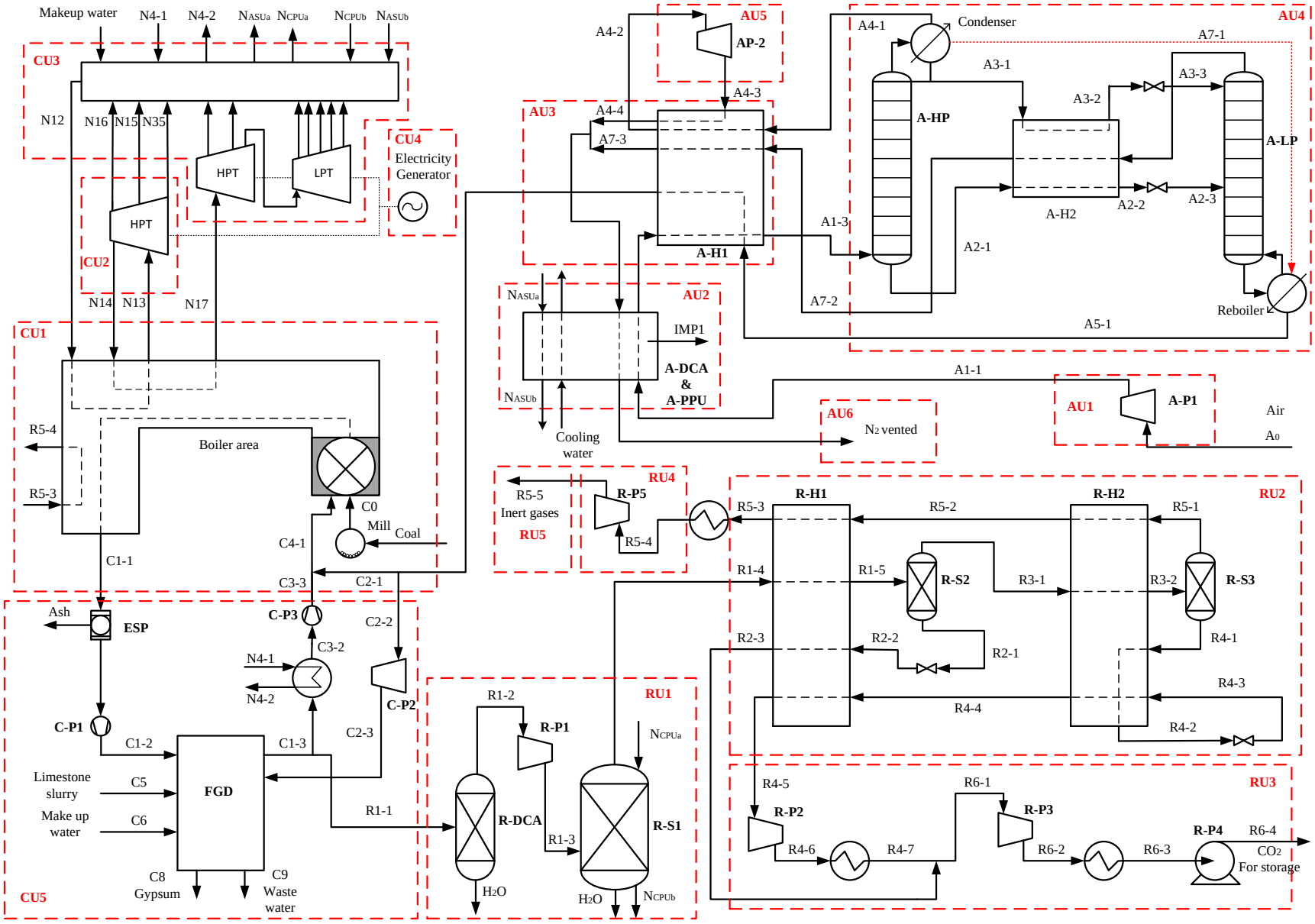
Makeup water
N4-1
N4-2
NASUa
NCPUa
NCPUb
NASUb
CU3
N12
N16
N15
N35
HPT
LPT
CU4
Electricity Generator
HPT
CU2
N14
N13
N17
CU1
R5-4
R5-3
Boiler area
C0
Mill
Coal
C4-1
C1-1
C3-3
C2-1
Ash
ESP
C-P3
C2-2
C3-2
N4-1
N4-2
C-P2
C-P1
C1-2
C1-3
C2-3
Limestone slurry
C5
Make up water
C6
FGD
R1-1
C8
Gypsum
C9
Waste water
CU5
R1-2
R-P1
R-DCA
R1-3
R-S1
H2O
H2O
NCPUa
NCPUb
RU1
R5-5
Inert gases
R-P5
R5-4
RU4
RU5
AU5
AP-2
A4-2
A4-3
AU3
A4-4
A7-3
A-H1
A1-3
A7-2
AU2
NASUa
IMP1
A-DCA & A-PPU
NASUb
Cooling water
AU6
N2 vented
A4-1
Condenser
A7-1
A3-1
A3-3
A3-2
A-HP
A-LP
A-H2
A2-2
A2-3
A2-1
Reboiler
A5-1
AU4
A1-1
AU1
A-P1
Air
A0
R-H1
R-H2
RU2
R5-3
R5-2
R5-1
R1-4
R1-5
R-S2
R3-1
R3-2
R-S3
R2-3
R2-2
R2-1
R4-1
R4-3
R4-4
R4-2
R4-5
R-P2
R6-1
R-P3
R-P4
R6-4
CO2
For storage
R4-6
R4-7
R6-2
R6-3
RU3

AU1: Main air compressor (MAC); AU2: Pre purification unit; AU3: Main heat exchanger; AU4: Distillation unit; AU5: N_2 turbine; AU6: VentedN_2; CU1: Boiler area; CU2: High pressure steam turbines; CU3: Steam cycle excluding high pressure turbines (Intermediate pressure and low pressure steam turbines, condenser, condensate pump, gland seal condenser, steam generator feed pump, steam seal regulator, the feed water heaters, deaerator, and steam generator pump); CU4: Electricity generator; CU5: Ash removal and desulphurization unit (electrostatic precipitator and glue gas desulphurization unit); RU1: first stage of CO_2 compression; RU2: Two stage flash CO_2 purification process; RU3: Second stage of CO_2 compression; RU4: Tail gas turbine; RU5: Vented inert gasses.

Figure 20: Flowsheet of oxy-combustion plant. This flowsheet was adapted from a similar one in (Fu and Gundersen, 2013)**.**

The vapour stream (R3-1) from flash drum (R-S2) is cooled to -54℃ in the sub ambient heat exchanger (R-H2). This stream is then flashed into a vapour and liquid stream by flash drum (R-S3). The vapour stream (R5-1) which contains mostly inert gasses is then heated in the multi stream sub ambient heat exchangers (R-H1 and R-H2). It's then heated against the hot flue gases in the boiler, and then reports to the tail gas turbine (R-P5) which recovers power before venting it to the atmosphere. The liquid stream (R4-1), from flash drum (R-S3) is then cooled to around -55.62℃ after expansion in a Joule-Thompson valve. It then provides cooling in the sub ambient heat exchangers on its way out of the double flash separation process. Stream (R4-5) is compressed to the same pressure as stream (R2-3) by compressor (R-P2). It's then cooled using cooling water before being combined with stream (R2-3). The combined stream is the compressed to 78bar by a two stage compressor with water intercooling (R-P3). The compressed carbon dioxide stream (R6-2) is then cooled to around 25℃ by sea water or chilled cooling water. At this temperature and pressure the CO_2 is its dense phase. It's then pumped to 150bar by pump (R-P4) for transport and storage in saline formations. The purity of the captured CO_2 is around 97.3%.

3.2. Air fired plant process description

Figure 21 is a flowsheet of the un-retrofitted air fired plant. The two major processes not included in the un-retrofitted plant are the upstream ASU and the downstream CPU. The un-retrofitted plant is fed air (stream A0) as an oxidant instead of oxygen. The major processes in the un-retrofitted pulverised coal fired plant are mostly identical to those of the oxy-combustion plant. Minor differences include: there's no steam extraction to the ASU and the CPU from the steam cycle (streams $N_{ASUa}, N_{CPUa}, N_{ASUb}$ and N_{CPUb} fall away), there's no boiler feed water extraction for flue gas recycle heating from the steam cycle (streams N4-1 and N4-2 fall away) and there's no flue gas recycle (streams C3-1, C3-2 and C3-3 fall away).

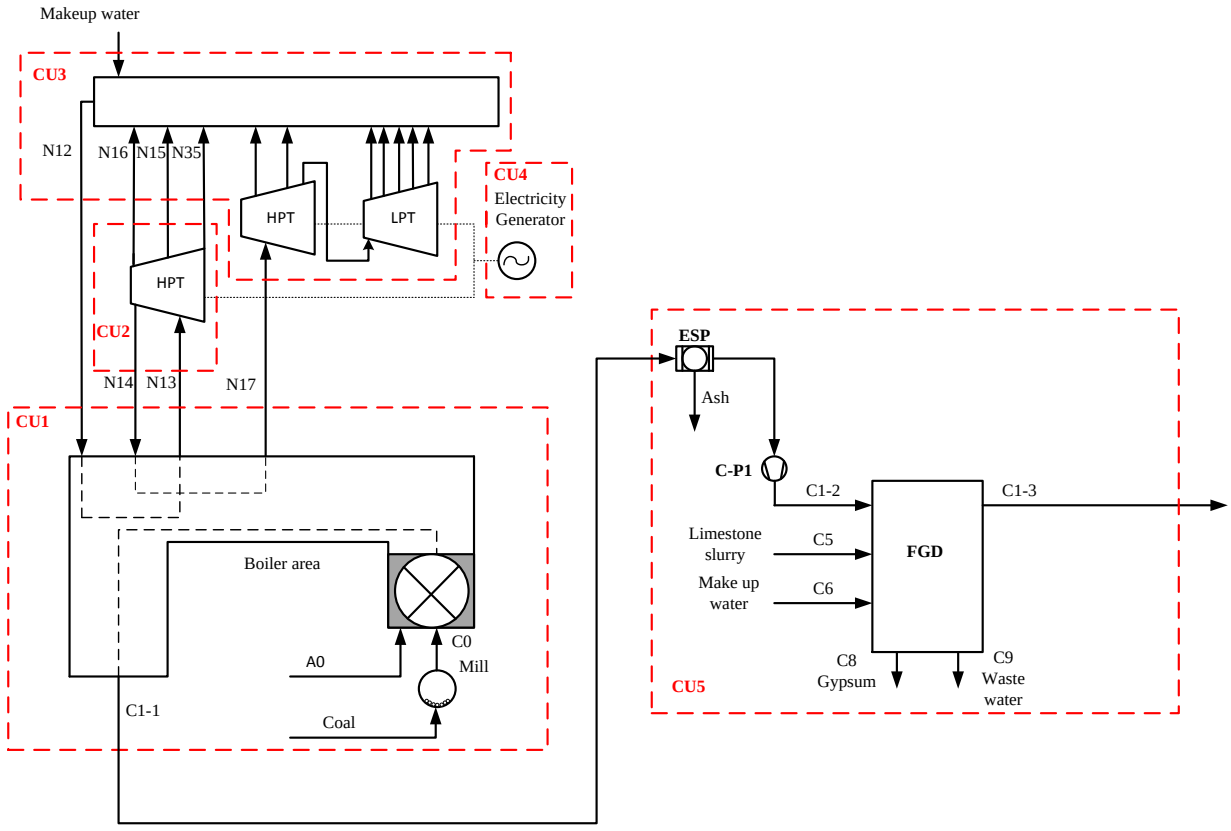

CU1: Boiler area; CU3: Steam cycle excluding high pressure turbines (Intermediate pressure and low pressure steam turbines, condenser, condensate pump, gland seal condenser, steam generator feed pump, steam seal regulator, the feed water heaters, deaerator, and steam generator pump); CU5: Ash removal and desulphurization unit (electrostatic precipitator and glue gas desulphurization unit).

Figure 21: Simplified flowsheet for un-retrofitted air fired plant.

4. Simulation

An un-retrofitted, air fired 546 MW net power plant and an oxy-combustion 562 MW net power plant were simulated using ASPEN plus V8.4. Using the simulation results from both models the thermal efficiency penalty of the oxy-combustion retrofit was then determined and compared with the oxy-combustion thermal efficiency penalty reported in Fu and Gundersen (2013). This was done in order to determine what effect if any loosening the assumptions made by Fu and Gundersen (2013) would have on the efficiency penalty findings made. Section 4.1 describes the ASPEN plus flowsheets for the Boiler Island, air fired plant steam cycle, flue gas desulphurization unit, baghouse and ESP. Section 4.2 describes the ASPEN plus flowsheets for the air separation unit, the oxy-combustion steam cycle and the compression and purification unit. The flowsheets described in Section 4.1 are used to simulate the air fired plant. The flowsheets described in Section 4.2 describe sections exclusive to the oxy-combustion plant and leaves out sections shared between the two models. These sections include: the boiler island, baghouse and electrostatic precipitators.

4.1. Air fired plant ASPEN plus flowsheet

4.1.1. Boiler Island

The boiler Island flowsheet is based loosely on the flowsheet developed by Aspen Tech (2011, pp. 5-52) (See Figure 22). The simulation template used for this model is Solids with English units. Wet coal (stream WETCOAL) is initially fed into the RSTOICH block called (DRYREACT) along with hot Nitrogen (stream NITROGEN). The hot Nitrogen is used to dry the wet coal. The RSTOIC block in conjunction with the calculator block then determine the products from the drying processes which are: dry coal, nitrogen and the water. The volatiles Nitrogen and water are flashed out using a FLASH2 block and the dry coal reports to the RYIELD block (block DECOMP). The RGIBBS block models the combustion of the dry coal through Gibbs free energy minimization. However the free energy of coal cannot be calculated on account of it being a non-conventional solid. So before feeding the dry coal to the reactor it first gets decomposed into its constituents elements using the RYIELD block in conjunction with the combustion calculator. The hot products from the RGIBBS reactor then report to a cooler block which flashes the products to 177℃ and 1.01325bar and transmits the reaction heat to the steam cycle using a multi stream heat exchanger.

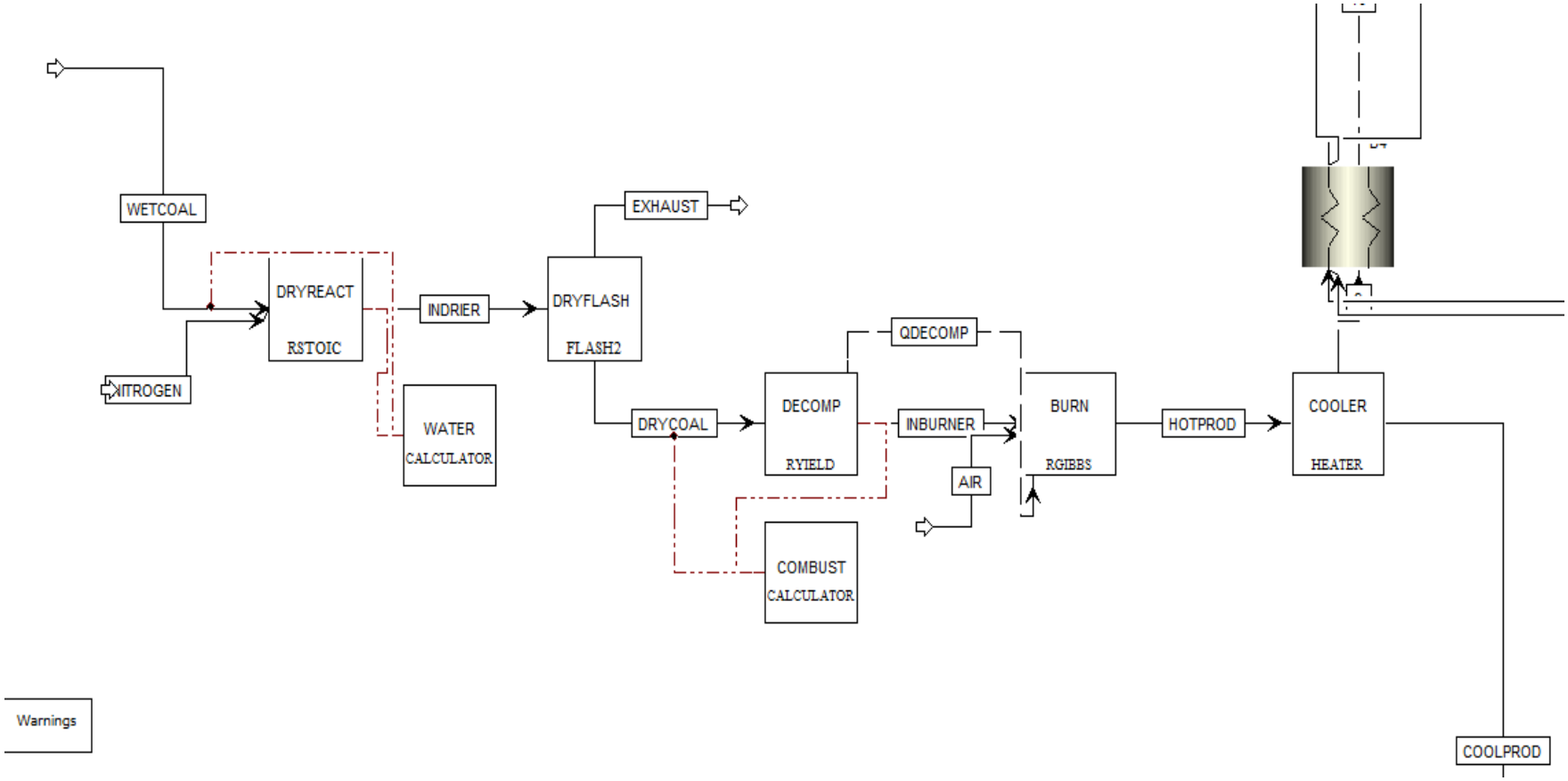

Figure 22: ASPEN plus flowsheet for boiler island.

4.1.2. Baghouse and ESP

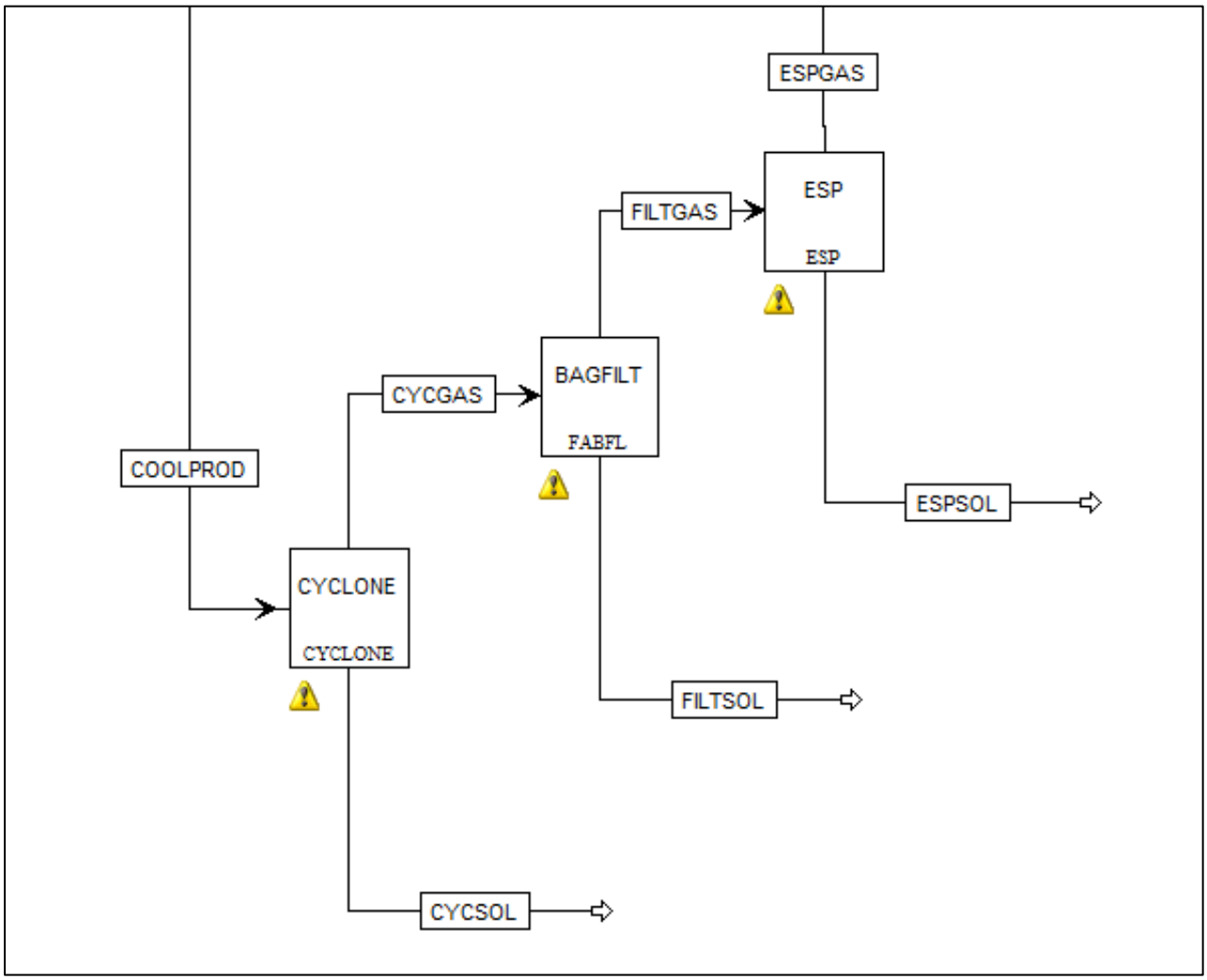

Figure 23: ASPEN plus flowsheet for baghouse and ESP.

The combustion products form the cooler (stream COOLPROD) are then sent to a gas solid separation train for particulate removal. This separation train is an extension on the Boiler Island model acquired from Aspen Tech (2011, pp. 5-52). The cyclone has a separation efficiency of 0.8, the efficiency correlation is Leith-Licht and the type is a Stairmand-HE. The bag filter was modeled using a FABFL block, the filtration velocity was calculated from baghouse characteristics and the unit was assigned a maximum pressure drop of 0.0344738bar. A plate model was selected for the ESP using the Crawford calculation method. It was assigned a separation efficiency of 0.995.

4.1.3. Air fired plant steam cycle

The ASPEN plus flowsheet for the air fired plant steam cycle is provided in Figure 25. It's based on a steam cycle developed by Almas (2012). The feed water heaters and the gland seal condenser were modeled using cross current heat exchangers. The model is composed of three high pressure turbines (HP), two intermediate pressure turbines (IP) and five low pressure turbines (LP). The deaerator and the condenser are modeled using heater blocks. The deaerator flashes its outlet stream to 176.38℃ and 9.21 bar and the condenser block flashes its outlet stream to 38.39℃ and 0.07bar.

4.1.4. Flue gas desulphurization

The flow sheet for the flue gas desulphurization unit is shown in Figure 26. The oxidant (stream C2-3), makeup water (stream MUWATER) and limestone slurry (stream 25) are fed into the unit using mixer blocks. The reaction and separation that normally take place in an absorption column are modeled using a combination of an RGIBBS (block FGDREACT) reactor and flash separator (block B53). The reaction in the RGIBBS reactor takes place at 1 atmosphere and 330.15 K. The flash block then separates out the wet gypsum product (stream GYPSUM) from the scrubbed flue gasses (stream C1-3) at the same conditions. The wet gypsum is then dried in a hydro cyclone (block B54) with a separation efficiency of 0.97 to produce the dry gypsum product (stream C8-GYPS) and waste water (stream C9-WATER).

4.2. Oxy-combustion ASPEN plus flowsheet

Since the baseline and oxy-combustion model share a Boiler Island, flue gas desulfurization unit and gas solid separation train only the air separation unit, oxy-combustion steam cycle and the compression and purification unit will be described.

4.2.1. Air separation unit

The flowsheet for the air separation unit is shown in Figure 24. The direct contact aftercooler was modeled using a flash block (B34) that removed all impurities apart from Argon. The main heat exchanger (A-H1) and the heat exchanger between the high pressure and low pressure column (A-H2) were modeled using a multi stream counter current heat exchangers. The high pressure column has 12 stages with feed coming in on the tenth stage. It has a distillate flow of 10.0443kmol/sec and a reflux ratio of 1.47. The distillate vapour fraction from the high pressure

column condenser is 0.46. The low pressure column has 23 stages and a distillate rate of 351.91 kg/sec. Stream A3-3 is fed on the first stage and stream A2-3 is fed on the stage 16 of the low pressure column. The heating that the cryogenic Nitrogen stream undergoes in the temperature swing adsorption unit occurs in a countercurrent heat exchanger. The heat exchanger transmits heat from the steam cycle into the Nitrogen stream using stream N_{ASUa}.

4.2.2. Compression and purification unit

The flowsheet for the initial compression and dewatering step is shown in Figure 29. Dewatering is achieved using a flash block (block B43) that flashes its products out at 308.15K and 1.01325bar. Three stage compression is achieved using a standard multi stage compressor (block R-P1). The flue gas then reports to the double flash separation unit Figure 27. Heat exchangers R-H1 and R-H2 are modeled using multi stream countercurrent heat exchangers. A flash block which operates at 247.15K and 31.3bar is used to simulate flash unit R-S2. Another flash block which operates at 219.15K and 31.1bar simulates flash unit R-S3. A standard multi stream compressor is used to model the compressor R-P3. A pump is used to model unit R6-4.

4.2.3. Oxy-combustion steam cycle

A detailed flowsheet of the oxy-combustion steam cycle is shown in Figure 28. The same blocks used to model the deaerator, condenser, feed water heaters, gland seal condenser and the turbines in the air fired model were used here. One of the differences between the two models is the steam extraction after the intermediate pressure turbines (N_{ASUa} and N_{CPUa}). This steam is then returned to the deaerator after its been used for heating in the air separation unit and the compression and purification unit (N_{ASUb} and N_{CPUb}). Another difference is the boiler feed water extracted after feed water heater 2 (stream N4-1). This water is used to pre heat the flue gasses recycled back to the boiler before being returned (N4-2) to front end of feed water heater 2.

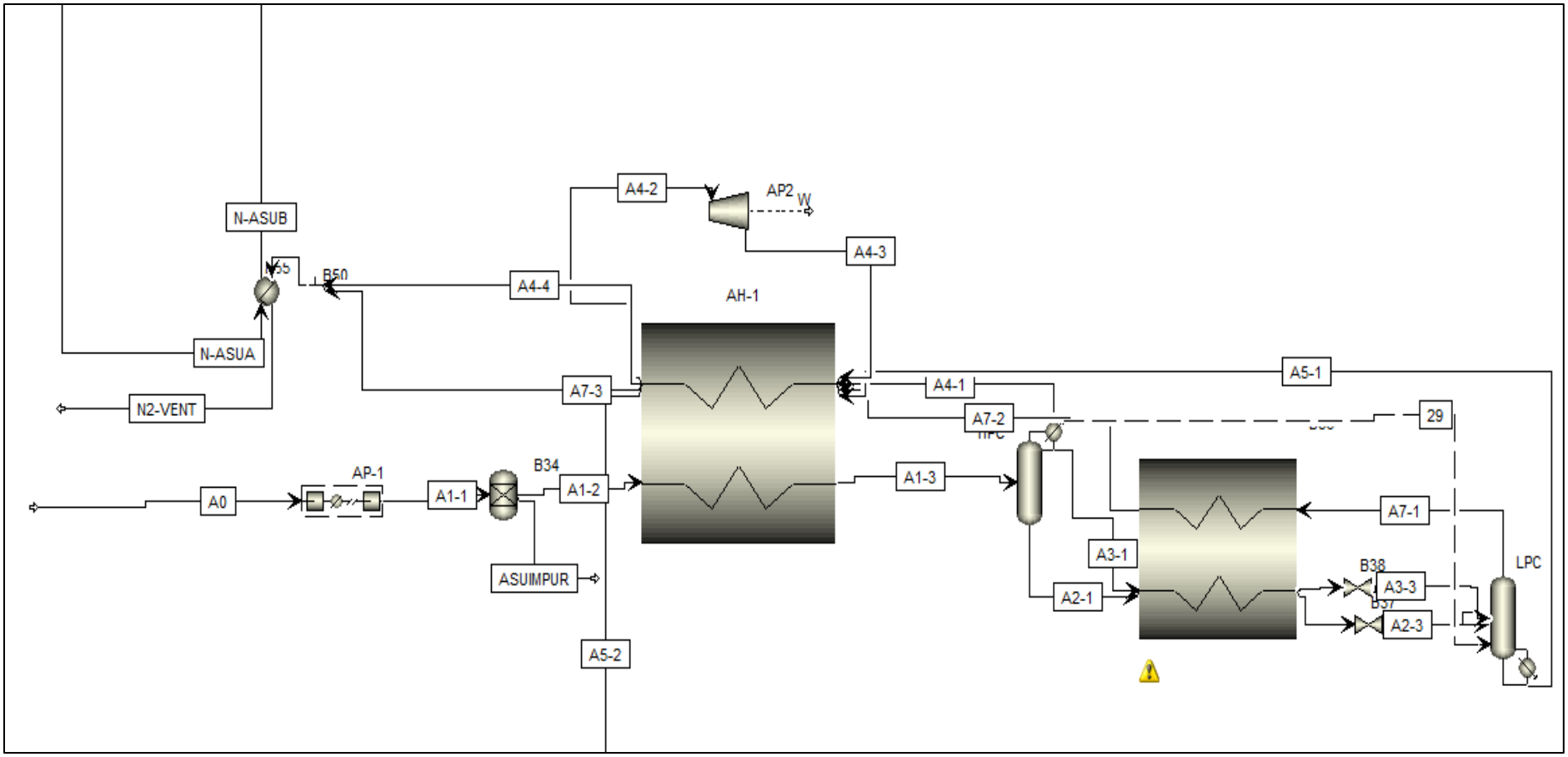

Figure 24: ASEPN plus flowsheet for air separation unit.

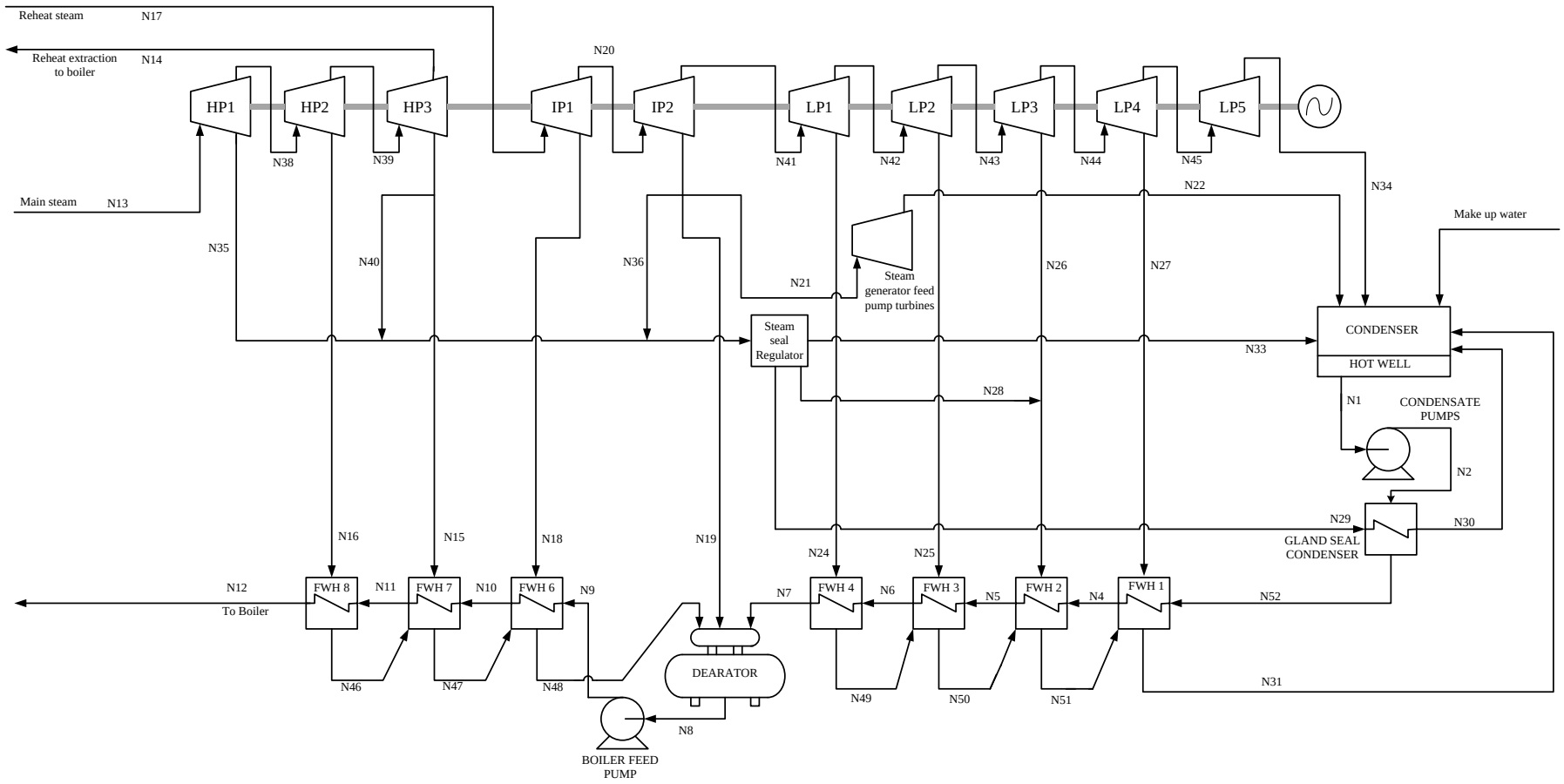

Figure 25: ASPEN plus flowsheet of air fired steam cycle.

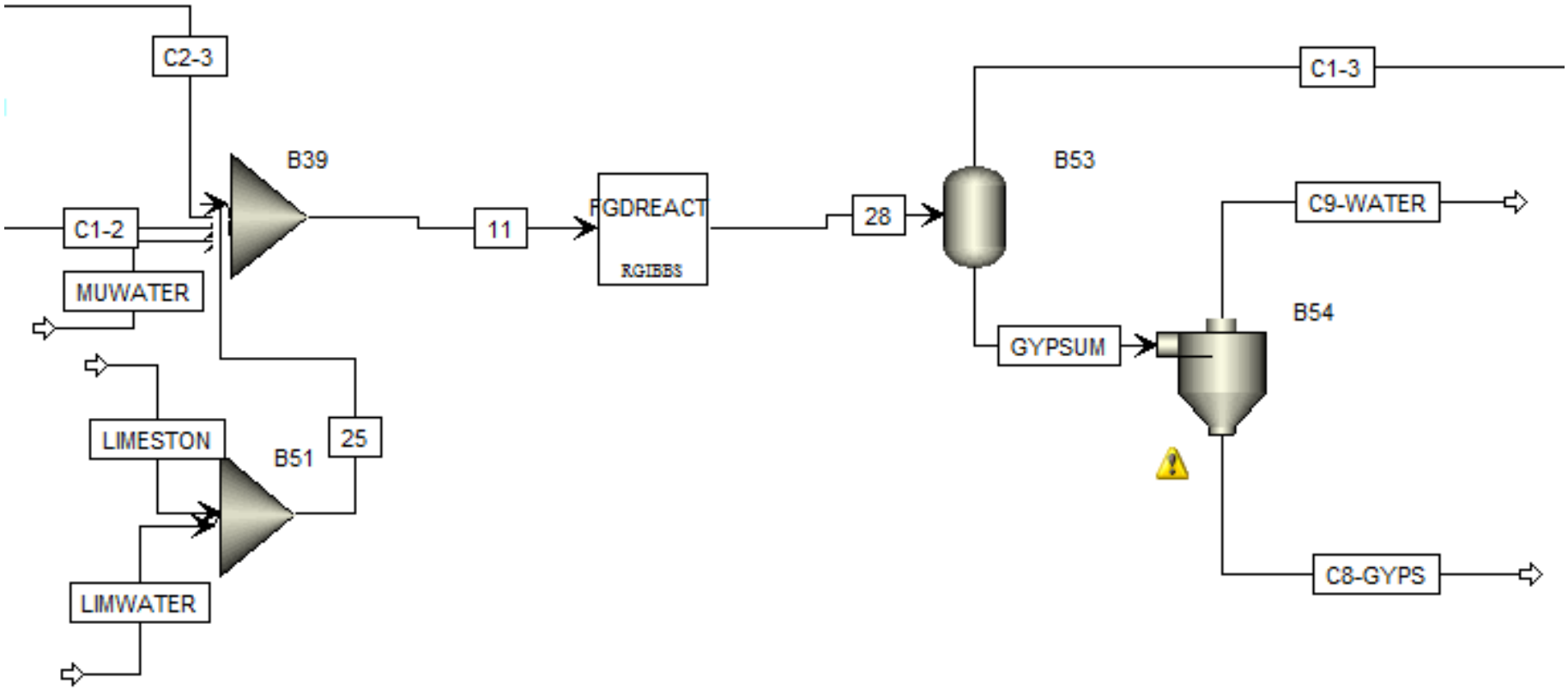

Figure 26: ASPEN plus flowsheet of flue gas desulphurization unit.

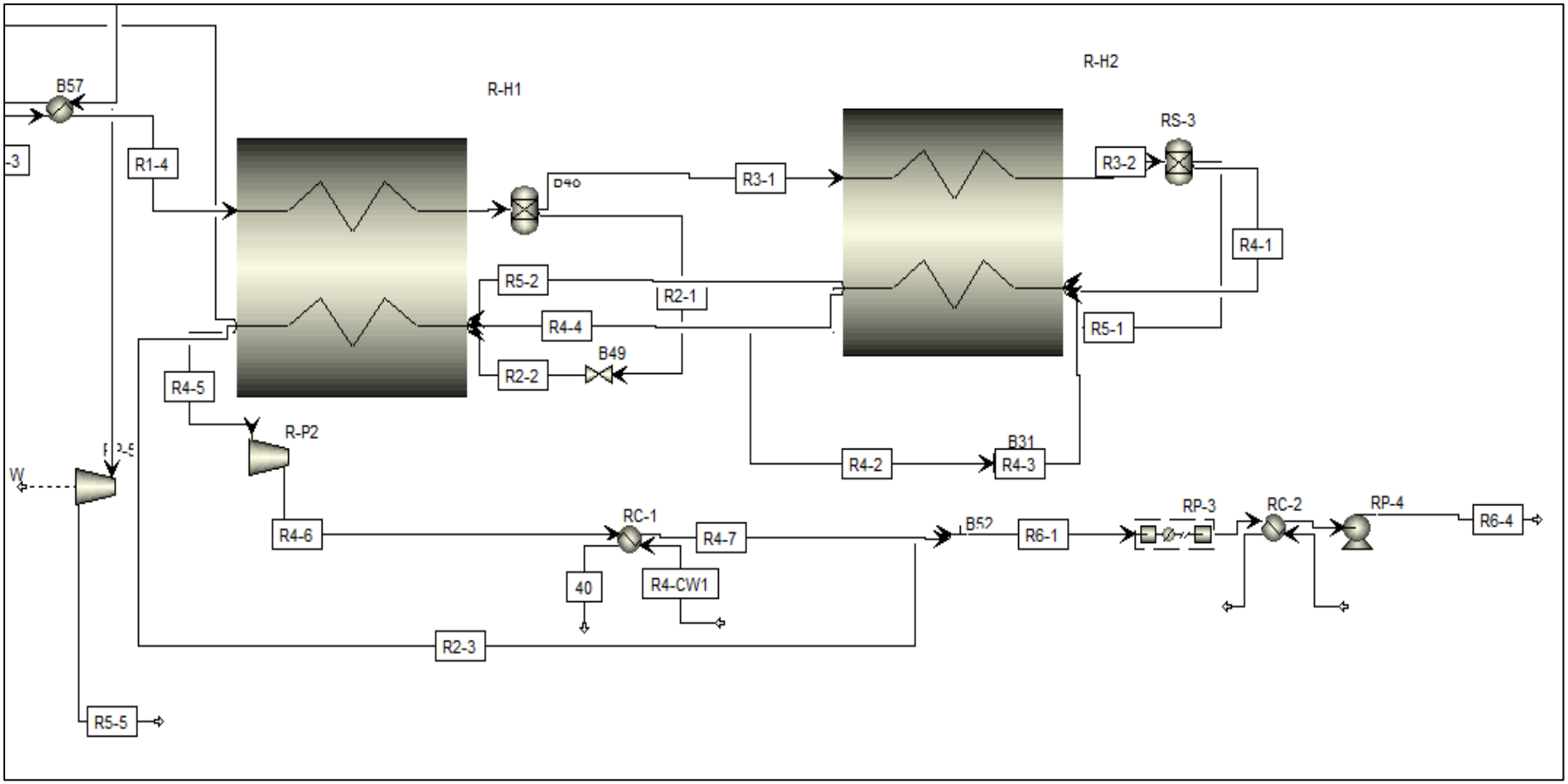

Figure 27: ASPEN plus flowsheet of double flash separation unit.

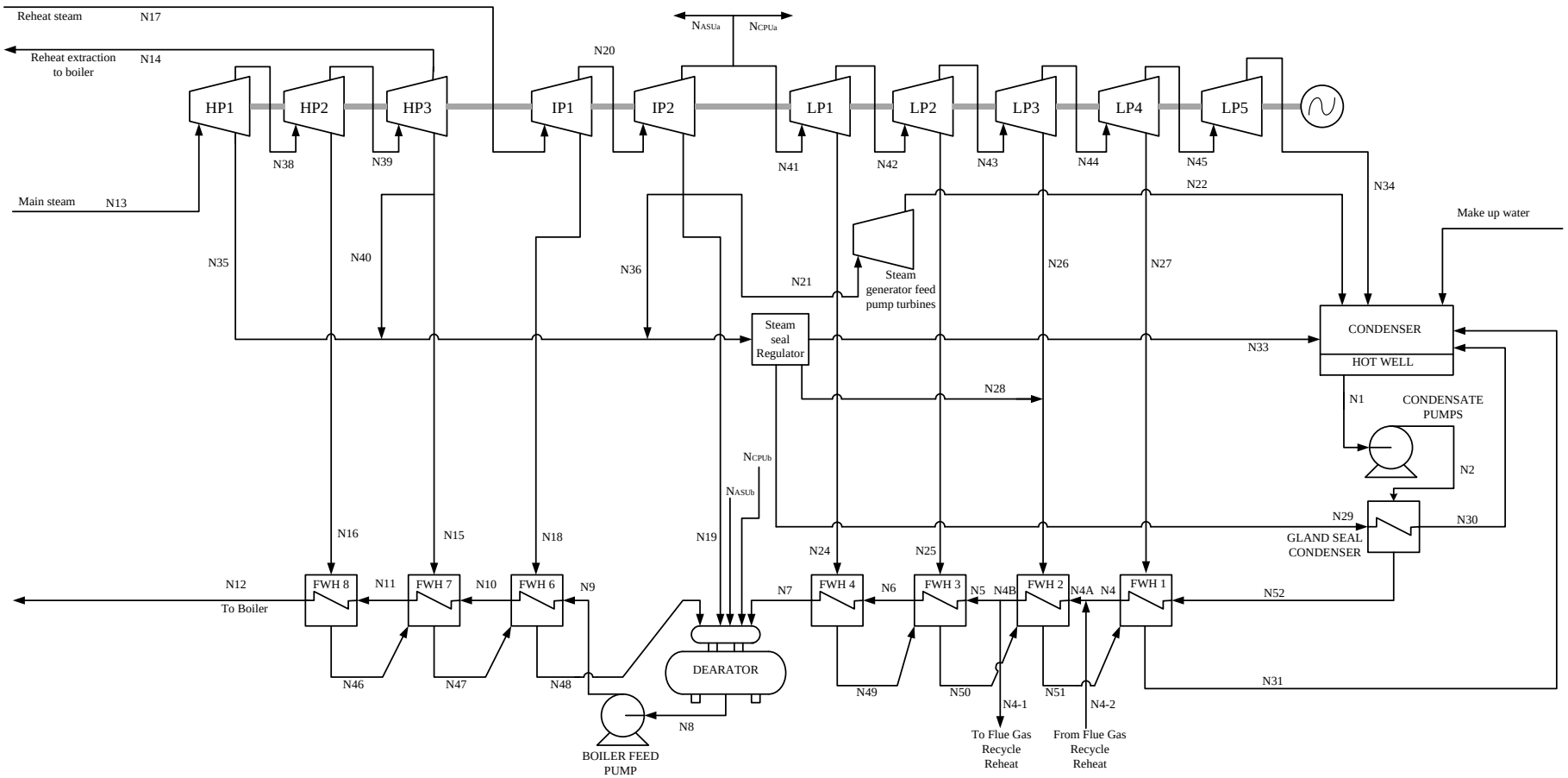

Figure 28: Detailed oxy-combustion steam cycle flowsheet.

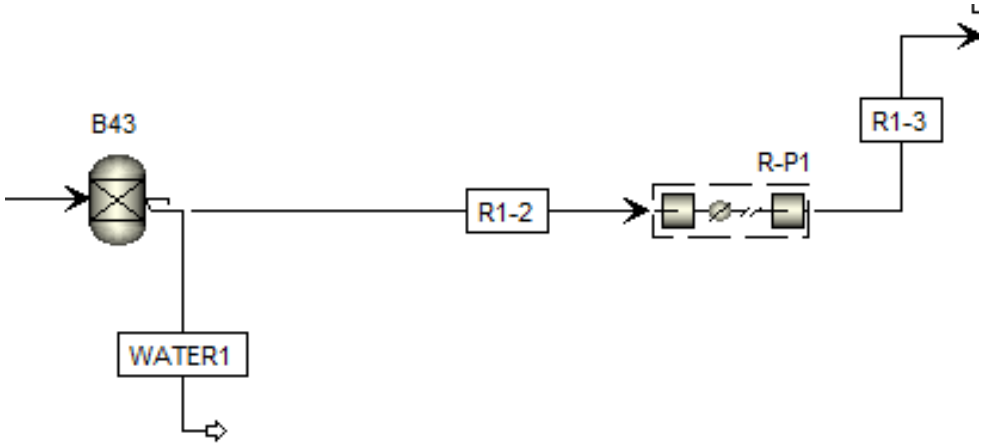

Figure 29: ASPEN plus flowsheet for compression and dewatering section before CO_2 separation in double flash separation unit.

4.3. Thermodynamic property package

The process was simulated using ASPEN PLUS V8.4. The Peng-Robinson (PR) property method was used for the ASU, combustion process and CPU. NBS/NRC steam tables are used in the steam cycle. Detailed computational specifications are listed in Table 3.

4.4. Coal characteristics and Limestone composition

Table 2 lists the coal characteristics and Table 1 gives the composition of the limestone fed to the FGD.

Table 1: Limestone composition

Component	Chemical formulae	Weight percent
Calcium carbonate	$CaCO_3$	80.4
Magnesium Carbonate	$MgCO_3$	3.5
silica	SiO_2	10.32
Aluminum Oxide	Al_2O_3	3.16
Iron Oxide	Fe_2O_3	1.24
Sodium Oxide	Na_2O	0.23
Potassium Oxide	K_2O	0.72
Balance		0.43
	Total	100

Table 2: Coal characteristics

	as received	dry
Proximate analysis (%)		
Moisture	11.12	0.00
Volatile matter	34.99	39.37
Ash	9.7	10.91
Fixed carbon	44.19	49.72
Ultimate analysis (%)		
Carbon (C)	63.75	71.73
Hydrogen (H)	4.50	5.06
Nitrogen (N)	1.25	1.41
Sulfur (S)	2.51	2.82
Chlorine (Cl)	0.29	0.33
Ash	9.70	10.91
Moisture (H2O)	11.12	0.00
Oxygen (O)	6.88	7.74
High heating value (HHV) (MJ/kg)	27.14	30.53
Low heating value (LHV) (MJ/kg)	26.17	29.45
Chemical exergy (MJ/kg)	31.95	

4.5. Computational specifications

Table 3: Computational specifications for both plants

Turbo-machinery units	
Isentropic efficiency of HP/IP/LP steam turbines	0.9/0.9/0.88
Steam turbine mechanical efficiency	0.996
Generator mechanical efficiency	0.985
Isentropic/mechanical efficiency of compressors	0.82/0.97
Isentropic/mechanical efficiency of fans	0.88/0.98
Isentropic/mechanical efficiency of the tail gas turbine	0.9/0.999
Pump efficiency (including motor driver)	0.736
gas outlet temperature of compression intercoolers (°C)	35
ASU and CPU	
Minimum temperature difference in sub-ambient heat exchangers (°C)	1.5
Temperature difference of the condenser/reboiler exchanger (°C)	1.5
Pressure drop in the pre-purification unit (bar)	0.15
Pressure drop in sub-ambient heat exchangers (%)	~3
Pressure drop in the HP column (bar)	0.1
Pressure drop in the LP column (bar)	0.1
Inlet/outlet temperatures of cooling water (°C)	25/35
Inlet/outlet temperatures of seawater (°C)	15/25
Minimum temperature difference in cooling water heat exchangers (°C)	10
Cooling water pressure (bar)	2
Steam cycle	
Pressure loss in feed water heaters (bar)	0.34
Condenser pressure (bar)	0.069

4.6. Results

The plant performance for a retrofitted (Oxy-combustion) and un-retrofitted (air fed) plant are compared in Table 4. Other auxiliaries in the table include: the coal handling and conveying, limestone handling and regent preparation, pulverizes, ash handling, precipitators, FGD pumps and agitators, steam turbine auxiliaries, circulating water pumps, cooling tower fans, transformer losses and the miscellaneous balance including the plant control systems and lighting. These auxiliaries are estimated to have load equal to 3.2% of a plants gross power production (Ciferno et al., 2008). The thermal efficiency of the un-retrofitted plant was determined to be 39.021% whilst that of the retrofitted plant was determined to be 29.772% giving an efficiency penalty of 9.249%, which is very close to the 9.4% penalty reported by Fu and Gundersen (2013). If the 789.385 MW (Gross) oxy-combustion plant were not retrofitted it would have an overall efficiency of 39.391%, which is very close to the 39.021% efficiency of the un-retrofitted 579.681MW (Gross) plant. Indicating that it is the ASU(which contributes 6.2%) and the CPU(which contributes 3.4%) which are responsible for the overall thermal efficiency penalty. This comes close to the contribution made by the ASU (6.3%) and CPU (3.4%) in the original paper (Fu and Gundersen, 2013).

Table 4: Plant performance comparison

	Basic	**Oxy-combustion**
Gross power generated (MW)	579.681	789.385
Air fans or RFG fan (MW)	N/A	3.525
Induced fan (MW)	14.410	16.072
Condensate pumps (MW)	0.680	0.931
ASU		
Main air compressor (MAC) (MW)	N/A	130.383
N2 turbine (MW)	N/A	-13.253
CPU		
CO2 compression(MW)	N/A	72.203
Tail gas turbine (MW)	N/A	-7.748
Other auxiliaries	18.55	25.26
Total auxiliaries (MW)	33.64	227.7
Net power (MW)	546.041	562.012
Net plant efficiency,%(HHV)	39.021	29.772
Coal feed (kg/s)	51.32	69.23
HHV (MJ/kg)	27.267	27.267
Thermal input of coal feed (MW)	1399.342	1887.694

5. Exergy analysis

5.1. Methodology

The exergy content of a stream of matter or quantity of heat is a measure of the amount of useful work that can be acquired from the total energy contained in the said matter or heat as it moves toward equilibrium with the environment. The energy that isn't converted to work is irreversibly lost as the system and the surroundings move to a higher state of entropy (Kotas,1985). In theory the minimum work input to a process (whether it be a separation process, compression process etc….) can be achieved if it stays infinitesimally close to equilibrium between its initial and final state. Such processes are called reversible processes. Conducting an exergy analysis on a process helps determine its thermodynamic efficiency by taking into account the exergy flows entering and leaving it. Hinderink, et al., (1996) provide a detailed means of determining the exergy content of multi component material streams containing both liquid and vapour phases ideal for use with flow-sheet simulators such as ASPEN plus V8.4. The exergy content of process streams containing liquid and solid phases were determined in the same manner. The exergy content of a stream of matter is the maximum amount of work attainable from it as it moves from its process conditions (T, P) to the dead state. The dead state being defined by thermal, mechanical and chemical equilibrium with the environment where each component is in its ambient chemical state, ambient partial pressure and ambient temperature (T_0, P_{00}) (Kotas,1985).

The total exergy content of a material stream $(\dot{E}_{tot})$ ignoring kinetic and potential exergy terms can be decomposed into three components (Hinderink et al., 1996):

$$\dot{E}_{tot} = \dot{E}_{ch} + \dot{E}_{ph} + \dot{E}_{mix} \qquad 5.1a$$

Here $\dot{E}_{ch}$, $\dot{E}_{ph}$ and $\dot{E}_{mix}$ represent the chemical, physical and mixing exergy respectively.

The exergy of mixing is the exergy difference between the mixed process components at (T, P), and the unmixed components also each at (T, P).

$$\dot{E}_{mix} = \left[\dot{F}h - \sum_i^n \left(\dot{F}_i h_i\right)\right] - T_0\left[\dot{F}s - \sum_i^n \left(\dot{F}_i s_i\right)\right] \qquad 5.1b$$

Here, $\dot{F}$ is the total stream molar flow, $\dot{F}_i$ is the component molar flow, h is the total stream enthalpy, h_i is the component molar enthalpy, s is the total stream molar entropy and s_i is the component molar entropy.

The physical exergy of a stream is the maximum work obtainable when each of its unmixed components are taken from the process conditions (T, P) to the reference conditions defined by the ambient temperature and pressure (T_0, P_0).

$$\dot{E}_{ph} = \left[\sum_i^n (\dot{F}_i h_i) - \sum_i^n (\dot{F}_{0,i} h_{0,i})\right] - T_0\left[\sum_i^n (\dot{F}_i s_i) - \sum_i^n (\dot{F}_{0,i} s_{0,i})\right] \quad 5.1c$$

In equation 5.1c, $h_{0,i}$ and $s_{0,i}$ are the component enthalpy and entropy at reference conditions (T_0, P_0) respectively. The chemical exergy of a material stream is determined by multiplying each components molar flow by its standard chemical exergy and summing this over all components in the stream. Here, $e^0_{ch,i}$ is the standard chemical exergy which takes each component to the final reference conditions (T_0, P_{00}).

$$\dot{E}_{ch} = \sum_i^n (\dot{F}_i e^0_{ch,i}) \quad 5.1d$$

The chemical exergy of the coal fed $(e^0_{ch,coal})$ was determined using equation 5.1e below (Fu and Gundersen, 2013). Here $(LHV)^0$ represents the lower heating value of the coal at reference conditions (T_0, P_0) and φ is the ratio of chemical exergy to the lower heating value determined using equation 5.1f. In equation 5.1f, the variables h, c, o and n are the mass fractions of hydrogen, carbon, oxygen and nitrogen in the ultimate analysis of coal (dry basis) respectively.

$$\varphi = e^0_{ch,coal}/(LHV)^0 \quad 5.1e$$

$$\varphi = 1.0437 + 0.1896(h/c) + 0.2499(o/c) + 0.0428(n/c) \quad 5.1f$$

The exergy content of a heat flow $(\dot{Q})$ transmitted through a control surface at temperature (T_r) can be determined using equation 5.1g below (Kotas,1985).

$$\dot{E}^Q = \dot{Q}\left(\frac{T_r - T_0}{T_r}\right) \quad 5.1g$$

The exergy loss or irreversibility of a unit operation can be determined using equation 5.1h below. Here $\dot{E}^{in}$ and $\dot{E}^{out}$ represent material, heat and work exergy flows moving in and out of the process respectively.

$$\dot{I} = \dot{E}^{in} - \dot{E}^{out} \quad 5.1h$$

The theoretical minimum work of separation is a thermodynamic ideal in which the separation unit operates reversibly and only needs to supply the required work to account for the exergy difference between the products and the feeds. It can be determined using equation 5.1i.

$$\dot{W}_{min} = \sum_{product} \dot{E}_{tot}^{product} - \sum_{feed} \dot{E}_{tot}^{feed} \quad 5.1i$$

Here, $\sum_{product} \dot{E}_{tot}^{product}$ represents the sum of the exergy of all the components in the product stream and $\sum_{feed} \dot{E}_{tot}^{feed}$ represents the sum of the exergy of all components in the feed stream.

5.2. Assumptions

In conducting their research Fu and Gundersen (2013) made the following simplifying assumptions: (1) The exergy of the ash is assumed to be zero. (2) The exergy of the limestone slurry is calculated as the exergy of its two main constituents: water (70 wt%) and calcium carbonate ($CaCO_3$). The exergy of gypsum is calculated in similar way; as the sum of the exergy of water (10 wt%) and solid gypsum ($CaSO_4.2H_2O$). The chemical exergy of ($CaCO_3$) and ($CaSO_4.2H_2O$) is obtained from (Szargut et al., 1988). (3) The reaction heat of the FGD unit is ignored. The chemical exergy of the waste water in the FGD unit is also ignored. (4) Ignoring the physical exergy of the solids (coal, limestone, gypsum). (5) Assuming the ambient air is composed only of N_2, O_2, Ar, CO_2 and H_2O. This ignores other noble gases and inorganic substances present in ambient air. (6) The exergy of impurities (H_2O and CO_2) in the ASU are ignored.

The new more relaxed set of assumptions used to conduct this revisit are: (1) The exergy of the ash is assumed to be zero. (2) The exergy of the limestone slurry and the gypsum was calculated as the exergy of components $CaCO_3, MgCO_3, SiO_2, Al_2O_3, Fe_2O_3, Na_2O, K_2O$, solid gypsum $CaSO_4.2H_2O$ and water where applicable. Their chemical exergies where all obtained from (Kotas,1985). (3) The physical exergy of the coal feed was ignored (4) The ambient air was assumed to be composed of ($N_2, O_2, Ar, CO_2, H_2O, Ne, He$ and CH_4).

5.3. Exergy analysis results and discussion

Table 5 places the main ASU exergy analysis results of those of Fu and Gundersen (2013) (under the column ‘Original work’) alongside those obtained in this thesis (under the column ‘Revisited work’). Figure 30 shows the distribution of exergy losses in the original work alongside those in

the revisited work. There is little discrepancy between the two sets of results. This could be attributed to the fact that the constituents added to the original air composition exist in trace amounts, and have standard chemical exergy values comparable with the main constituents accounted for in the original work. Including the exergy of the impurities separated out in the temperature swing adsorption unit also made little difference. This stream of impurities contains only trace elements, so its flowrate is simply too small for it to possess a significant amount of exergy.

The units contributing the most to ASU process irreversibility are the main air compressor followed by the distillation column. The irreversibility's in the compressor can be reduced by increasing compressor efficiency, increasing the number of isothermal stages in the compressor and decreasing the compressor operating temperature.

Table 5: Results of ASU exergy analysis

Air separation unit results	**Original work**	**Revisited work**
Air compressor irreversibility (MW)	34	37.941
Distillation irreversibility (MW)	29.6	30.026
Heat exchanger irreversibility (MW)	11.5	18.729
A-DCA & A-PPU (MW)	8.5	12.266
Nitrogen turbine (MW)	1.9	2.478
Exergy input (main air compressor) (MW)	128	130.383
N_2 turbine output (MW)	10.2	13.253
Minimum work of separation (MW)	26.9	30.026
Specific power consumption (kWh/kgO_2)	0.23	0.251
Specific minimum work of separation (kWh/kgO_2)	0.053	0.058
Nitrogen vented (MW)	12.6	9.07

All actions would approximate reversible operation, reduce compression work and reduce the irreversibility's in the intercoolers (Kotas,1985). Increasing the compressor efficiency or the number of compression stages is likely infeasible though as this would require replacing the unit. Lowering the operating temperature of a compressor may effect overall operation significantly. So a study this action would have on downstream processes would be required.

(a) (b)

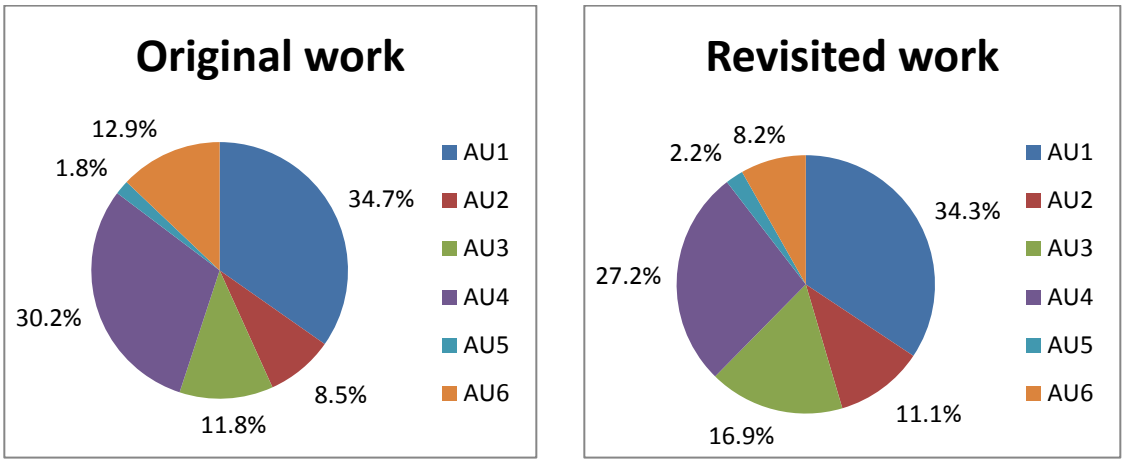

Figure 30: Distribution of exergy losses in ASU: a) Original work of Fu and Gundersen (2013); b) revisited work. The Figure is presented in color.

The irreversibility's in the distillation column are associated with irreversible heat and mass transfer between the ascending vapour and descending liquid within the column. Reversible operation can be approximated in a distillation column by increasing the number stages. This reduces irreversibility's associated with heat transfer by reducing the temperature disparity between the ascending gas and descending liquid at each stage (Kotas,1985). It also reduces reboiler duty and enhances mass transfer by having the operation run closer to the equilibrium curve (Fu and Gundersen, 2012). This can be achieved with intermediate condensers and reboilers (Kotas,1985). One could also improve the mass transfer in the column by artificial irrigation through a sparger using an external pump on each stage, which overcomes the reduced wetted surface that come with low reflux ratios associated with low reboiler duties (Bhole, et al., 2016) . The exergy losses in the main heat exchanger can be overcome by optimizing the temperature profiles between its hot and cold streams.

Table 6: Major results for combustor and steam cycle exergy analysis

Combustion & steam cycle	**Original work**	**Revisited work**
Boiler area irreversibility (MW)	1158	885.218
HP turbine irreversibility (MW)	13	17.929
Rest of the steam cycle irreversibility (MW)	112	104.23
Coal exergy input (MW)	2211	1961.928
Gross power output (MW)	792	789.386

Table 6 and Figure 31 place the results of the combustor and steam cycle exergy analysis (major results and exergy loss distribution) in the original work alongside those in the revisited work. Much like the ASU there is little difference here between the two sets of results, with the major contributor to process irreversibility being the boiler area in both cases. The similarity between the two could again be attributed to the fact that the trace elements added to the feed and infiltration air have chemical exergies very similar to the constituents in the original work. The additional solid components included in the limestone slurry and gypsum product also have compositions and chemical exergies too low to make a significant impact on the FGD unit irreversibility. Including the physical exergies of the slurry feed solid components had little impact because the stream is fed into the flue gas desulphurization unit at the environmental state ($T_{0,}P_0$), and so the exergy of mixing (which in this case is very small on account of the solid components being immiscible in water) along with the chemical exergy were the only total exergy components that weren't zero. The gypsum product and the FGD waste water's relatively low temperature, flowrate and immiscible solid content result in it having physical and mixing exergy values too low to make a real difference. Accounting for the reaction heat from the flue gas desulphurization unit also made little difference. This heat is delivered at a relatively low temperature resulting in it having low exergy content. Any minor differences between the two sets of results are more likely as a result of the different sources from which the standard chemical exergies were obtained.

(a) (b)

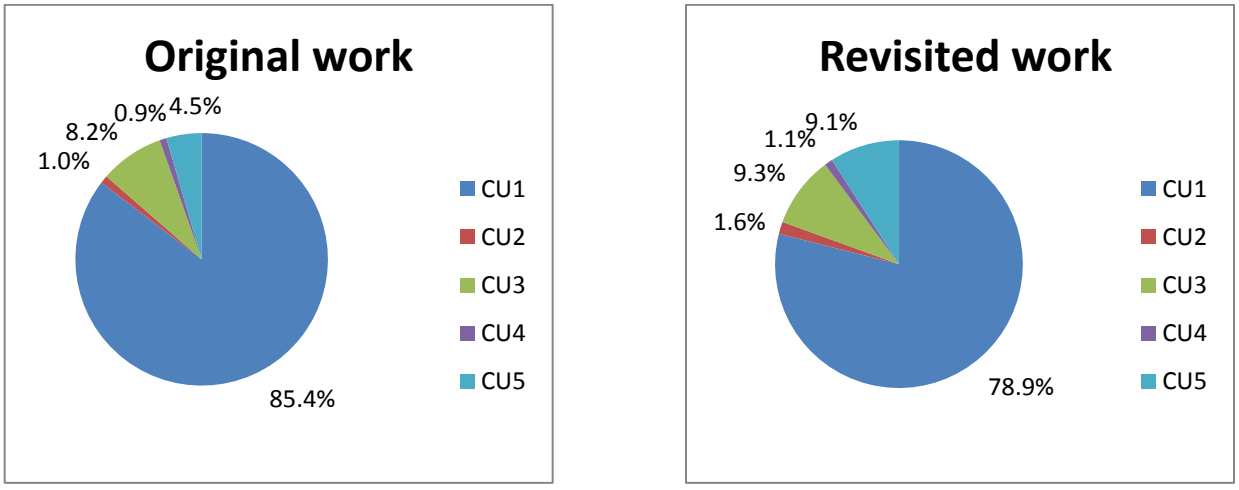

Figure 31: Distribution of exergy losses over combustor and steam cycle: a) Original work; b) Revisited work. The Figure is presented in color.

Causes for the large irreversibility associated with combustion include: the degradation of very orderly chemical exergy to lower quality thermal energy or 'heat', incomplete combustion, irreversible transmition of heat to the working fluid and exhaust losses to down-stream flue gas treatment units (Kotas,1985). Recycling the flue gas before the FGD would improve boiler efficiency as this process robs the flue gas of sensible heat (Mousavian & Mansouri, 2011). The boilers operating pressure could be increased. As mentioned before this increases the saturation temperature of the water separated out in the flue gas condenser and makes it feasible to integrate this unit with the steam cycle (Chen et al., 2012). Switching to ultra-supercritical steam cycle conditions can reduce boiler irreversibility by increasing the temperature at which the working fluid accepts heat. This action can also decrease the irreversibility's in the steam cycle by increasing the gross power output. This is likely infeasible though as it would require replacement of many major plant units.

Table 7: Major results for compression and purification unit exergy analysis

CPU	**Original work**	**Revisited work**
Exergy "power input" (MW)	73	78.606
Tail gas turbine output (MW)	9	7.748
Net power consumption (MW)	64	64.456
Specific work $(kWh/kgCO_2)$	0.114	0.114
Minimum work of separation (MW)	37	33.905
Minimum specific work $(kWh/kgCO_2)$	0.067	0.06
Irreversibility of [RU1] (MW)	17.3	21.195
Irreversibility of [RU3] (MW)	7	7.481

(a) (b)

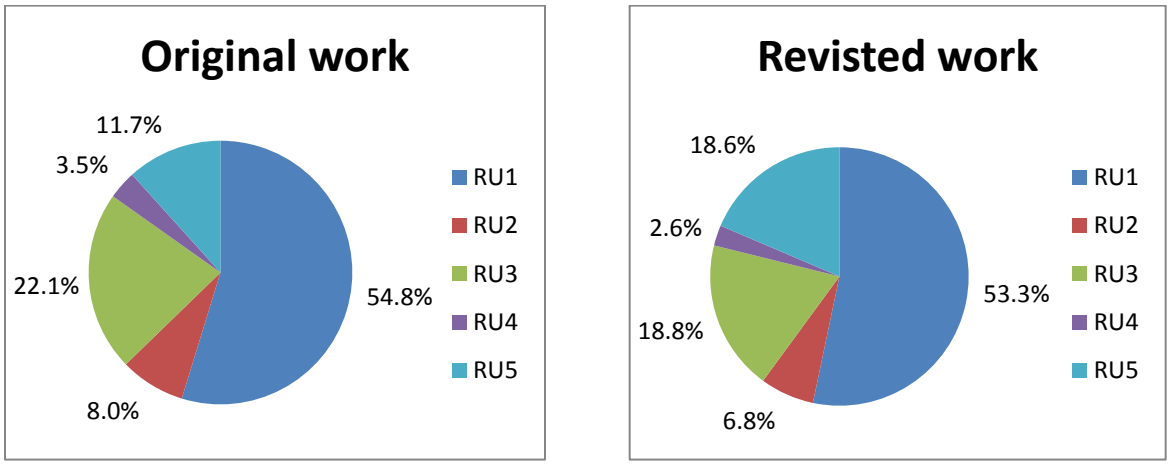

Figure 32: Distribution of exergy losses over compression and purification process: a) Original work; b) Revisted work. The Figure is presented in color.

Table 7 and Figure 32 place the results of the CPU exergy analysis (major results and exergy loss distribution) in the original work alongside those in the revisited work. The results are very similar, with the carbon dioxide compression processes being responsible for the majority of the exergy losses in both sets of results. The same recommendations made for possibly reducing the exergy losses associated with compression processes and heat exchangers in the ASU apply here.

(a) (b)

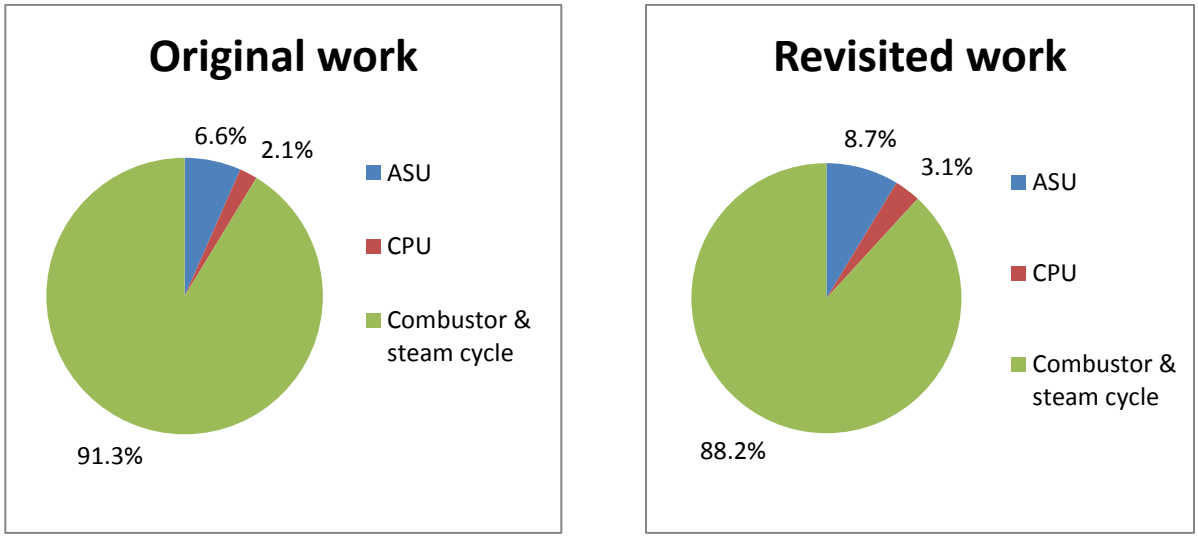

Figure 33: Distribution of exergy losses over entire plant: a) Original work; b) Revisited work. The Figure is presented in color.

Figure 33 shows the distribution of exergy losses over the entire plant in both the original, and the revisited work. The combustor and the steam cycle are responsible for the majority of the exergy losses in both sets of results.

If the minimum work of separation in both the ASU and CPU could be achieved this efficiency penalty would come down to 3% with the ASU contributing 1.5% and the CPU contributing 1.7%. This is similar to the results obtained by Fu and Gundersen (2013) were this minimum efficiency penalty was determined to be 3.4%, with the ASU contributing 1.4% and the CPU contributing 2%.

Figure 34 shows the effect of compressor efficiency on plant performance. The net plant efficiency increases from 28.6% to 30.694% as the compressor isentropic efficiencies increase from 0.74 to 0.9. This is similar to the effect it had in the original work where the net thermal efficiency increased form 29.3% to 31.4%.

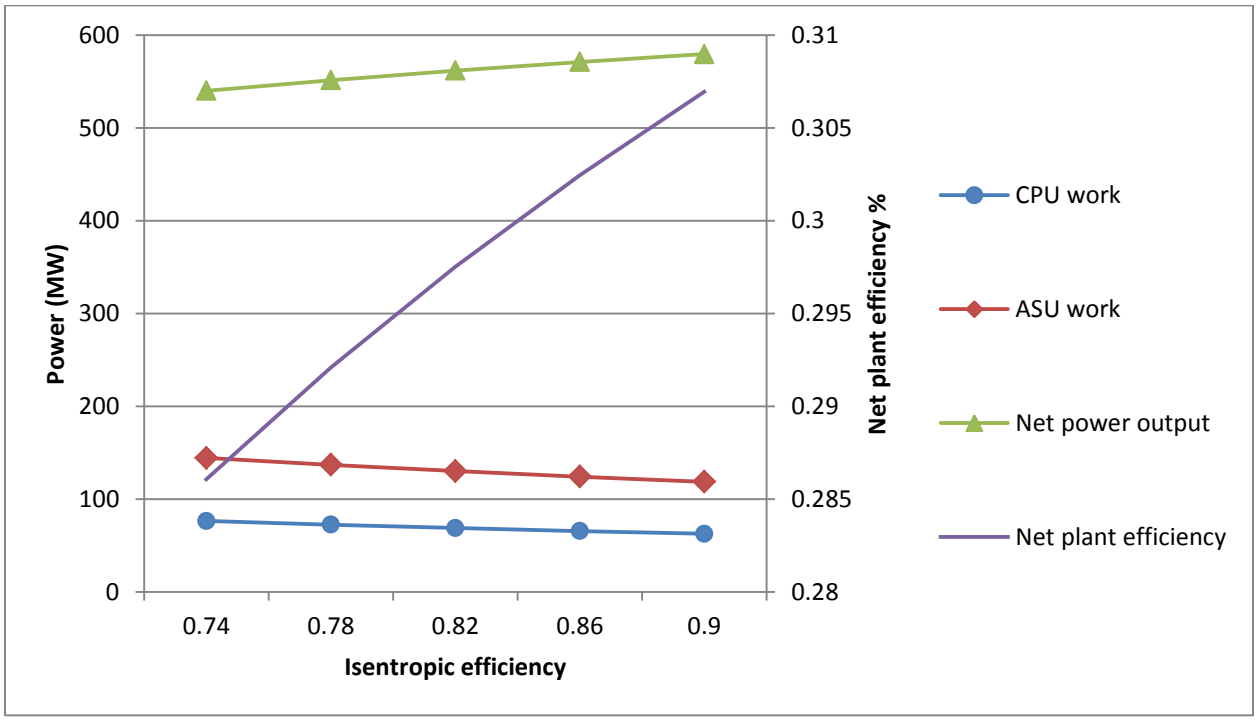

Figure 34: Effect of compressor isentropic efficiency on plant performance. The Figure is presented in color.

6. Heat integration

A heat integration study identical to that in the original work by Fu and Gundersen (2013) was performed to determine again if loosening the assumptions from the original work would alter the original findings. The exergy analysis indicates that the compression processes in the ASU and CPU are chiefly responsible for the energy penalty associated with oxy-combustion. This study attempts to determine the feasibility of using the heat evolved in the multi-stage compression processes to pre heat the boiler feed water in the steam cycle. This would reduce their impact on overall plant performance as less steam would need to be extracted from the turbines for boiler feed water pre heating which increases the retrofitted plants overall gross power output. This paper investigates the thermal efficiency improvement achievable in 4 integration schemes. Each integration scheme is investigated as a case study. In one of the case studies (case study 2), the temperature of the compression heat in the main air compressor is lifted by reducing the number of its compression stages. This allows the compressor to be integrated with higher pressure feed water heaters and so reduction of steam extraction at higher pressure turbines can be achieved. This reduces compressor efficiency and increases compression work though.

6.1. Decomposing the steam cycle

Figure 28 is a detailed flowsheet of the oxy-combustion steam cycle referred to in this section. The gland seal condenser preheats the boiler feed water to 39.05℃ before it reports to the low pressure feed water heaters (N3). The four low pressure feed water heaters (FWH1-4) heat this stream further to 145.85℃ before it reports to the deaerator which removes dissolved gasses. Water leaving the deaerator is pumped to 290 bar and further heated to 290.8℃ in the three remaining feed water heaters in the high pressure section (FWH6-8). As the boiler feed water flows through a FWH it's heated by steam extracted from turbines and condensate from higher pressure FWH's ahead of it. A larger portion of the heating is done by the extracted steam. Compression heat, carried by the hot gasses in the compressors in the ASU and CPU can be used to heat the boiler feed water and thus reduce the demand for extracted steam. It's important then to know the heat contribution of each extracted steam level so as to accurately determine the required steam flow to satisfy the demand that cannot be met by the compression heat. The heat loads in each feed water heater are decomposed in Figure 35. The contributions made by

extracted steam and higher pressure condensate are separated out in each feed water heater. The bottom arrow moving from right to left represents the heated boiler feed water. The boiler feed water heat demand in each feed water heater was determined using results from ASPEN plus. The streams moving from left to right in a step wise manner from one feed water heater to the next are the cooled extracted steam flows. Though their contributions are separated out, their actually mixed in each FWH. As the condensate moves from one FWH to the next it's flashed to a lower pressure and condensed again at a lower saturation temperature. Hence the sudden drop in temperature as a stream moves from one FWH to next. The heat loads of the extracted steam flows could not be determined directly through ASPEN plus. So they were estimated instead using steam tables.

6.2. Integration steps

Each integration study is carries out in the following steps:

1. Determine the supply temperature of the compression heat and thus the FWH's for which the compression heat can be integrated.
2. Draw the grand composite curve (GCC) which determines the minimum utility requirements at different temperature levels for a heat exchanger network (Smith, 2005).
3. Use the grand composite curve along with Figure 35 to determine the demand for extracted steam in each FWH. Only the extracted steam load in each FWH is taken into consideration. The contribution made by the condensate from higher pressure FWH's (including the gland seal condenser) is neglected. This means the compressed gases are cooled to temperatures higher than 49.08℃ at the exit of FWH1.
4. The compressed gasses are further cooled to 35℃ after leaving FWH1to reduce compression work.

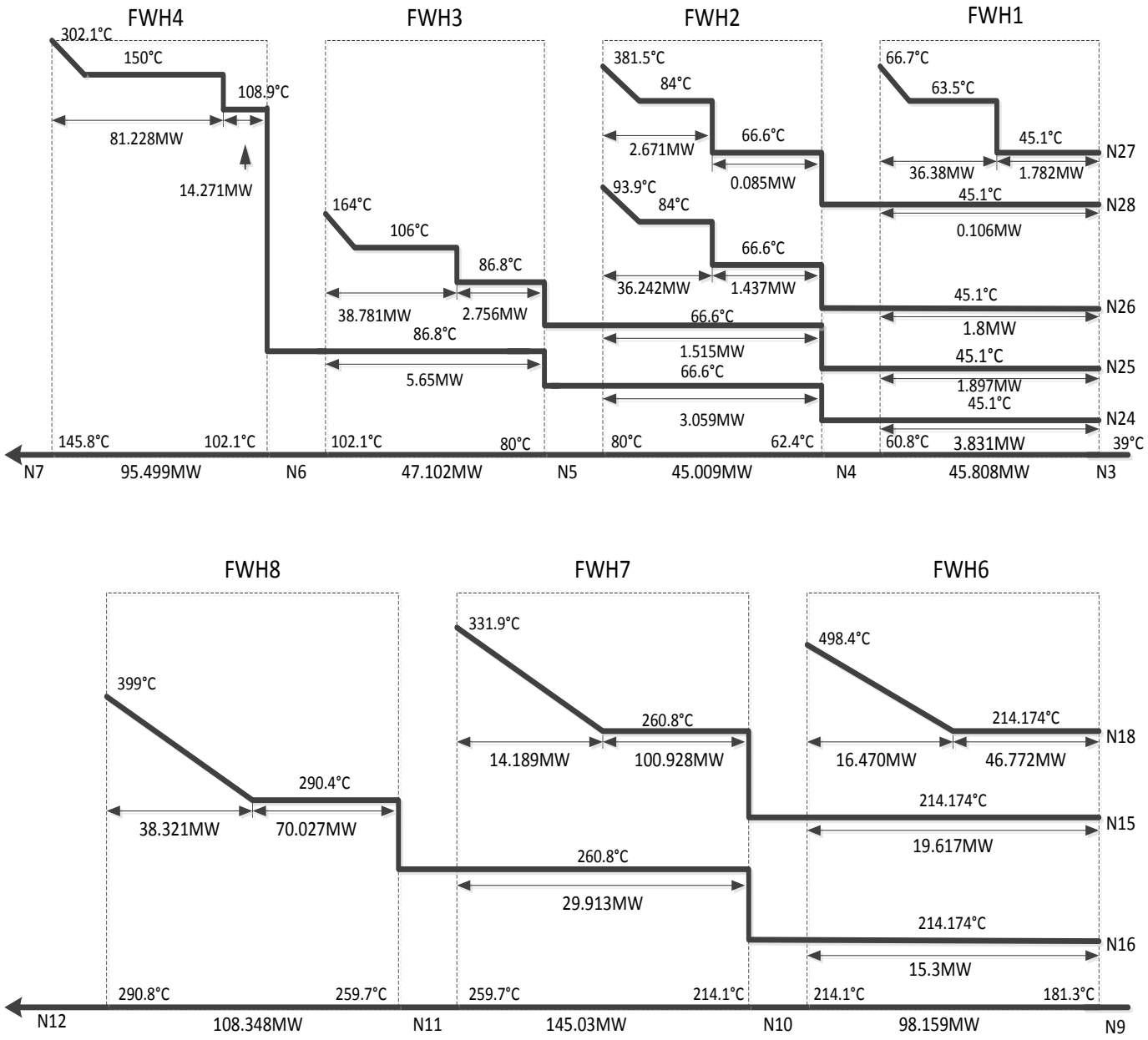

Figure 35: Decomposed heat loads in the each FWH (before integration).

In conducting this heat integration study the following assumptions are made:

1. The minimum temperature difference for the gas water heat exchangers is 10℃. Since the boiler feed water is fed to FWH1 at 39.08℃, this means the compressed gases can be cooled at most to around 49.08℃ in FWH1.
2. The pressure drop on the gas side of the gas water heat exchangers is neglected.
3. The pressure levels of extracted steam are maintained.
4. The compressor efficiency is the same for all compression stages.
5. The steam seal regulator and the deaerator are not influenced by the heat integration.

6.3. Case Studies

The heat integration potential for 4 case studies is investigated: in case 1 and 2 only the ASU is integrated, in case 3 only the CPU is integrated and in case 4 both the ASU and the CPU are integrated. When integrating the CPU only the compression heat from compressors R-P1 and R-P3 is integrated.

Detailed below is a description of the four case studies:

Case 1: The main air compressor has three stages with intercooling. The compression ratio for each stage is equal (i.e. 1.77).

Case 2: The main air compressor (MAC) has two stages with intercooling. With equal compression ratio for each stage (i.e. 2.35)

Case 3: Compressor R-P1 has five stages with equal pressure ratio and compressor R-P3 has 2 stages with equal pressure ratio.

Case 4: The compression schemes in case 1 (three stage compression in ASU) and case 3 (multi stage compression in CPU) are used.

Table 8 gives the stage characteristics across each compressor case 1, case 2 and case 3. Table 9 gives the boiler feed water CP's across each feed water heater.

Table 8: Stage number, inlet temperature ($\boldsymbol{Tin}\,(\boldsymbol{Kelvin})$), outlet temperature ($\boldsymbol{Tout}\,(\boldsymbol{Kelvin})$), cooling duty ($\Delta\boldsymbol{H}(\boldsymbol{MW})$), compression ratio (Comp ratio) and $\boldsymbol{CP}(\boldsymbol{MW}/℃)$ at each stage and in every compressor for case 1, case 2 and case 3.

Case 1					
A-P1					
Stage number	$Tin\,(Kelvin)$	$Tout\,(Kelvin)$	$\Delta H(MW)$	Comp ratio	$CP(MW/℃)$
Stage 1	362.363	308.15	34.667	1.77	0.64
Stage 2	374.471	308.15	42.511	1.77	0.64
Stage 3	374.471	308.15	43.818	1.77	0.64
Case 2					
A-P1					
Stage number	$Tin\,(Kelvin)$	$Tout\,(Kelvin)$	$\Delta H(MW)$	Comp ratio	$CP(MW/℃)$
Stage 1	398.173	308.15	57.69	2.35	0.64
Stage 2	411.453	308.15	67.761	2.35	0.64
Case 3					
R1-2					
Stage number	$Tin\,(Kelvin)$	$Tout\,(Kelvin)$	$\Delta H(MW)$	Comp ratio	$CP(MW/℃)$
Stage 1	370.421	308.15	10.157	1.99	0.163
Stage 2	370.57	308.15	10.264	1.99	0.164
Stage 3	370.861	308.15	10.483	1.99	0.167
Stage 4	371.415	308.15	10.954	1.99	0.173
Stage 5	372.397	308.15	12.046	1.99	0.187
R6-1					
Stage number	$Tin\,(Kelvin)$	$Tout\,(Kelvin)$	$\Delta H(MW)$	Comp ratio	$CP(MW/℃)$
Stage 1	357.226	308.15	8.722	1.88	0.178
Stage 2	366.913	308.15	1.711	1.88	0.291

Table 9: boiler feed water CP's across feed water heaters 1, 2 and 3.

	$CP(MW/℃)$
FWH4	2.185324394
FWH3	2.131327059
FWH2	2.55735
FWH1	2.101298532

The following takes case 1 as an illustrative example. The three hot streams from the outlet of each compression stage of compression process A-P1 are (see Table 8): H1(89.213℃ →35℃), H2(101.321℃ →35℃), H3(101.321℃ →35℃). Therefore the compression heat can be integrated with FWH1-3. The CP value (specific heat capacity multiplied by mass flow rate) for the hot gasses in the first compression stage of A-P1 (H1) was determined to be 0.64(MW/℃). This value was also assigned to the total heat capacities of H2 and H3. The CP's for the boiler feedwater flowing through feed water heaters (FWH) 1, 2 and 3 were determined to be 2.1, 2.56 and 2.13 respectively (see Table 9). Assuming that no steam is extracted for FWH1-3 (i.e. the heat is supplied only by the compressed gasses), and that the contribution made by the condensate form FWH4 and the steam from the steam seal regulator (N28) are negligible the following grand composite curve (GCC) (Figure 36) was produced. Based on the grand composite curve, the minimum hot utility demand in FWH3 is 32.611MW, in FWH2 is 11.72MW and in FWH3 is 3.952MW. One can then use Figure 35 to determine the required extracted steam flowrates to satisfy the minimum utility demand that cannot be met by the compression heat in each FWH. These flowrates are shown in Table 10. The new decomposed heat loads (compression heat not included) are shown in Figure 37. Figure 38 shows the decomposed heat loads in FWH1-3 with the compression heat included. The solid line running along the bottom of Figure 38 represents the boiler feed water. The dotted line running along the top represents the compressed gasses. Each FWH in Figure 38 has been divided into 3 sections to better depict the heat contributions made by the extracted steam, the compressed gasses and the mixed condensates. The section to left represents the contribution made by the extracted steam, the section in the center represents the contribution made by the compressed gasses and the section to the right represents the contribution made by the condensates.

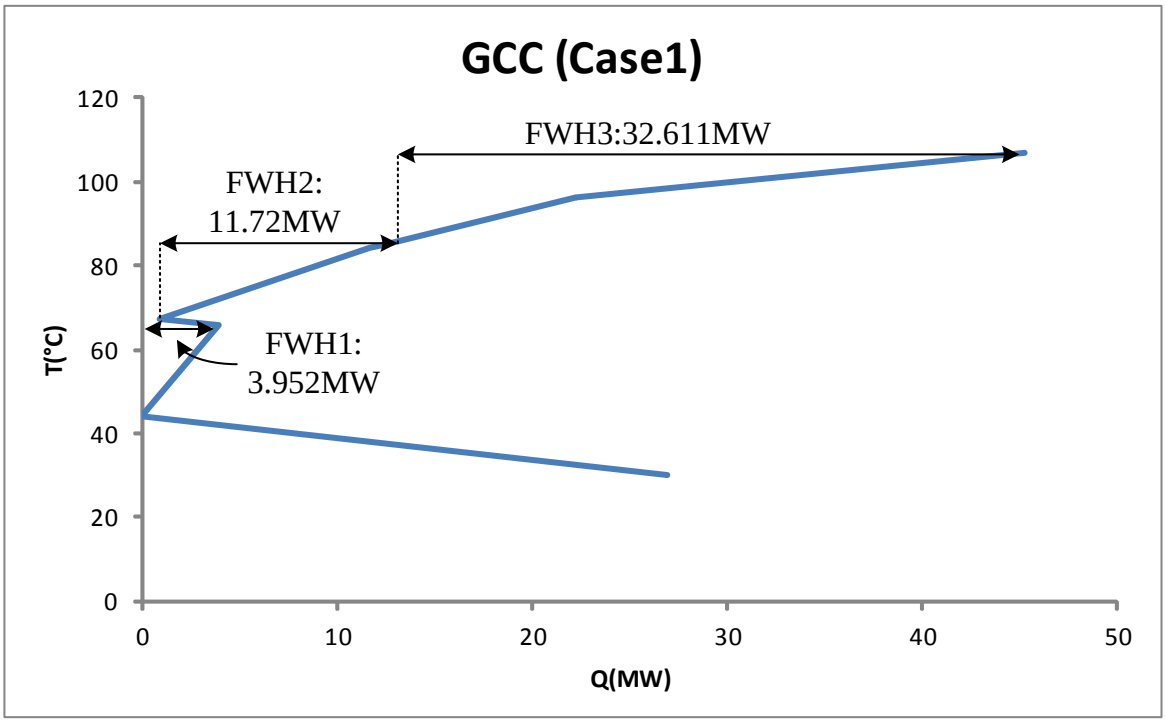

Figure 36: The GCC for FWH1-3 in Case 1.

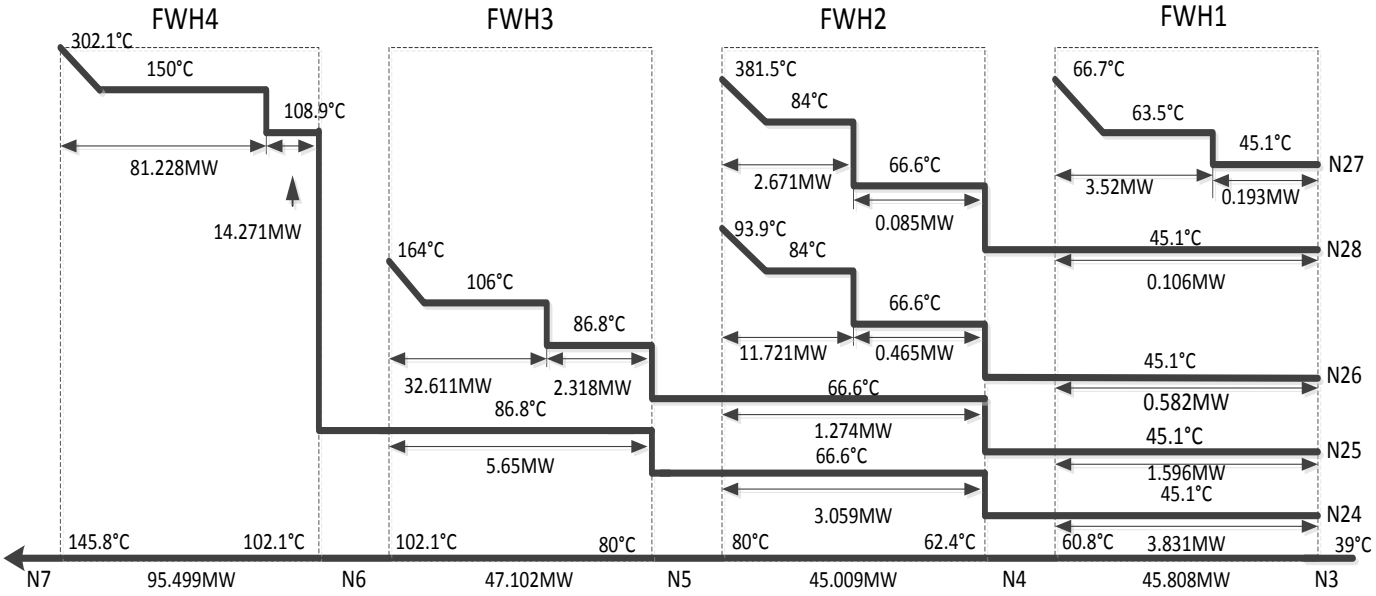

Figure 37: Decomposed heat loads in the each FWH (for case 1). Compression heat not included.

6.4. Results of heat integration study

The main heat integration results are shown in Table 10. Recorded in the results for each case study are: the highest temperature of the compressed gasses, the work in the ASU and CPU, the gross power output, the net power output, the thermal efficiency and the extracted steam flows. Figures 39-41 are the GCC for cases 2, 3 and 4 respectively. Case 1 gave a net thermal efficiency improvement of 0.36% which is close that reported in the original work of 0.38%. Case 2 gave a net thermal efficiency improvement of 0.289% while that in the original work gave an improvement of 0.38%. Case three gave a net thermal efficiency improvement of 0.296% while that in the original work gave an improvement of 0.27%. Finally, case 4 gave a net thermal efficiency improvement of 0.679% while that in the original work gave an improvement of 0.72%.

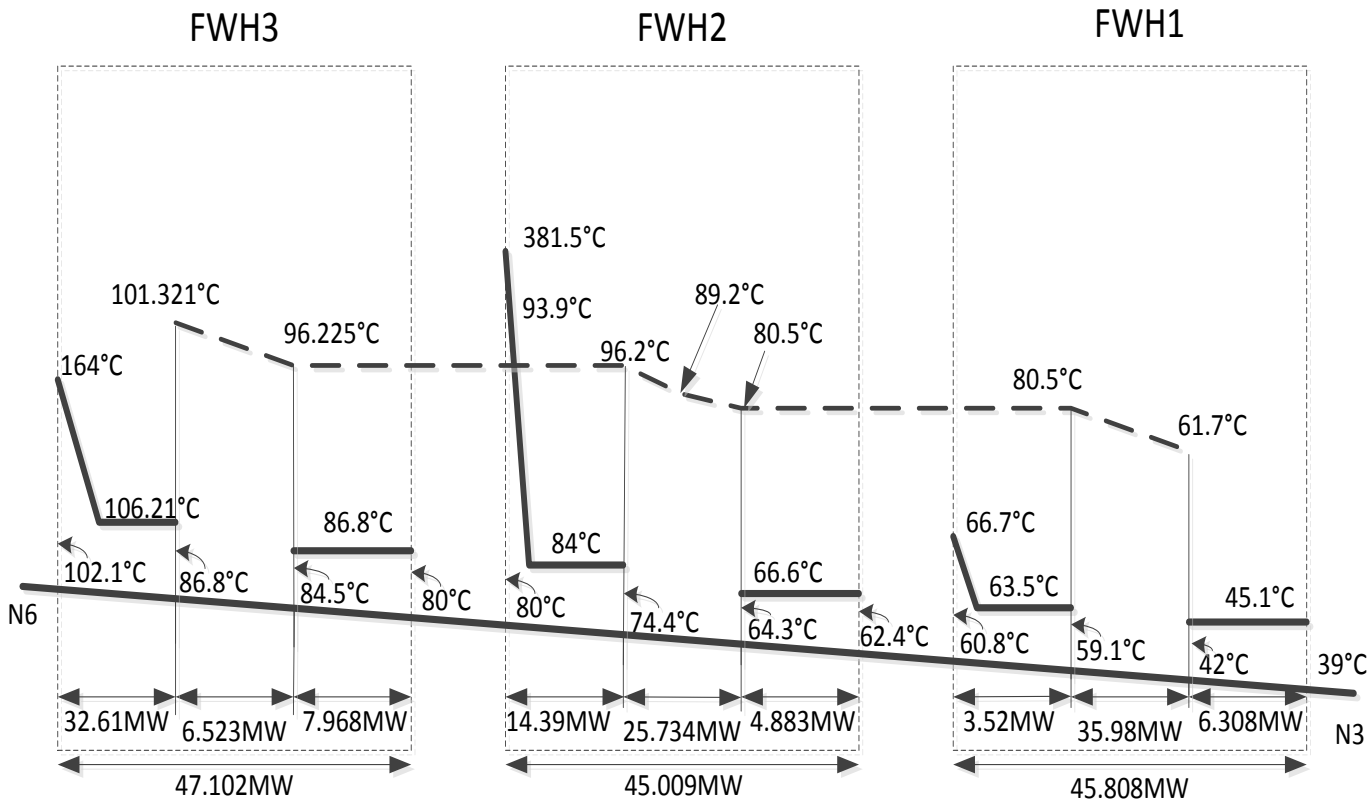

Figure 38: Decomposed heat loads in FWH1-3 (for case 1). Compression heat included.

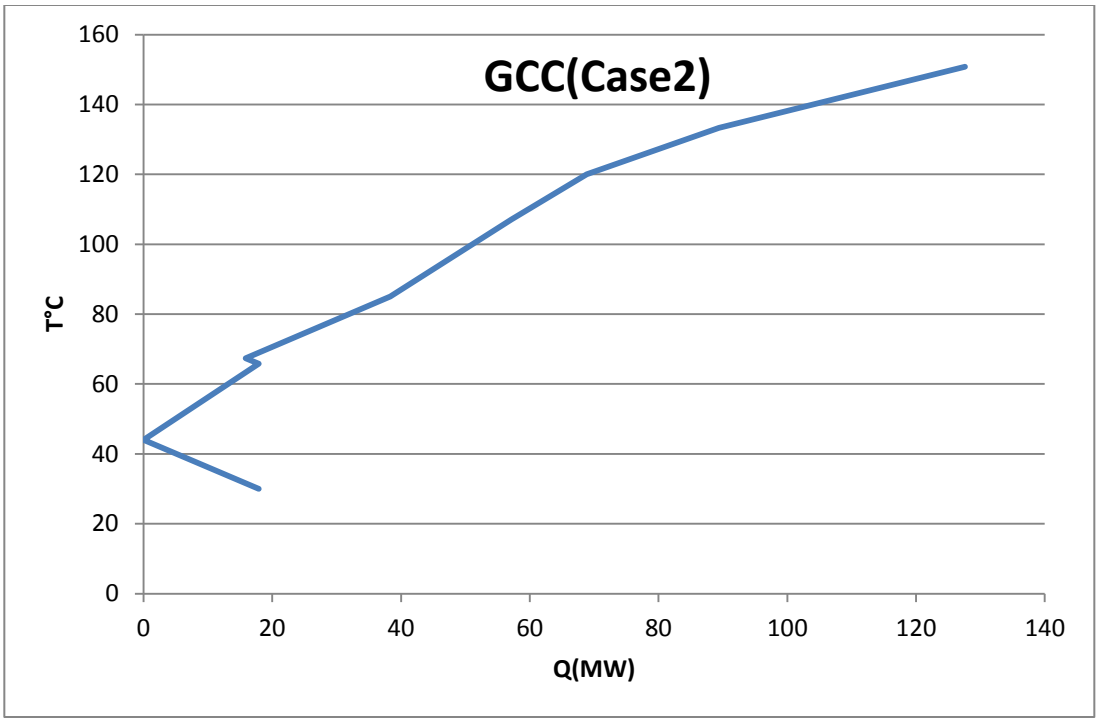

Figure 39: GCC for case 2.

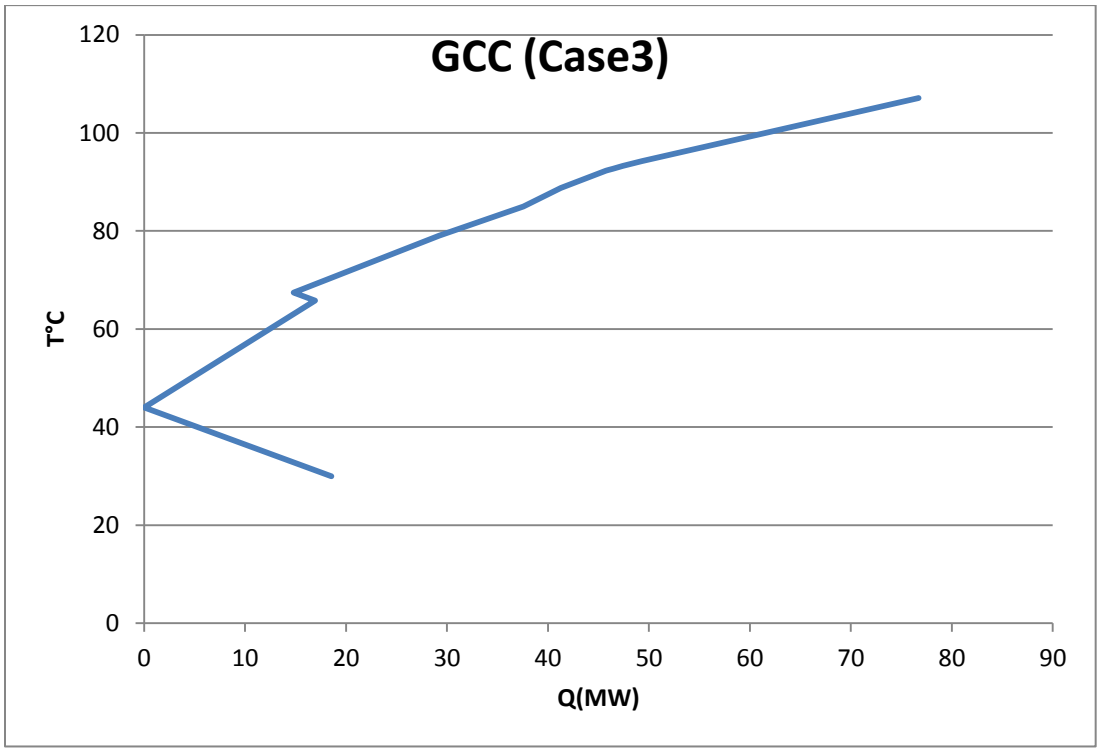

Figure 40: GCC for case 3.

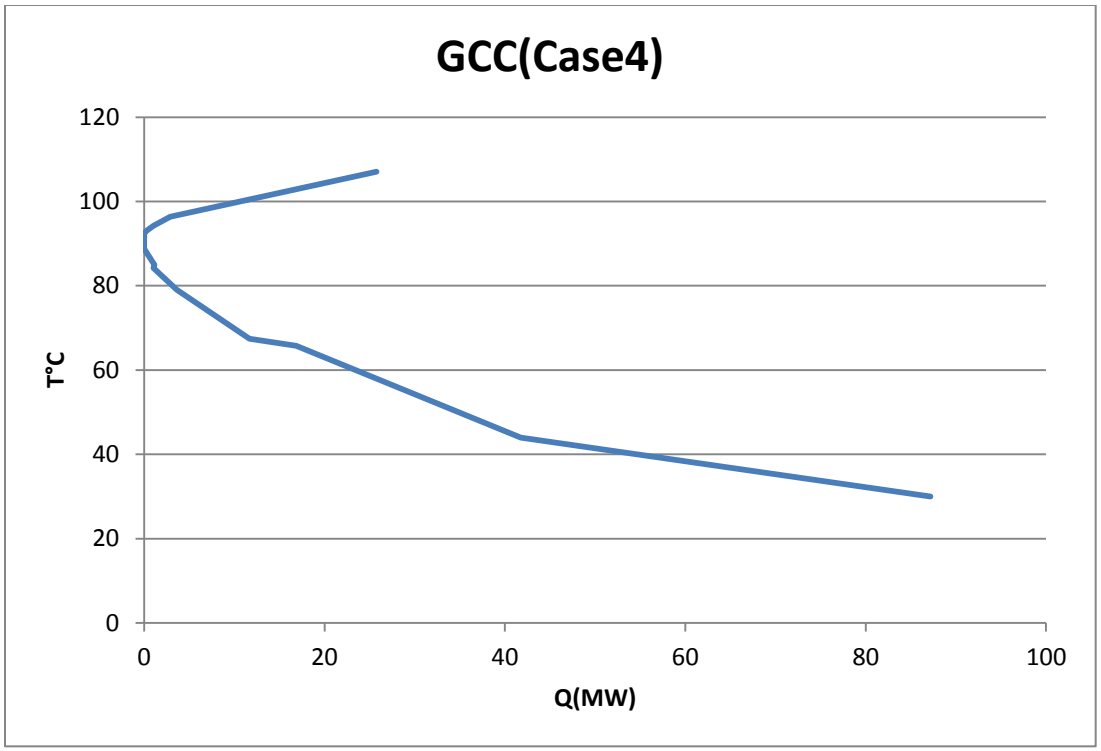

Figure 41: GCC for case 4.

Table 10: Main heat integration results

Heat integration results	Without integration	Case 1	Case 2	Case3	Case 4
Highest, T_{gas}, ℃	101.321	101.321	138.303	99.247	101.321
Work in the ASU, MW	117.129277	116.065	120.5489	117.1293	116.065
Work in the CPU, MW	64.4558263	64.45583	64.455826	61.46114	61.46114
Gross power, MW	789.385988	795.3038	798.2644	791.9864	798.1468
Net power, MW	561.628488	568.6106	567.08728	567.2236	574.4482
Thermal efficiency, %	29.7520872	30.12196	30.041265	30.04849	30.43121
Steam flow, kg/sec					
N15	60.901	60.901	60.901	60.901	60.901
N16	47.501	47.501	47.501	47.501	47.501
N18	24.844	24.844	24.844	24.844	24.844
N24	33.232	33.232	28.825778	33.232	33.232
N25	16.456	13.84143	7.9853661	16.456	10.92487
N26	15.617	5.051985	9.6898242	9.807298	0
N27	15.457	1.679231	7.6071171	7.196444	0

7. Conclusions

The efficiency penalty associated with oxy-combustion was found to be 9.249%, whilst that in the original work was 9.4%. In this work the theoretical minimum energy consumption in the ASU and CPU results in a net plant thermal efficiency penalty of 3% whilst that in the original work is 3.4%. The irreversibility around the flue gas desulphurization unit was found to be 21.195 MW whilst that in the original work was 17.3MW. The actual and minimum specific work of separation in the ASU was found to be 0.251(kWh/kgO_2) and 0.058(kWh/kgO_2) respectively whilst those in the original work were found to be 0.23(kWh/kgO_2) and 0.058(kWh/kgO_2) respectively. The actual and minimum specific work of separation in the CPU was found to be 0.114($kWh/kgCO_2$) and 0.06($kWh/kgCO_2$) respectively whilst those in the original work were found to be 0.114($kWh/kgCO_2$) and 0.067($kWh/kgCO_2$) respectively.

Relaxing the assumptions in the original work of Fu and Gundersen (2013) had little impact on the exergy analysis results. The components added to the air composition exist in trace amounts and have chemical exergy values not large enough to make a real impact. The same can be said for the impurities accounted for in the ASU. The physical exergy of the limestone slurry was determined to be zero on account of the fact that the stream is fed in at the environmental state. As a result the only total exergy component for the limestone slurry feed that isn't zero apart from the chemical exergy is the exergy of mixing. However even the exergy of mixing proved insignificant on account of the solid limestone components being immiscible in water. The gypsum products relatively low temperature, flowrate and immiscible solid content result in it too having physical and mixing exergy values too low to make a real difference. The reaction heat from the flue gas desulphurization unit is delivered at too low a temperature to have a large enough exergy content to make difference.

The net thermal efficiency increased steadily from 28.6% to 30.694% when the isentropic efficiency in all compressors was increased from 0.74 and 0.9. This was similar to the result in the original work were the thermal efficiency increased from 29.3% to 31.4%. Integrating both the ASU and CPU with the steam cycle improved the thermal efficiency by 0.679% in this work, and by 0.72% in the original work.

8. Bibliography

Almås, K. (2012) *Coal-fired Power Plants based on Oxy-combustion with Carbon Capture : Combustion Conditions and Water Consumption*. Norwegian University of Science and Technology.

Beér, J. M. (2007) 'High efficiency electric power generation: The environmental role', *Progress in Energy and Combustion Science*, 33(2), pp. 107–134.

Bhole, S, L., Patil, N, P., Patil, V, S. and Gharpure, M, G. (2016) 'Improvement in stage efficiency and Reduction in Energy Consumption of Ditillation Through Artificial Irrigation', *Journal of Advanced Chemical Sciences*, 2(2), pp. 219–222.

Buhre, B. J. P., Elliott, L. K., Sheng, C. D., Gupta, R. P. and Wall, T. F. (2005) 'Oxy-fuel combustion technology for coal-fired power generation', *Progress in Energy and Combustion Science*, 31(4), pp. 283–307.

Burnard, K. and Bhattacharya, S. (2011) *Power generation from coal: Ongoing Developments and Outlook*.

Chen, L., Yong, S. Z. and Ghoniem, A. F. (2012) 'Oxy-fuel combustion of pulverized coal: Characterization, fundamentals, stabilization and CFD modeling', *Progress in Energy and Combustion Science*. Elsevier Ltd, 38(2), pp. 156–214.

Ciferno, J., Haslbeck, J., Black, J., Kuehn, N., Lewis, E., Rutkowski, M., Woods, M. and Vaysman, V. (2008) *Pulverized Coal Oxycombustion Power Plants Volume 1 : Bituminous Coal to Electricity Final Report*.

Coal Industry Advisory Board (2010) '"Power Generation from Coal: Measuring and Reporting Efficiency Performance and CO2 Emissions"', pp. 1–111.

Edenhofer, O., Pichs-Madruga, R., Sokona, Y., Minx, J. C., Farahani, E., Susanne, K., Seyboth, K., Adler, A., Baum, I., Brunner, S., Eickemeier, P., Kriemann, B., Savolainen, J., Schlomer, S., von Stechow, C. and Zwickel, T. (2014) 'Climate Change 2014: Mitigation of Climate Change', *Working Group III Contribution to the Fifth Assessment Report of the Intergovernmental Panel on Climate Change*, 3, pp. 1–1435.

EU Commission (2005) *"Winning the battle against global climate change"*. Brussels.

Folger, P. (2010) *Carbon capture: a technology assessment*. Lincon.

Fu, C. and Gundersen, T. (2012) 'Techno-economic analysis of CO 2 conditioning processes in a coal based oxy-combustion power plant', *International Journal of Greenhouse Gas Control*. Elsevier Ltd, 9,

pp. 419–427.

Fu, C. and Gundersen, T. (2012b) 'Using exergy analysis to reduce power consumption in air separation units for oxy-combustion processes', *Energy*. Elsevier, 44(1), pp. 60–68.

Fu, C. and Gundersen, T. (2013) 'Exergy Analysis and Heat Integration of a Coal-Based Oxy-combustion Power Plant', *Energy & Fuels*, 27, pp. 7138–7149.

Hanak, D. P., Biliyok, C., Yeung, H. and Bia??ecki, R. (2014) 'Heat integration and exergy analysis for a supercritical high-ash coal-fired power plant integrated with a post-combustion carbon capture process', *Fuel*. Elsevier Ltd, 134, pp. 126–139. doi: 10.1016/j.fuel.2014.05.036.

Hands, B, A. (1986) *Cryogenic Engineering*. London: Academic press.

Herold, J., Rüster, S. and Hirschhausen, C. Von (2010) *Carbon capture; transport and storage in Europe: A problematic energy bridge to nowhere?*, *FEEM Note di Lavoro*.

Hinderink, A. P., Kerkhof, F. P. J. M., Lie, A. B. K., De Swaan Arons, J. and Van Der Kooi, H. J. (1996) 'Exergy analysis with a flowsheeting simulator - I. Theory; calculating exergies of material streams', *Chemical Engineering Science*, 51(20), pp. 4693–4700.

Hough, S. (2009) 'Supercritical Rankine Cycle', pp. 1–11.

Houghton JT, Y, D., DJ, G., M, N., PJ, van der L., X, D., K, M. and C, J. (2001) *Climate Change 2001: The Scientific Basis*, *Climate Change 2001: The Scientific Basis*.

Hu, Y. (2011) *CO2 capture from oxy-fuel combustion power plants*. KTH Royal Institue of Technology.

IEA (International energy agency) (2013) *World Energy Outlook 2013*, *International Energy Agency*. Paris, France.

IEAGHG (2010) *OXYFUEL COMBUSTION OF PULVERISED COAL*.

Kanniche, M., Gros-Bonnivard, R., Jaud, P., Valle-Marcos, J., Amann, J. M. and Bouallou, C. (2010) 'Pre-combustion, post-combustion and oxy-combustion in thermal power plant for CO2 capture', *Applied Thermal Engineering*. Elsevier Ltd, 30(1), pp. 53–62.

Kotas, T, J. (1985) *The Exergy Method of Thermal Plant Analysis*. Essex: Butterworths.

Kumar Mohanty, D., Venkatesh BITS Pilani K Birla Goa Campus, V. K., Nagar, Z. and -, G. (2014) 'Performance Analysis of a Combined Cycle Gas Turbine Under Varying Operating Conditions', *Mechanical Engineering: An International Journal (MEIJ)*, 1(2), pp. 11–25.

Lockwood, T. (2014) *Developments in oxyfuel combustion of coal*. London.

Mancuso, L., Wheeler, F., Ferrari, N. and Wheeler, F. (2013) 'Integration of carbon capture unit with power generation : technology advances in oxy-combustion plants', in *3rd Oxy-fuel Combustion conference*, pp. 1–22.

Molina, A. and Shaddix, C. R. (2007) 'Ignition and devolatilization of pulverized bituminous coal particles during oxygen/carbon dioxide coal combustion', *Proceedings of the Combustion Institute*, 31, pp. 1905–1912. doi:

Mousavian, S. M. and Mansouri, M. T. (2011) 'Conceptual feasibility study of retrofitting coal-fired power plant with oxy-fuel combustion', *Proceedings of the Institution of Mechanical Engineers, Part A: Journal of Power and Energy*, 225(6), pp. 689–700.

Petit, R. J., Raynaud, D., Basile, I., Chappellaz, J., Ritz, C., Delmotte, M., Legrand, M., Lorius, C. and Pe, L. (1999) 'Climate and atmospheric history of the past 420,000 years from the Vostok ice core, Antarctica', *Nature*, 399, pp. 429–413.

Pipitone, G. and Bolland, O. (2009) 'Power generation with CO2 capture: Technology for CO2 purification', *International Journal of Greenhouse Gas Control*, 3(5), pp. 528–534.

Smith, R. (2005) *Chemical Process Design and Integration*. West Sussex: John Wiley & Sons LTD.

Soundararajan, R. (2015) *Oxy-combustion coal based power plants with CO2 capture : Process integration approach to reduce capture penalty*. Norwegian University of Science and Technology.

Suda, T., Masuko, K., Sato, J., Yamamoto, A. and Okazaki, K. (2007) 'Effect of carbon dioxide on flame propagation of pulverized coal clouds in CO2/O2 combustion', *Fuel*, 86(12–13), pp. 2008–2015.

Szargut, J., Morris, D, R. and Steward, F, R. (1988) *Exergy Analysis of Thermal, Chemical & Metallurgical Processes*. New York: Hemisphere.

Szatkowski, A. (2009) *Modeling Carbon Dioxide Capture from a Supercritical Power Plant with ASPEN Plus*. Lehigh University.

Toftegaard, M. B., Brix, J., Jensen, P. A., Glarborg, P. and Jensen, A. D. (2010) 'Oxy-fuel combustion of solid fuels', *Progress in Energy and Combustion Science*. Elsevier Ltd, 36(5), pp. 581–625.

Wallace, F, J. and Linning, W, A. (1970) *Basic Engineering Thermodynamics*. Pitman publishing.

Zhu, Q. (2013) *Developments in fluidised bed combustion technology*.

Zhu, Q. (2015) 'High-efficiency power generation – review of alternative systems', pp. 1–120.

9. Appendix

9.1. Oxy-combustion stream results

Stream information for Figure 20

Stream name	A0	A1-1	A1-2	A1-3	A2-1	A2-2	A2-3	A3-1	A3-2
$T(K)$	298.15	308.15	301.15	99.03734	99.68747	89.71747	83.66103	95.7022	92.2022
$P(Pa)$	101325	560000	560000	560000	560000	560000	140000	560000	560000
$\dot{M}(Kg/sec)$	630	630	626.0947	626.0947	343.8243	343.8243	343.8243	152.3348	152.3348
$\dot{E}_{tot}$	1.335408	93.77704	93.77491	239.5887					
Mole fractions									
H_2O	0.009901	0.009901	0	0	0	0	0	0	0
N_2	0.773085	0.773085	0.781124	0.781124	0.599869	0.599869	0.599869	0.986242	0.986242
O_2	0.207423	0.207423	0.20958	0.20958	0.384252	0.384252	0.384252	0.011565	0.011565
NO_2	0	0	0	0	0	0	0	0	0
NO	0	0	0	0	0	0	0	0	0
S	0	0	0	0	0	0	0	0	0
SO_2	0	0	0	0	0	0	0	0	0
SO_3	0	0	0	0	0	0	0	0	0
H_2	0	0	0	0	0	0	0	0	0
Cl_2	0	0	0	0	0	0	0	0	0
HCl	0	0	0	0	0	0	0	0	0
CO	0	0	0	0	0	0	0	0	0
CO_2	0.000365	0.000365	0	0	0	0	0	0	0
Ar	0.009201	0.009201	0.009297	0.009297	0.015879	0.015879	0.015879	0.002192	0.002192
Ne	1.78E-05	1.78E-05	0.00E+00	0.00E+00	0.00E+00	0.00E+00	0.00E+00	0.00E+00	0.00E+00
He	4.95E-06	4.95E-06	0.00E+00	0.00E+00	0.00E+00	0.00E+00	0.00E+00	0.00E+00	0.00E+00
CH_4	1.78E-06	1.78E-06	0.00E+00	0.00E+00	0.00E+00	0.00E+00	0.00E+00	0.00E+00	0.00E+00

Stream information for Figure 20

Stream name	A3-3	A4-1	A4-2	A4-3	A4-4	A5-1	A5-2	A7-1	A7-2
$T(K)$	80.44114	95.7017	283.5021	183.8431	283.5431	92.65846	283.3626	80.80727	101.6291
$P(Pa)$	140000	560000	525000	100000	100000	140000	140000	140000	140000
$\dot{M}(Kg/sec)$	152.3348	129.5864	129.5869	129.5869	129.587	144.595	144.5978	351.91	351.91
$\dot{E}_{tot}$		42.26689	22.61173	6.8808	2.901254	104.6933	20.01084		62.60298
Mole fractions									
H_2O	0	0	0	0	0	0	0	0	0
N_2	0.986242	0.993974	0.993954	0.993954	0.99395	0.01392	0.013769	0.977734	0.978109
O_2	0.011565	0.004866	0.004884	0.004884	0.004887	0.95524	0.95538	0.017654	0.017332
NO_2	0	0	0	0	0	0	0	0	0
NO	0	0	0	0	0	0	0	0	0
S	0	0	0	0	0	0	0	0	0
SO_2	0	0	0	0	0	0	0	0	0
SO_3	0	0	0	0	0	0	0	0	0
H_2	0	0	0	0	0	0	0	0	0
Cl_2	0	0	0	0	0	0	0	0	0
HCl	0	0	0	0	0	0	0	0	0
CO	0	0	0	0	0	0	0	0	0
CO_2	0	0	0	0	0	0	0	0	0
Ar	0.00	0.00116	0.001163	0.001163	0.001163	0.03084	0.030852	0.004613	0.00456
Ne	0	0	0	0	0	0	0	0	0
He	0	0	0	0	0	0	0	0	0
CH_4	0	0	0	0	0	0	0	0	0

Stream information for Figure 20

Stream name	C0	C1-1	C1-2	C1-3	C2-1	C2-2	C2-3	C3-1	C3-2
$T(K)$	298.15	450.15	455.2405	330.15	283.3149	283.3149	371.1071	330.15	339.25
$P(Pa)$	101325	101353	95579.06	101325	140000	140000	310000	101325	101325
$\dot{M}(Kg/sec)$	69.23	720.9656	719.7264	700.0573	141.7975	2.769991	2.76389	504.0413	504.0413
$\dot{E}_{tot}$	1961.928	373.3308			19.5229	0.381376			
Mole fractions									
H_2O	N/A	0.20086	0.20098	0.151031	0	0	0	0.151031	0.151031
N_2	N/A	0.082446	0.080458	0.086038	0.015538	0.015538	0.012942	0.086038	0.086038
O_2	N/A	0.002467	0.002577	0	0.953738	0.953738	0.956302	0	0
NO_2	N/A	4.72E-08	4.88E-08	0	0	0	0	0	0
NO	N/A	0.000248	0.000252	0	0	0	0	0	0
S	N/A	5.01E-09	5.03E-09	0	0	0	0	0	0
SO_2	N/A	0.004147	0.004199	0.002081	0	0	0	0.002081	0.002081
SO_3	N/A	1.32E-06	1.36E-06	0	0	0	0	0	0
H_2	N/A	7.97E-04	0.000793	4.31E-06	0	0	0	4.31E-06	4.31E-06
Cl_2	N/A	2.81E-09	2.87E-09	0	0	0	0	0	0
HCl	N/A	1.05E-03	0.001057	0.001127	0	0	0	0.001127	0.001127
CO	N/A	1.15E-02	0.01152	4.5E-10	0	0	0	4.5E-10	4.5E-10
CO_2	N/A	0.670607	0.672307	0.73181	0	0	0	0.73181	0.73181
Ar	N/A	2.58E-02	0.025851	0.027727	0.030723	0.030723	0.030756	0.027727	0.027727
Ne	N/A	2.05E-06	2.06E-06	2.19E-06	0	0	0	2.19E-06	2.19E-06
He	N/A	2.87E-06	2.88E-06	3.07E-06	0	0	0	3.07E-06	3.07E-06
CH_4	N/A	2.01E-18	1.94E-18	0.000176	0	0	0	0.000176	0.000176

Stream information for Figure 20

Stream name	C4-1	R1-1	R1-2	R1-3	R1-4	R1-5	R2-1	R2-2	R2-3
$T(K)$	333.1793	330.15	308.15	308.15	308.15	246.444	247.15	244.5487	297.5544
$P(Pa)$	110000	101325	101325	3200000	3200000	3200000	3140000	2200000	2200000
$\dot{M}(Kg/sec)$	645.5265	196.3765	181.8462	182.1927	182.5083	182.1927	116.928	116.928	116.9522
$\dot{E}_{tot}$		78.60571			110.0563				71.68589
Mole fractions									
H_2O	0.112981	0.151031	0	0	0	0	0	0	0
N_2	0.067622	0.088143	12.52083	0.101365	0.103855	0.101365	0.014467	0.014467	0.014857
O_2	0.240925	0	0	0	0	0	0	0	0
NO_2	0	0.00E+00	0	0	0	0	0	0	0
NO	0	0	0	0	0	0	0	0	0
S	0	0.00E+00	0	0	0	0	0	0	0
SO_2	0.001557	0.002014	0.654577	0.002452	0.002373	0.002452	0.000356	0.000356	0.000345
SO_3	0	0.00E+00	0	0	0	0	0	0	0
H_2	3.22E-06	4.13E-06	7E-05	5.07E-06	4.86E-06	5.07E-06	7.36E-07	7.36E-07	7.07E-07
Cl_2	0	0.00E+00	0	0	0	0	0	0	0
HCl	0.000843	1.12E-03	0.20788	0.001328	0.001325	0.001328	0.000193	0.000193	0.000193
CO	3.36E-10	5.30E-10	5.8E-08	5.3E-10	6.24E-10	5.3E-10	7.56E-10	7.56E-10	8.93E-10
CO_2	0.547443	0.729738	162.8537	0.862183	0.859817	0.862183	0.976756	0.976756	0.976368
Ar	0.02849	2.77E-02	5.609142	0.032667	0.032626	0.032667	0.008228	0.008228	0.008237
Ne	1.64E-06	2.19E-06	0	0	0	0	0	0	0
He	2.30E-06	3.06E-06	0	0	0	0	0	0	0
CH_4	1.32E-04	2.51E-04	0	0	0	0	0	0	0

Stream information for Figure 20

Stream name	C5	C6	C8	C9	ASH	ASUimpure	RDCA-H2O
$T(K)$	298.1	298.15	330.4	330.4	450.1	301.1	308.1
$P(Pa)$	101325	101325	105000	105000	91146.25	560000	101325
$\dot{M}(Kg/sec)$	17.97	29.17	9.179	60.497	6.605	4.254	13.823
$\dot{E}_{tot}$	1.485113	1.457263	0.877792	3.365371		0.431624	0.870997
Mole fractions							
H_2O	0.923606	1	0.371404	0.999861		0.962141	0.998802
N_2	0	0	1.05E-08	2.81E-08		0	0
O_2	0	0	0	0		0	0
NO_2	0	0	0	0		0	0
NO	0	0	0	0		0	0
S	0	0	0	0		0	0
SO_2	0	0	1.1E-06	2.96E-06		0	0
SO_3	0	0	0	0		0	0
H_2	0	0	7.32E-13	1.97E-12		0	0
Cl_2	0	0	0	0		0	0
HCl	0	0	1.14E-07	3.06E-07		0	0
CO	0	0	4.35E-17	1.17E-16		0	0
CO_2	0	0	5.44E-06	1.46E-05		0.035473	0
Ar	0	0	4.84E-08	1.3E-07		0	0
Ne	0	0	1.96E-12	5.27E-12		0.001732	1.45E-05
He	0	0	5.35E-13	1.44E-12		0.000481	2.03E-05
CH_4	0	0	1.59E-10	4.29E-10		0.000173	0.001163
$CaSO_4$	0	0	0	0		N/A	0
$CaSO_3$	0	0	0	0		N/A	0
$CaSO_4.2H_2O$	0	0	0.47338	9.08E-05		N/A	0
C	0	0	0	0		N/A	0
$CaCO_3$	0.057531	0	0	0		N/A	0
$MgCO_3$	0.002973	0	0.024462	4.69E-06		N/A	0
SiO_2	0.012301	0	0.101217	1.94E-05		N/A	0
Al_2O_3	0.00222	0	0.018264	3.5E-06		N/A	0
Fe_2O_3	0.000556	0	0.004576	8.78E-07		N/A	0
Na_2O	0.000266	0	0.002187	4.19E-07		N/A	0
K_2O	0.000547	0	0.004504	8.64E-07		N/A	0

Stream information for Figure 20

Stream name	R3-1	R3-2	R4-1	R4-2	R4-3	R4-4	R4-5	R4-6	R4-7
$T(K)$	247.15	223.5572	219.15	230	219.5904	228.8804	295.1004	374.164	308.064
$P(Pa)$	3140000	3140000	3110000	3110000	900000	900000	900000	2200000	2200000
$\dot{M}(Kg/sec)$	65.2647	65.2647	39.4782	39.4782	39.4782	39.4782	39.4782	39.4782	39.4782
$\dot{E}_{tot}$									
Mole fractions									
H_2O	0	0	0	0	0	0	0	0	0
N_2	0.243402	0.243402	0.022263	0.022263	0.022263	0.022263	0.022263	0.022263	0.022263
O_2	0	0	0	0	0	0	0	0	0
NO_2	0	0	0	0	0	0	0	0	0
NO	0	0	0	0	0	0	0	0	0
S	0	0	0	0	0	0	0	0	0
SO_2	0.005878	0.005878	0.000531	0.000531	0.000531	0.000531	0.000531	0.000531	0.000531
SO_3	0	0	0	0	0	0	0	0	0
H_2	1.22E-05	1.22E-05	1.1E-06	1.1E-06	1.1E-06	1.1E-06	1.1E-06	1.1E-06	1.1E-06
Cl_2	0	0	0	0	0	0	0	0	0
HCl	0.003184	0.003184	0.000288	0.000288	0.000288	0.000288	0.000288	0.000288	0.000288
CO	1.6E-10	1.6E-10	1.57E-11	1.57E-11	1.57E-11	1.57E-11	1.57E-11	1.57E-11	1.57E-11
CO_2	0.674912	0.674912	0.963314	0.963314	0.963314	0.963314	0.963314	0.963314	0.963314
Ar	0.072613	0.072613	0.013604	0.013604	0.013604	0.013604	0.013604	0.013604	0.013604
Ne	0	0	0	0	0	0	0	0	0
He	0	0	0	0	0	0	0	0	0
CH_4	0	0	0	0	0	0	0	0	0

Stream information for Figure 20

Stream name	R5-1	R5-2	R5-3	R5-4	R5-5	R6-1	R6-2	R6-3	R6-4
$T(K)$	219.15	228.94	297.64	624.04	297.5558	300.2651	308.15	298.15	316.0496
$P(Pa)$	3110000	3110000	3110000	3110000	105000	2200000	7800000	7800000	15000000
$\dot{M}(Kg/sec)$	25.7865	25.7865	26.06432	26.06432	26.06432	156.4062	156.4062	156.4062	156.444
$\dot{E}_{tot}$			13.48728	16.15213	7.38779				105.1234
Mole fractions									
H_2O	0	0	0	0	0	0	0	0	0
N_2	0.517732	0.517732	0.524551	0.524551	0.524551	0.01644	0.01644	0.01644	0.016882
O_2	0	0	0	0	0	0	0	0	0
NO_2	0	0.00E+00	0	0	0	0	0	0	0
NO	0	0	0	0	0	0	0	0	0
S	0	0.00E+00	0	0	0	0	0	0	0
SO_2	0.012511	0.012511	0.011973	0.011973	0.011973	0.0004	0.0004	0.0004	0.000388
SO_3	0	0.00E+00	0	0	0	0	0	0	0
H_2	2.59E-05	2.59E-05	2.45E-05	2.45E-05	2.45E-05	8.28E-07	8.28E-07	8.28E-07	7.95E-07
Cl_2	0	0.00E+00	0	0	0	0	0	0	0
HCl	0.006777	6.78E-03	0.006684	0.006684	0.006684	0.000217	0.000217	0.000217	0.000217
CO	3.39E-10	3.39E-10	3.95E-10	3.95E-10	3.95E-10	5.69E-10	5.69E-10	5.69E-10	6.72E-10
CO_2	0.31714	0.31714	0.312753	0.312753	0.312753	0.973355	0.973355	0.973355	0.972915
Ar	0.145814	1.46E-01	0.144014	0.144014	0.144014	0.009588	0.009588	0.009588	0.009598
Ne	0.00E+00	0.00E+00	0	0	0	0	0	0	0
He	0.00E+00	0.00E+00	0	0	0	0	0	0	0
CH_4	0.00E+00	0.00E+00	0	0	0	0	0	0	0

9.2. Oxy-combustion steam cycle results

Stream information for Figure 28

Stream name	N13	N14	N17	N35	N16	N38	N39	N40	N15
$T(K)$	872	605.1	894.3	835.5	672.1	835.5	672.1	605.1	605.1
$P(Pa)$	24233000	4900000	4522000	20000000	7700000	20000000	7700000	4900000	4900000
$\dot{M}(Kg/sec)$	612.05	502.491	502.491	0.559	47.513	611.49	563.977	0.569	60.917
$\dot{E}_{tot}$	1010.435	604.3969	803.665		62.7414				73.69794
Stream name	N18	N20	N36	N19	N-ASUA	N-CPUA	N41	N21	N24
$T(K)$	771.6	771.6	654.7	654.7	654.7	654.7	654.7	654.7	575.2
$P(Pa)$	2138000	2138000	949000	949000	949000	949000	949000	949000	501000
$\dot{M}(Kg/sec)$	24.85	477.64	0.507	15.322	2.231	0.041	423.225	36.315	33.24
$\dot{E}_{tot}$					2.43481	0.044776			
Stream name	N42	N25	N43	N44	N26	N27	N22	N45	N34
$T(K)$	575.2	437.2	437.2	367.1	367.1	339.8	328.2	339.8	315.2
$P(Pa)$	501000	132000	132000	58000	58000	24000	13789.47	24000	7000
$\dot{M}(Kg/sec)$	389.984	16.46	373.524	357.903	15.621	15.462	36.315	342.441	342.441
$\dot{E}_{tot}$									
Stream name	Mu water	N33	N1	N2	N30	N29	N52	N31	N4-2
$T(K)$	298.1	652.6	311.5	311.6	316.2	652.6	312.2	295.7	343.2
$P(Pa)$	101325	949000	7000	1689000	949000	949000	1689000	24000	1586000
$\dot{M}(Kg/sec)$	5.187	0.362	466.363	466.363	0.349	0.349	466.363	81.708	96.88
$\dot{E}_{tot}$	0.259149								6.393821
Stream name	N4	N4A	N51	N4B	N4-1	N50	N5	N49	N6
$T(K)$	334	335.6	316.8	353.2	353.2	324.3	353.2	343	375.2
$P(Pa)$	1586000	1586000	58000	1586000	1586000	132000	1586000	501000	1551000
$\dot{M}(Kg/sec)$	466.363	563.243	66.247	563.243	96.88	49.701	466.365	33.24	466.365
$\dot{E}_{tot}$					6.965723				
Stream name	N7	N-CPUB	N-ASUB	N8	N9	N48	N10	N47	N11
$T(K)$	419	449.5	449.5	449.5	454.5	411.3	487.3	459	532.8
$P(Pa)$	1517000	949000	949000	921000	28958000	2138000	28958000	4900000	28889000
$\dot{M}(Kg/sec)$	466.365	0.041	2.231	612.05	612.05	133.281	612.05	108.431	612.05
$\dot{E}_{tot}$		0.007672	0.417211						
Stream name	N46	N12	N28						
$T(K)$	481.6	563.3	652.6						
$P(Pa)$	7700000	24233000	949000						
$\dot{M}(Kg/sec)$	47.513	612.05	0.924						
$\dot{E}_{tot}$		283.7696							

9.3. Baseline power plant stream results

Stream information for Figure 21

Stream name	C0	C1-1	C1-2	C1-3	C5	C6	C8	C9	A0
$T(K)$	298.1	450.1	456.6	330.1	298.1	298.1	330.4	330.4	298.1
$P(Pa)$	101325	101325	96956.88	101325	101325	101325	105000	105000	101325
$\dot{M}(Kg/sec)$	51.32	564.062	559.165	588.232	16.931	22.27	6.899	9.26	513.426
$\dot{E}_{tot}$									
Mole fractions									
H_2O	N/A	0.089862	0.089862	0.150819	0.923052	1	0.086704	0.999997	0.015761
N_2	N/A	0.749679	0.749679	0.701897	0	0	1.99E-08	2.29E-07	0.791425
O_2	N/A	0.006108	0.006108	0.005995	0	0	2.82E-09	3.25E-08	0.185902
NO_2	N/A	3.64E-07	3.64E-07	1.85E-11	0	0	4.41E-14	5.09E-13	0
NO	N/A	0.001285	0.001285	1.51E-15	0	0	3.06E-22	3.53E-21	0
S	N/A	1.81E-09	1.81E-09	0	0	0	0	0	0
SO_2	N/A	0.002118	0.002118	0	0	0	0	0	0
SO_3	N/A	9.72E-07	9.72E-07	0	0	0	0	0	0
H_2	N/A	0.000289	0.000289	0	0	0	0	0	0
Cl_2	N/A	4.22E-10	4.22E-10	9.32E-05	0	0	4.55E-09	5.25E-08	0
HCl	N/A	0.000224	0.000224	2.11E-05	0	0	4.97E-10	5.73E-09	0
CO	N/A	0.002032	0.002032	0	0	0	0	0	0
CO_2	N/A	0.142087	0.142087	0.135267	0	0	2.35E-07	2.71E-06	0.000238
Ar	N/A	0.006257	0.006257	0.005853	0	0	2.38E-09	2.75E-08	0.00661
Ne	N/A	2.40E-05	2.40E-05	2.24E-05	0	0	4.66E-12	5.38E-11	2.53E-05
He	N/A	3.36E-05	3.36E-05	3.14E-05	0	0	1.27E-12	1.47E-11	3.55E-05
CH_4	N/A	3.03E-20	3.03E-20	0	0	0	0	0	3.19E-06
$CaSO_4$	N/A	0	0	0	0	0	0.668997	0	0
$CaSO_3$	N/A	0	0	0	0	0	0	0	0
$CaSO_4.2H_2O$	N/A	0	0	0	0	0	0	0	0
C	N/A	0	0	0	0	0	0	0	0
$CaCO_3$	N/A	0	0	0	0.057948	0	0.01879	0	0
$MgCO_3$	N/A	0	0	0	0.002995	0	0.035542	0	0
SiO_2	N/A	0	0	0	0.01239	0	0.14706	0	0
Al_2O_3	N/A	0	0	0	0.002236	0	0.026536	0	0
Fe_2O_3	N/A	0	0	0	0.00056	0	0.006648	0	0
Na_2O	N/A	0	0	0	0.000268	0	0.003177	0	0
K_2O	N/A	0	0	0	0.000551	0	0.006545	0	0

9.4. Baseline power plant steam cycle results

Stream information for Figure 25

Stream name	N13	N14	N17	N35	N16	N38	N39	N40	N15
$T(K)$	872	605.1	894.3	835.5	672.1	835.5	672.1	605.1	605.1
$P(Pa)$	24233000	4900000	4522000	20000000	7700000	20000000	7700000	4900000	4900000
$\dot{M}(Kg/sec)$	450	369.449	369.449	0.411	34.933	449.589	414.656	0.418	44.789
Stream name	N18	N20	N36	N19	N41	N21	N24	N42	N25
$T(K)$	771.6	771.6	654.7	654.7	654.7	654.7	575.2	575.2	437.2
$P(Pa)$	2138000	2138000	949000	949000	949000	949000	501000	501000	132000
$\dot{M}(Kg/sec)$	18.271	351.178	0.373	11.265	312.84	26.7	24.571	288.269	12.167
Stream name	N43	N44	N26	N27	N22	N45	N34	Mu water	N33
$T(K)$	437.2	367.1	367.1	339.8	328.2	339.8	315.2	298.1	652.6
$P(Pa)$	132000	58000	58000	24000	13789.47	24000	7000	101325	949000
$\dot{M}(Kg/sec)$	276.102	264.555	11.547	11.429	26.7	253.126	253.126	5.187	0.266
Stream name	N1	N2	N30	N29	N52	N31	N4	N51	N50
$T(K)$	311.5	311.6	310.1	652.6	312.2	297	334	319	321.5
$P(Pa)$	7000	1689000	949000	949000	1689000	24000	1655000	58000	132000
$\dot{M}(Kg/sec)$	345.93	345.93	0.257	0.257	345.93	60.393	345.93	48.965	36.738
Stream name	N5	N49	N6	N7	N8	N9	N48	N10	N47
$T(K)$	354.5	340.1	376.6	420.4	449.5	454.5	411.3	487.3	459
$P(Pa)$	1586000	501000	1551000	1517000	921000	28958000	2138000	28958000	4900000
$\dot{M}(Kg/sec)$	345.93	24.571	345.93	345.93	450	450	97.993	450	79.722
Stream name	N11	N46	N12	N28					
$T(K)$	532.8	481.6	564	652.6					
$P(Pa)$	28889000	7700000	28855000	949000					
$\dot{M}(Kg/sec)$	450	34.933	450	0.68					